3D *in vitro* models as tool for studying tissue repair and remodelling of soft and hard tissues

Maria Elisabeth Schröder

Doctoral Thesis for the degree of Philosophiae Doctor (Ph.D)

Department of Biomaterials

Institute of Clinical Dentistry

Faculty of Dentistry

University of Oslo

Norway

2023

Table of contents

ACKNOWLEDGEMENTS

LIST OF PAPERS

This thesis is based on the following papers and will be referred to in the text by their Roman numerals:

Paper I.

$25(OH)D_3$ alone and combined with vitamin K2 exert more favorable effects than $1,25(OH)_2D_3$ on markers of bone regeneration in 3D spheroids of human periodontal ligament cells. Schröder M, Eriksson Agger A, He J, Skallerud BH, Haugen HJ, Syversen U, Reseland JE. Manuscript.

Paper II.

Vitamin K2 modulates vitamin D-induced mechanical properties of human 3D bone spheroids *in vitro*. Schröder M, Aurstad Riksen E, He J, Skallerud BH, Møller ME, Lian AM, Syversen U, Reseland JE. Journal of Bone and Mineral Research Plus. 2020; 4(9): e10394

Paper III.

Osteoblasts in a perfusion flow bioreactor – tissue engineered constructs of TiO_2 scaffolds and cells for improved clinical performance. Schröder M, Reseland JE, Haugen HJ. Cells. 2022; 11: 1995

ABBREVIATIONS

AA	Ascorbic acid
ALP	Alkaline phosphatase
BMP	Bone morphogenetic protein
BMUs	Basic multicellular units
BTE	Bone tissue engineering
BXR	Biaxial rotating bioreactor
cDNA	Complementary DNA
CLSM	Confocal laser scanning microscopy
DKK-1	Dickkopf-related protein-1
dsDNA	Double-stranded DNA
ECM	Extracellular matrix
ELISA	Enzyme-linked immunoassay
FGF-2	Fibroblast growth factor-2
G-CSF	Granulocyte-colony-stimulating factor
IL-6	Interleukin-6
IL-8	Interleukin-8
MBAA	Multiplex bead array assay
MCP-1	Monocyte chemoattractant protein-1
M-CSF	Macrophage-colony stimulating factor
mRNA	messenger RNA
MSCs	Mesenchymal stem cells
OC	Osteocalcin
OPG	Osteoprotegerin
OPN	Osteopontin
PDL	Periodontal ligament
RANK	Receptor activator of nuclear factor κB
RANKL	Receptor activator of nuclear factor κB ligand
RCCS	Rotary cell culture system
RT-qPCR	Reverse transcription quantitative polymerase chain reaction
Runx2	Runt-related transcription factor 2
RWV	Rotating wall vessel
TiO_2	Titanium dioxide
TRAP	Tartrate-resistant acid phosphatase
VDR	Vitamin D receptor
VEGF	Vascular endothelial growth factor
$1,25(OH)_2D_3$	1,25-dihydroxyvitamin-D_3
$25(OH)D_3$	25-hydroxyvitamin-D_3
2D	Two-dimensional
3D	Three-dimensional

1. INTRODUCTION

1.1 Soft and hard tissues of the periodontium

The periodontium is a complex structure made up of two soft tissues (gingiva and periodontal ligament (PDL)) and two hard tissues (root cementum and alveolar bone) (Figure 1). It attaches the teeth to the bone of the jaws and provides support during their function (1, 2).
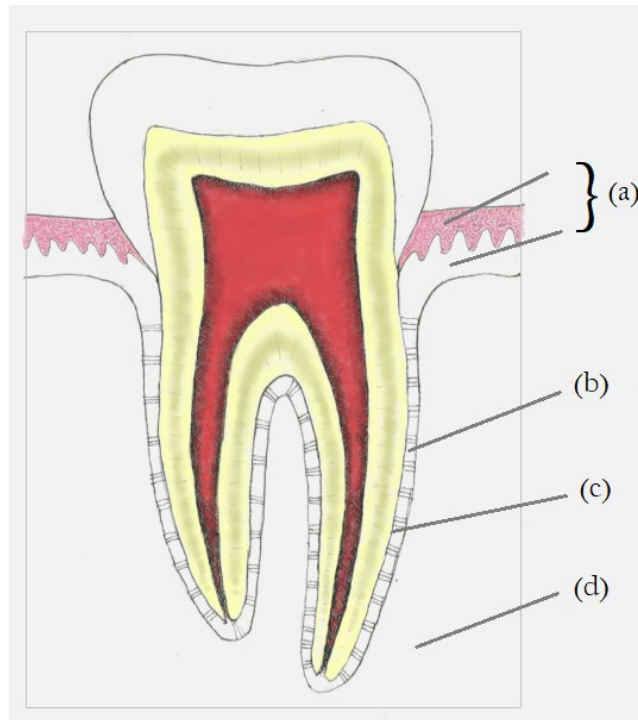
Figure 1. Overview of the tissues of the periodontium. (a) Gingiva with upper epithelial and lower connective tissue components. (b) Periodontal ligament. (c) Cemetum. (d) Alveolar bone. Figure modified after (3).

Characteristic for the periodontium tissues is their specialized structure, which directly relates to their function. The gingiva facing the tooth consists of epithelial structures and underlying connective tissue components (Figure 1a). As part of the gingiva, the junctional epithelium provides the epithelial attachment to the tooth and functions as a barrier against microbial infection (1).

Extending from the gingiva is the PDL (Figure 1b), a dense fibrous connective tissue, ranging from 0.15–0.38 mm in width (4), which links the tooth root to the bone forming the socket wall. Its main functions are to support the teeth in their sockets, protect them from excessive mechanical forces generated during mastication, act as a sensory receptor for the masticatory system and provide a cell reservoir for tissue homeostasis, repair and regeneration (1, 5). During mastication, the PDL experiences mechanical loading (*e.g.* compression, stretch, fluid shear forces and combinations of these), which plays a crucial role for its remodelling and

1

homeostasis (6, 7). Structurally, the PDL is made up of a ground substance (mainly water, proteoglycans and glycoproteins), in which collagen fibre bundles, cells, nerves and blood vessels are embedded (8). The collagen fibre bundles are mainly composed of collagens Type I and III, in addition, Types V, VI, XII and XIV are present in minor amounts in the ligament (9-12). The fibres form a complex three-dimensional (3D) meshwork between the periodontium's two mineralized tissues, the cementum and alveolar bone, in which their ends are firmly inserted (1). The combination and interaction of the viscous fluid phase and the elastic collagen fibres account for the viscoelastic properties of the PDL (13-15).

Fibroblasts are associated with the collagen fibres in the PDL and inhabit about 25% of the ligament volume in human premolar teeth (5). These fibroblasts are derived from a cell population in the inner layer of the dental follicle (16). PDL fibroblasts are active secretory cells responsible for the high turnover and remodelling of the PDL's extracellular matrix (ECM), allowing the tooth to adapt to positional changes (5). They are furthermore characterized by high alkaline phosphatase (ALP) activity (17), an enzyme involved in mineralization (18) and cementum formation (19), and by expression of bone-related proteins like osteopontin (OPN) and osteocalcin (OC) (20). PDL fibroblasts are suggested to play a pivotal role in forming new cementum, bone and fibrous attachment during periodontal regeneration (21, 22).

Besides fibroblasts, the PDL contains bone-forming cells (osteoblasts) and bone-resorbing cells (osteoclasts), epithelial cells (rests of Mallassez), monocytes, macrophages, cells resorbing cementum and dentin (odontoclasts) and undifferentiated mesenchymal cells, capable of differentiating into fibroblasts, cementoblasts and osteoblasts (1).

As mentioned earlier, the primary function of the cementum (Figure 1c), the hard tissue covering the entire surface of the tooth root, is to provide anchorage to the PDL fibres (1). The fourth component of the periodontium, the alveolar bone (Figure 1d), is a specialized part of the maxillary and mandibular bones, lining the whole tooth socket. Due to the embedded PDL collagen fibres bundles, it is also termed bundle bone. In between these fibres, osteoblasts lay down an intrinsic collagen fibre network (23, 24). A characteristic of the alveolar bone is its rapid remodelling, which occurs as a response to tooth migration and mechanical loading during mastication (23). The rest of the alveolar process comprises cortical plates of compact bone and a central spongy bone (24). Structure and composition of compact and spongy bone, as well as the remodelling of alveolar bone, are comparable to other bone sites in the body (23).

1.2 Bone structure, cells, remodelling and mechanical properties

Histologically, lamellar (mature) bone is composed of cortical (compact) and cancellous (trabecular, spongy) bone (Figure 2a).
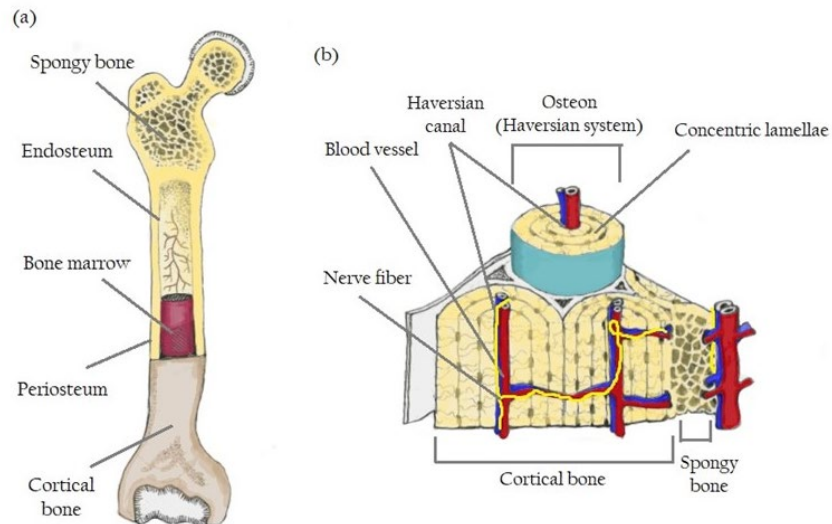
Figure 2. Structure of bone. (a) Components of long bone (b) Microstructure of bone with Haversian system. Figure modified after (25).

Cortical bone makes up 80% of the skeleton's bone mass (26) and has a protective and mechanical function (27). The outer surface of cortical bone is surrounded by the periosteum, a fibrous connective tissue that contains blood vessels, nerves and osteogenic cells, while the inner layer is surrounded by the endosteum (28). Cancellous bone makes up 20% of the bone mass (26) and has a metabolic function (27). It comprises a network of trabecular rods and plates enclosing a cavity harbouring the bone marrow (28). The basic structural unit in the cortical bone is the Haversian system, also termed osteon (Figure 2b). It is made up of concentric sheets of collagen fibrils, termed lamellae, which are arranged in a circular pattern around a cavity, the Haversian canal, which encompasses blood- and lymphatic vessels, and nerves (29, 30).

Bone is composed of an organic matrix (20–40%; including 2-5% cells and < 3% lipids), water (5-10%) and inorganic mineral (50-70%) (28, 31). Collagens, predominately Type I, with trace amounts of Types III and V, make up 90% of the organic matrix in mineralized bone. The remaining 10% compose of non-collagenous proteins (32) including glycoproteins (*e.g.* ALP), RGD-containing glycoproteins (*e.g.* OPN, bone sialoprotein), γ-carboxy glutamic acid-containing proteins (*e.g.* OC), proteoglycans, and serum proteins. Many of these are involved

in regulating the bone mineralization process or the modulation of bone cell activity (28). Type I, III and V collagens are fibrillar collagens, composed of a triple helix motif (glycin – proline – hydroxyproline) (33). The inorganic component of bone is composed of carbonated hydroxyapatite [$Ca_{10}(PO_4)_6(OH)_2$], which is embedded in the form of plate-like mineral crystals (20-80 nm in length and 2-5 nm thick), between the collagen fibrils (34, 35). Moreover, bone is lined and penetrated by several different types of cells (36). Osteoblasts (4-6% of resident cells) are large cells with cuboidal shape, present on the bone surface, which synthesize and secrete the bone's organic matrix and regulate its mineralization (36, 37). Osteocytes are terminally differentiated osteoblasts and the principal cell type in adult bone (90–95% of resident cells) (38). Bone lining cells are quiescent osteoblasts with elongated or flattened morphology, which cover bone surfaces in the adult skeleton that do not undergo remodelling (39). Their function in bone is not fully understood, however, they are suggested to serve as a membrane to separate bone and interstitial fluids (40, 41) and to be involved in bone remodelling (42, 43). The fourth cell type, osteoclasts, carry out bone resorption to initiate the remodelling of the bone matrix (36). More details on each bone cell type are given in the following paragraphs.

Osteoblasts originate from pluripotent mesenchymal stem cells (MSCs), and their differentiation to osteogenic lineage cells involves Wnt pathways, bone morphogenetic protein (BMP) signalling, and the expression of several osteoblast-specific transcription factors, among them runt-related transcription factor 2 (Runx2) and osterix (44). The development of pre-osteoblasts into mature, matrix-synthesizing osteoblasts follows three sequential stages: proliferation, matrix maturation and mineralization (45). The characteristic expression of osteoblast phenotype-related genes during each stage is shown in Figure 3. Actively secreting osteoblasts in human bone have a relatively short average life-span of around three months (46). At this point, 50-80% of osteoblasts will undergo apoptosis (47), while a smaller portion will develop into bone-lining cells (30). In addition, 10-20% of osteoblasts will be completely embedded within the newly synthesized matrix and switch their phenotype to osteocytes (30, 48). Osteocytes within the mineralized matrix sit within small spaces (lacunae) and form long, cytoplasmic extensions that travel in small channels (canaliculi). This osteocyte lacuna-canalicular network serves as a connection to cells resident on the bone surface and the vasculature. Osteocytes are also involved in regulating phosphate homeostasis via the secretion of endocrine factors (*e.g.* fibroblast growth factor 23). Moreover, osteocytes regulate the activities of osteoclasts and osteoblasts during bone remodelling through expression and release

of signalling molecules (49), and are the main mechanoresponsive cells in bone (50). Mechanical loading due to physical activity is one of the main drivers of bone mass and architecture (51, 52), and osteocytes may sense mechanical stimuli in the form of matrix strain, pressure, fluid flow and/or shear stress (49). Osteocytes may experience fluid flow-induced shear stress *in vivo* when interstitial fluid is forced through the narrow channels of the lacuna-canalicular network within the mineralized ECM (50). This shear stress has been estimated to range from 0.8–3 Pa in a theoretical model (53). Mechanoresponsive signalling pathways in bone cells include mitogen-activated protein kinase signalling, Wnt/β-catenin, calcium, prostaglandins, nitric oxide, and estrogen (54).
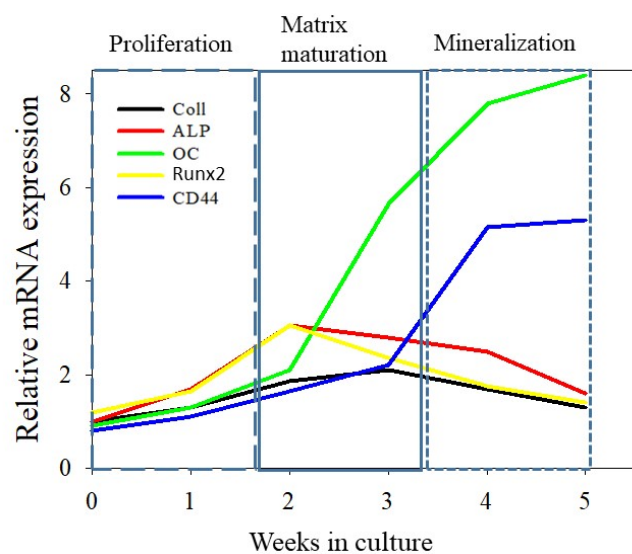
Figure 3. Gene expression pattern during differentation of primary human osteoblasts. Relative mRNA expression of collagen (Coll), alkaline phosphatase (ALP), osteocalcin (OC), runt-related transcription factor 2 (Runx2) and adhesion molecule CD44 (CD44) obtained from 2D monolayer cultures. Data is shown as expression relative to house keeping genes at time point 0 (relative fold-change) (Reseland 2001, unpublished data).

Osteoclasts are multinucleated cells formed by the fusion of mononuclear precursor cells of the monocyte-macrophage lineage (55). Osteoclast formation is dependent on macrophage-colony stimulating factor (M-CSF) and interaction of receptor activator of nuclear factor κB (RANK) ligand (RANKL), produced mainly by osteocytes (56, 57) and in minor amounts by stromal and other osteogenic lineage cells, with the transmembrane RANK receptor on the surface of osteoclast precursors (58-60). To prevent excessive osteoclast formation, osteoprotegerin (OPG), produced by stromal cells, osteoblasts and periodontal ligament fibroblasts (58, 61), acts as a soluble decoy receptor (62) by binding to RANKL and hence preventing the

RANK/RANKL interaction (63). Hence, the RANKL/OPG ratio is crucial for bone mass and strength (63).

The actions of osteoclasts resorbing bone and osteoblasts forming new bone are linked during the bone remodelling within discrete temporary anatomic structures termed basic multicellular units (BMUs) (64, 65). The BMUs are located within cavities that require remodelling, contain osteoblasts, osteoclasts and blood vessels (66), and are covered by bone lining cells, which form the bone remodelling compartment (42). The remodelling cycle within the BMU follows several sequential stages: recruitment and activation of mononuclear osteoclast precursors, differentiation into multinucleated osteoclasts, resorption, reversal, pre-osteoblast recruitment, osteoblast differentiation, bone formation and termination (Figure 4) (67).
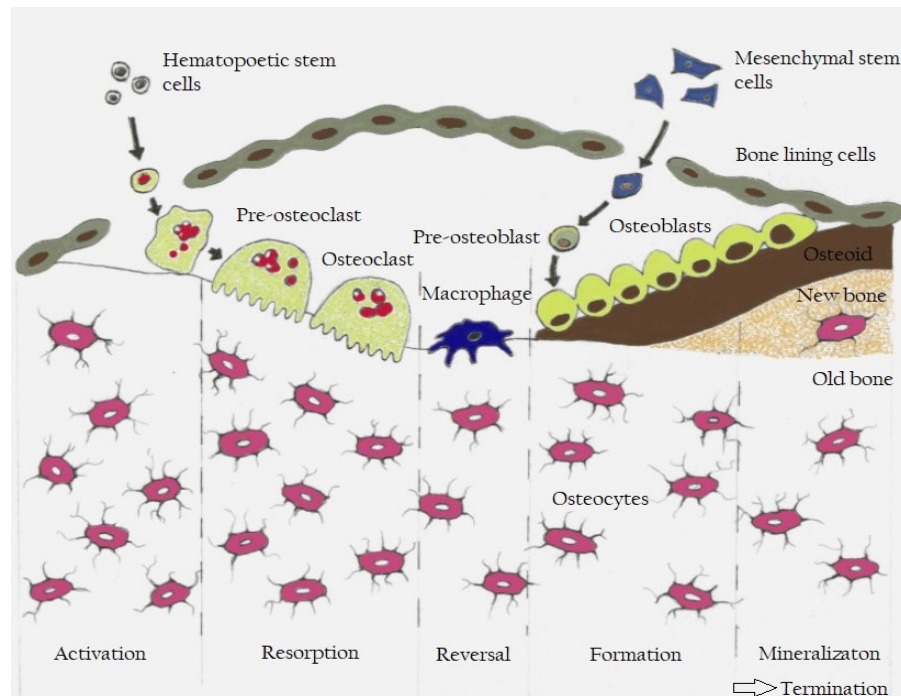
Figure 4. Overview of the bone remodelling cycle. Figure adapted from (68).

The couplings signals which regulate the reversal from resorption to the new bone formation during remodelling are suggested to include resorption products (growth factors derived from the bone matrix) and osteoclast-derived factors which stimulate osteoblast differentiation and function (further details can be found in (69)). Osteocytes play a crucial role in the termination of remodelling by secreting sclerostin and dickkopf-related protein-1 (DKK-1), the antagonist of the Wnt signalling pathway, which prevents further osteoblastic bone formation (38).

Bone remodelling underlies endocrine (parathyroid hormone, 1,25-dihydroxyvitamin-D$_3$ (1,25(OH)$_2$D$_3$), calcitonin, thyroid hormone, growth hormone, glucocorticoids and sex hormones) and paracrine (prostaglandins, cytokines, transforming growth factor-ß, BMPs) regulation (67). Bone remodelling functions to provide calcium and phosphate ions at sites of increased demand, adapt the skeleton to its mechanical environment and replacement of damaged or old bone with newer and healthier bone. Most remodelling sites in the skeleton develop randomly, while the minor part may be targeted to damaged areas (70). Microcracks may trigger targeted remodelling in bone, disrupting the osteocyte-canalicular network and leading to osteocyte apoptosis (71).

The remodelling rate and its tissue mass, as well as its macro- and microarchitecture and material properties (quality, amount and interaction of the mineral- and collagen matrix, presence of microdamage), are all factors that influence the mechanical properties of bone (28, 72, 73). The mineral phase of bone is associated with its stiffness and strength (74). Moreover, the collagen fibre network, in particular its organization (collagen fibril orientation, presence of collagen cross-links and post-translational modifications) (75) and structural integrity, play a crucial role in bone's toughness (flexibility) (76). The matricellular protein periostin, named after its expression in the periosteum and PDL of adult mice (77), has also been demonstrated to affect the mechanical properties of bone by influencing its material properties (78, 79), as well as its microdamage accumulation and repair (79). In addition, non-collagenous proteins in the bone matrix, among them OC and OPN, have been suggested to influence bone's toughness and fracture resistance (80).

1.3 Bone repair and bone grafting

Bone is one of the few tissues that can repair and regenerate itself without fibrous scar formation (81). Bone fractures can heal via a primary (direct) or secondary (indirect) pathway (82), depending on the degree of displacement and mechanical stability of the fracture site (81, 83, 84). Primary intramembranous healing, in which lost bone tissue is directly remodelled into the lamellar bone and the Haversian system, requires rigid fixation and reduction of fracture ends. In the case of an unstable fracture site, which is much more common (82), healing occurs through the secondary pathway, in which new bone is formed through a cartilage intermediate (endochondral ossification) (85).

The indirect fracture healing pathway is characterized by three overlapping phases: Inflammatory phase (haematoma and acute inflammation), the repair phase (soft- and hard

callus formation) and the remodelling phase (substitution of hard callus with lamellar bone) (86).

Bone grafting represents a common approach in clinical practice to enhance bone regeneration in cases where the self-healing capacity of bone is insufficient (*e.g.* large bone defects caused by a traumatic fracture, tumour resection, infection or skeletal abnormalities) (87). Autologous bone (bone transplanted within the same individual) is still the gold standard among all available grafts since it provides osteogenic cells, growth factors and a suitable scaffold matrix for bone regeneration, without risk for immuno-rejection (87, 88). However, the need for a second surgery, possible donor site complications and the relatively small volume of these grafts limit their usage (89, 90). Allografts (bone transplanted from a donor of the same species) (91) and xenografts (bone transplanted from a different species) (88) are available in greater quantities but harbour a potential risk for immuno-rejection and transmission of diseases. Due to the need for tissue processing and sterilizing, they often lack viable cells and most growth factors (91, 92).

Bone grafting with synthetic materials, so called bone graft substitutes, and their combination with MSCs/osteoprogenitor cells and/or growth factors, referred to as bone tissue engineering (BTE), represents an alternative to the limitations and current shortage of natural bone grafts (93-95). An ideal bone graft substitute material combines the following properties: highly porous with an interconnected porosity to allow for cell growth, transport of nutrients and removal of waste products (96). The minimum pore size is considered to be >100 μm, pores >300 μm are recommended for bone ingrowth and vascularization (97). Moreover, the material should possess suitable surface properties for the attachment, migration, proliferation and differentiation of bone cells, mechanical properties comparable to implantation site, and controlled biodegradability to maintain 3D stability during bone ingrowth (94, 96). Another requirement is biocompatibility (94), referring to the ability of the material to perform its desired function in the host without eliciting any undesirable local or system effects (98). Furthermore, the material should be osteoconductive, providing a suitable scaffold to support and direct the bone growth over its surface (99), and enable direct bone-to-implant contact, referred to as osseointegration (100). Another desirable property of a bone substitute material is osteoinductivity, which refers to its ability to stimulate and activate MSCs and osteoprogenitor cells from the surrounding tissues of the host to differentiate into osteoblasts (101).

Synthetic bone substitutes like calcium sulphate, calcium phosphate ceramics/cements, bioactive glass and combinations of these, are characterized by high biocompatibility and

chemical similarity with bone (96, 102), however, their low mechanical properties (brittleness, low fatigue strength), in particular in porous form, limits the application to low- or non-load bearing bone defects (103, 104). Previously, a porous (porosity up to 90%) titanium dioxide (TiO_2) ceramic with improved compressive strength (up to 3.4 MPa (105), which is in the range of trabecular bone (106)), has been fabricated by polymer sponge replication using commercially available TiO_2 powder (for details on fabrication process please see (105, 107)). The scaffolds structural parameters were carefully optimized to allow for cellular adhesion, viability, and differentiation (105, 107). Characteristic for the scaffolds is their large, interconnected pore volume (spherical macropores with a diameter of 400 μm, strut diameter 50 -100 μm) in order to allow cells to migrate into the constructs and proliferate (105). Although the scaffolds do not provide or mimic cues of the natural ECM (integrin binding motifs), the surface chemistry is suitable for the attachment of mouse MC3T3-E1 pre-osteoblasts and human MSCs (107-110). Indeed, several *in vitro* studies demonstrated that MC3T3-E1 fibroblasts adhere well to the TiO_2 surface and are spread out in the open pores and struts of the scaffolds (107-109). The mRNA expression of the cell adhesion marker integrin ß1 of MC3T3-E1 cells has been found to be reduced following day one to seven of culture on the TiO_2 scaffolds, indicating increased adhesion. Moreover, an increase in fibronectin mRNA expression was detected over 21 days, indicating initiation of ECM deposition. Furthermore, the scaffolds promote the differentiation of MC3T3-E1 pre-osteoblasts to mature osteoblasts as indicated by a decrease of Type I collagen mRNA expression and high OC mRNA levels over 21 days, in line with increased ALP activity and calcium deposition (109).

TiO_2 has been widely studied as a material for bone defect healing (111-114) and BTE (108, 109) because of its biocompatible (115) and bioactive properties (116).

1.4 *In vitro* models mimicking tissues

Two-dimensional (2D) cultures, in which cells are grown as flat monolayers on a polystyrene or glass surface exposed to growth medium, represent the simplest and most cost-effective *in vitro* model applied to mimic native cellular tissue environment. However, these models are less good predictors of *in vivo* cellular behaviour and responses since they fail to replicate the tissue's complex and dynamic 3D environment (117, 118). Indeed, research has shown that cellular architecture, growth rate, metabolism and drug sensitivity differ radically in 3D and 2D cultures (119, 120). 3D *in vitro* models mimicking tissues can be categorized into scaffold-based or scaffold-free. Both categories include static and dynamic models (121). Scaffold-based models rely on using an exogenous template to support cellular attachment, migration, 3D

growth and tissue formation. The scaffold may be further modified with growth factors and/or factors involved in cellular differentiation to enhance tissue formation (122). Scaffold-based 3D culture has also been combined with microfluidic devices to simulate a dynamic culture environment by applying fluid flow. For this approach, microfluidic devices can be modified with micro-channels and/or pillars to provide a substrate for cellular attachment and 3D growth, also known as organ-on-a-chip systems (118). Scaffold-free tissue models are based on cellular self-organization into aggregates or larger constructs without the inclusion of any template guiding 3D growth (122, 123). These models include cell sheets and spheroids (122). Cells sheets represent 3D shaped functional tissue models, fabricated by expansion of cells into a confluent, ECM-rich sheet, and subsequent layering or draping on a surface coated with a thermo-responsive polymer (124-126). Spheroids can be formed by self-organization of monotypic or heterotypic cells using various methods (reviewed in detail in (121, 127, 128)). For example, low-adhesion or ultra-low attachment plates may be used to inhibit cellular attachment and promote aggregation into spheroids (also referred to as forced floating or liquid overlay technique) (129). Moreover, the hanging drop method, in which the cell suspension is placed in droplets on an inverted surface, enables cell aggregation by surface tension and gravitational forces (130, 131). In addition, hydrogels like Matrigel can be applied to enable 3D cell growth into spheroids (128). Spheroids can also be formed and cultured by agitation-based (dynamic) approaches (*e.g.* in a rotary cell culture system (RCCS)) (132).

1.5 Matrix composition, distribution of nutrients and oxygen, and their effects on cells in 3D tissue models

Cellular phenotype, behaviour and drug response *in vivo* are defined by the tissue microenvironment and niche in which, besides the 3D architecture, the biochemical composition and stiffness of the ECM and molecular concentration gradients in oxygen, pH and soluble molecules (nutrients, growth factors, cellular metabolites) play a central role (133, 134). Hence, to create realistic human 3D tissue models *in vitro*, their design and culture conditions need to be carefully considered (134, 135).

Scaffolds provide a framework for 3D growth and tissue formation in 3D models and may also direct cellular behaviour and function through their surface chemistry or through providing or mimicking biochemical and mechanical cues present in the native ECM (*e.g.* decellularized tissue matrix or hydrogels) (134, 136). Hydrogels, 3D networks of crosslinked polymer chains that absorb large amounts of water (136, 137), from natural sources such as Type I collagen, matrigel, fibrin or hyaluronan (136), provide binding ligands for cell adhesion and subsequent

integrin expression, which will direct cell fate through intracellular signalling pathways and regulate the deposition of self-generated ECM components by the cells (134, 136, 138). Likewise, synthetic hydrogels, *e.g.* polyethylene glycol- or polylactic acid-based may be modified with ECM-derived peptide sequences to provide integrin-binding motifs (139). This may represent an advantage over the use of synthetic/bioprinted scaffolds or organ-on-a-chip systems which usually lack natural ECM components (140, 141).

Within 3D tissue models, using scaffolds or scaffold-free models such as spheroids, the supply of oxygen and nutrients as well as the removal of waste products is dependent on passive diffusion mechanisms (142, 143). Oxygen tension (pO2) measurements within 3D tissue models using O2 sensitive microelectrodes demonstrate an oxygen concentration gradient from the surface to the core of the 3D constructs. Moreover, pO2 distribution within 3D tissue models is dependent on oxygen diffusion rate and cellular consumption rate (144, 145), the latter which is cell type specific (146).

Static spheroid cultures experience a diffusion depleted zone in the range of 150 - 200 µm for most molecules (147, 148). Diffusion limitations, in particular the limited supply of oxygen, may induce a hypoxic/anoxic spheroid core (148) in contrast to the spheroid surface where the cells are directly exposed to oxygen and medium and can actively proliferate (147). Spheroids with a radius of 25-50 µm cultured at 21% O2 have a pO2 of around 3.3% in their core, 100 µm spheroids a pO2 of 1.6% and spheroids with radii > 175 µm 0% (148, 149). Even irrigated spheroids experience anoxia at radii > 600 µm (148). In comparison, cells in tissues experience between 1% and 14% pO2, also referred to as physiological hypoxia (150), and oxygen tension levels in bone range between < 1% and 6% (151). Hypoxia and glucose starvation in large spheroids may induce metabolic changes in the cellular metabolism such as the switch from oxidative phosphorylation to aerobic glycolysis (148). A study by Pilz *et al.* further demonstrated that molecule/drug size may be another factor influencing the diffusion into spheroids (152). They analyzed the transport of nanoprobes into the ECM of different types of spheroids as well as their ECM viscosity and observed that smaller molecules (up to 10 nm) can diffuse freely through the ECM while larger molecules experience higher viscosity and hence diffusion limitations (152).

Matrix composition, substrate stiffness and molecular concentration gradients have a profound effect on cell migration, proliferation, cell fate and drug response in 3D tissue models (135, 144, 148, 153-157). Higher substrate stiffness in 3D matrices is associated with increased cell migration (135, 154) and lower stiffness with the preservation of the stem cell state (153, 155). Physiological hypoxia is a known driver of angiogenic signalling cascades and a regulator of

cell differentiation (144, 158, 159). During bone repair, hypoxia signalling stimulates angiogenesis, progenitor cell migration and differentiation (160). In 3D triple cultures of osteoblasts, osteocytes and osteoclasts, physiological hypoxia has been shown to negatively impact osteoblast and osteocyte phenotype marker expression and activity (161).

1.6 3D *in vitro* models mimicking bone

To date, several 3D *in vitro* models to study bone cell communication, bone remodelling/mineralization or bone diseases and the effect of various treatments on these processes have been proposed (156, 157, 162-171).

Collagen hydrogels have gained interest for the generation of 3D *in vitro* models of bone due to their close resemblance to the bone organic matrix and their remodelling capacity (164, 165, 167, 172). Bakkalci *et al.* developed a 3D bone model from rat calvarial osteoblasts in stiff, plastic compressed collagen gels which contained distinct mineralized nodules of immature (woven) bone (167). Bernhardt *et al.* fabricated a 3D *in vitro* bone model based on collagen gels, transwell inserts and human primary cells in which the three major cell types of bone, osteoblasts, osteoclasts and osteocytes, are spatially arranged in a similar *in vivo*-like manner. Interestingly, this model also allows for the separate analysis of each cell type (172). Domaschke *et al.* co-cultured osteoclast-like cells and osteoblasts on Type I collagen/hydroxyapatite sponge scaffolds and observed active remodelling and mineralization within the model (164).

A few bone-on-a-chip models exist up to date (171, 173, 174). Galván-Chacón *et al.* developed a 3D bone model mimicking aspects of the trabecular architecture, mineral content and dynamic environment of bone (171). They used two-photon polymerization laser lithography to print a 3D structural model of bone from a polymer, which was coated with biomimetic hydroxyapatite, seeded with human MSCs and integrated into a microfluidic system, to study bone cell-ECM interactions and other cellular processes involved in bone regeneration (171).

Spheroid cultures are frequently used to create 3D *in vitro* models of bone since they promote the maturation of the osteoblast/osteocyte phenotype and the crosstalk between bone cells (162, 163, 175-177). 3D aggregates of pre-osteoblasts/osteoblasts and/or osteoclasts in which the cells form their own (mineralized) ECM are also termed osteospheres (162, 178). Osteospheres have previously been fabricated using various techniques, among them low adhesion plates in combination with agitation (176, 179), magnetic levitation (180) and by rotational culture (162, 163, 181). Osteospheres have previously been used to study the effect of various drugs/agents

on the bone microenvironment and the mechanical properties of bone (168-170). Moreover, spheroids have been used as model system to study the bone mineralization process as well as the effect of various drugs on mineral deposition (156, 166). Koblenzer *et al.* fabricated murine MC3T3-E1 pre-osteoblast spheroids in non-adherent V-shaped plates and characterized the mineralized bone matrix and mineralization stages using advanced imaging techniques. They observed a native murine bone-like matrix in the model within 28 days (156). Vermeulen *et al.* established a mineralized bone spheroid model from human mesenchymal stromal cells and calcium/phosphate supplementation of the culture medium in microwell array plates. They demonstrated the suitability of the spheroids to serve as model systems for the screening of novel drugs promoting or inhibiting mineralization (166). Other studies have explored the potential of combining bone spheroids with biomaterials (157, 182). Heo *et al.* proposed a vascularized 3D bone model by incorporating human MSCs and human umbilical vein endothelial cell spheroids into fibrin hydrogels. The model exhibited pre-vascular network formation and enhanced osteogenic differentiation capacity (182).

1.7 The role of vitamins in soft and hard tissue remodelling and repair

Nutrition, in particular adequate intake of glucose, protein, fatty acids, amino acids, vitamins, and minerals, plays a crucial role in wound healing and tissue regeneration (183, 184). Vitamins A, B, C, D, E and K have been proposed to affect wound healing (183, 185), bone and oral health and periodontal tissues (186, 187).

Vitamin A, a fat-soluble vitamin composing a group of organic compounds including retinol and β-carotene (188), is known for its stimulating effect on epithelial growth, fibroblasts, granulation tissue, angiogenesis, collagen synthesis, epithelialization and fibrous tissue growth, hence promoting and enhancing wound healing (189). Vitamin A supplementation can counteract the inhibitory effect of steroid therapy on wound healing (190). Vitamin A and its precursor pro-vitamin A are involved in bone metabolism. Vitamin A promotes osteoblast differentiation, inhibits mineralization, and modulates the production of bone-related proteins, depending on its concentration. Pro-vitamin A stimulates osteoblast differentiation and bone formation while inhibiting osteoclast activity and bone resorption (191).

B-complex vitamins function as co-factors in several metabolic processes during wound healing and are required for collagen synthesis and cross-linking (192, 193). Vitamin B-complex supplementation benefits wound healing after periodontal flap surgery (194).

Vitamin C (ascorbic acid, (AA)) is required for collagen synthesis by acting as a co-factor in the hydroxylation of pro-collagen (195) and has an essential role in neutralizing reactive oxygen

species which damage cells and hence impair tissue healing (184, 196). Vitamin C deficiency is associated with impaired wound healing, bone fractures, gingival bleeding and inflamed gums (197). Barrios-Garay *et al.* concluded in a recent meta-analysis that vitamin C administration accelerates bone formation and fracture healing in animal models, mainly by modulating the activities of osteoblasts and osteoclasts, however, they found no beneficial effect in human studies (198). Vitamin C supplementation has been shown to improve wound healing upon tooth extraction (199, 200) and may be used to enhance the osseointegration of dental implants (187).

Vitamin D is a steroid hormone, which exists in several forms including D_2 (ergocalciferol) and D_3 (cholecalciferol). 25-hydroxyvitamin-D_3 ($25(OH)D_3$) is its storage form in the body and $1,25(OH)_2D_3$ its active form (201). Vitamin D deficiency has been shown to be associated with impaired fracture healing in animals (202), however, its influence on fracture healing in humans remains controversial (203). Still, it has been suggested to be involved in all stages of fracture healing through its effect on inflammatory cells, cytokines, growth factors, osteoblast, osteoclasts and mineralization (203). Indeed, vitamin D is crucial for bone mineralization through regulation of the body's calcium and phosphate homeostasis (204). Vitamin D deficiency is a risk factor for periodontal disease (205, 206) and may be associated with delayed post-surgical periodontal healing (207).

Vitamin E may improve wound healing and tissue regeneration through its function as an anti-oxidant (208). Vitamin E supplementation improved impaired wound healing in diabetic mice (209) and accelerated gingival wound healing in rats (210). Vitamin E is involved in the regulation of bone remodelling through direct effects on osteoblasts and osteoclasts and orchestration of key signalling pathways of bone resorption and formation (further details can be found in (211)). A higher intake of fruit, vegetables, vitamins A, B, C, E and omega-3 fatty acids was associated with improved healing after non-surgical periodontal therapy (212).

Vitamin K is a fat-soluble vitamin first identified for its role in blood coagulation (213, 214). Two main forms exist: vitamin K1 (phylloquinone) and vitamin K2 (menaquinone) (215). While vitamin K1 is mainly stored in the liver, K2 can be found in tissues all over the body (216, 217). Both Vitamin K and K2 act as a co-factor in the activation of several vitamin K-dependent proteins (218) including coagulation factors and proteins involved in bone mineralization (OC) or inhibition of soft tissue calcification (matrix Gla protein) (219). Vitamin K2 stimulates bone formation by inducing and upregulating the expression of osteogenic genes (220-222), inhibiting osteoblast apoptosis (223) and promoting collagen accumulation via activation of the steroid and xenobiotic receptor (221). In addition, vitamin K2 prevents bone

resorption by inducting osteoclast apoptosis (224), inhibiting the expression of RANKL and stimulating OPG expression (225).

Periodontitis is characterized by inflammatory-driven destruction of periodontal soft and hard tissues (226). Moreover, osteoporosis is associated with disrupted bone remodelling, leading to decreased bone mass and increased fracture risk (227). Research into these diseases and for the development of regenerative therapies has been performed in animal models (228-231). However, animal models are costly, may be too complex, and the responses may vary from those in humans (232, 233). Currently, there is a need for *in vitro* models, allowing the study of single cells as well as co-cultures, to identify cellular and molecular mechanisms involved in the remodelling and repair of soft and hard tissues (234, 235).

2. AIMS AND HYPOTHESES OF THE THESIS

The overall objective of the thesis was to create clinically relevant scaffold-free and scaffold-based 3D *in vitro* models, mimicking the cellular structures in soft and hard tissues, and applying these models to study cellular and molecular mechanisms involved in tissue repair and remodelling. Factors to consider when developing an *in vitro* model include 3D tissue microarchitecture, the inclusion of mechanical stimuli (fluid flow, shear stress, hydrostatic pressure, strain, compression) and appropriate growth factors or stimulatory agents (121, 236-238).

In this thesis, mechanical stimuli in the form of fluid flow-derived shear forces were applied in the scaffold-free and scaffold-based 3D *in vitro* models. It was hypothesized that fluid flow-derived shear forces are needed in both scaffold-free and scaffold-based 3D tissue models to mimic *in vivo* conditions.

Furthermore, vitamin supplementation was applied in the scaffold-free 3D *in vitro* model. It was hypothesized that vitamin supplementation in scaffold-free 3D tissue models can enhance cellular mechanisms involved in remodelling and repair.

The research questions and specific aims were as follows:

1. **Can 3D clinostat spheroids be a model of soft and hard tissues (paper I/II)**?
   Assess the performance of soft and hard tissue cells in 3D spheroids fabricated and cultured in a liquid low-shear stress cell culture system.

2. **Can stimulatory factors added to the medium enhance the regeneration and remodelling of soft and hard tissues in the generated models (paper I/II)?**
   Assess the performance of vitamin D and K2 in 3D spheroids of soft and hard tissue cells.

3. **Will fluid flow-derived shear forces in combination with 3D scaffolds enhance bone regeneration (paper III)? Are there any similarities in cellular/molecular responses from cells exposed to shear forces in scaffolds and in spheroids (paper I/II/III)?**
   Assess the performance/potential of fluid flow in a perfusion flow bioreactor system on bone cells in TiO$_2$ scaffolds.

The experimental strategy used to approach the aims of the thesis and to verify the hypotheses of the research is shown in Figure 5.
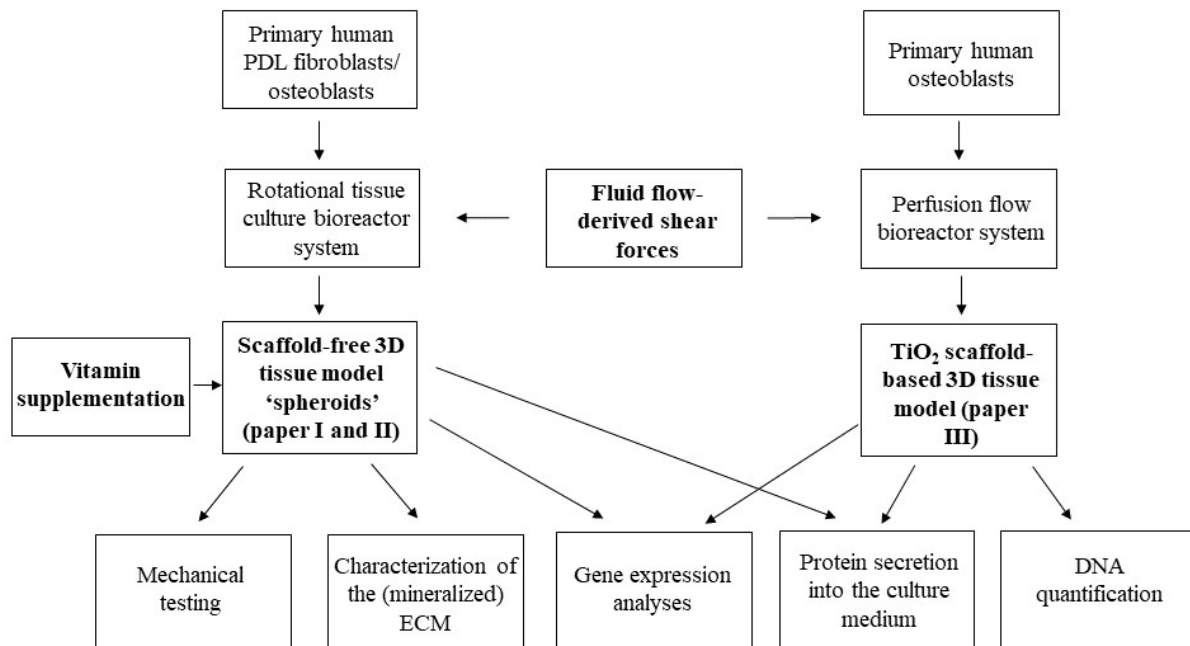
Figure 5. Experimental flow chart illustrating how the aims of the thesis were approached to verify the hypotheses. The numbers of the respective papers are indicated in parentheses.

3. SUMMARY OF RESULTS

Paper I

$25(OH)D_3$ alone and combined with vitamin K2 exert more favorable effects than $1,25(OH)_2D_3$ on markers of bone regeneration in 3D spheroids of human periodontal ligament cells.
Schröder M, Eriksson Agger A, He J, Skallerud BH, Haugen HJ, Syversen U, Reseland JE.

Spheroids of human PDL fibroblasts were generated in a liquid low-shear stress RCCS to mimic the cellular structures within the PDL in a scaffold-free 3D *in vitro* model. To stimulate cellular processes involved in tissue healing, bone remodelling and repair, the culture medium of the spheroids was supplemented with vitamin D (0.1 µM), both its active form, $1,25(OH)_2D_3$, and its precursor metabolite, $25(OH)D_3$, and vitamin K2 (1 µM). $25(OH)D_3$ induced an increase in the secretion of factors involved in inflammation and angiogenesis (interleukin-6 (IL-6) and fibroblast growth factor-2 (FGF-2)), enhanced the secretion of soluble ALP to the culture medium, and inhibited DKK-1 and sclerostin protein release, indicating stimulation of osteogenesis. $1,25(OH)_2D_3$ was less effective in promoting these effects. Vitamin K2 enhanced collagen Type I deposition in the outer rim of the PDL fibroblast spheroids. Moreover, both vitamin D forms exerted additive and synergistic effects in combination with vitamin K2 in the spheroids. The expression of several genes involved in vitamin D metabolism (vitamin D receptor (*VDR*), 1α-hydroxylase (*CYP27B1*) and 24-hydroxylase (*CYP24A1*)) was detected in the spheroids. However, the expression of 1α-hydroxylase was low, which may explain the independent effects of $25(OH)D_3$ in the PDL fibroblast spheroids.

Paper II

Vitamin K2 modulates vitamin D-induced mechanical properties of human 3D bone spheroids *in vitro*.
Schröder M, Aurstad Riksen E, He J, Skallerud BH, Møller ME, Lian AM, Syversen U, Reseland JE. 2020.

Spheroids of primary human osteoblasts were fabricated in a liquid low-shear stress RCCS to mimic the cellular structures and 3D organization within bone. Vitamins D and K2 may have an impact on bone density, remodelling and fracture risk, and were thus assessed in this 3D *in vitro* model of bone. $25(OH)D_3$ enhanced the stiffness and mineral deposition of the bone spheroids and had an effect on the secretion of factors beneficial for bone remodelling and repair (OPG, DKK-1, granulocyte-colony-stimulating factor (G-CSF), ALP, OPN). Vitamin K2

improved the flexibility of the spheroids, altered the distribution of collagen Type I, and elevated the levels of the collagen-associated matrix protein periostin. In addition, vitamin K2 enhanced the expression the RANKL and OPG at the mRNA level and the secretion of DKK-1 and G-CSF, indicating stimulation of cellular processes involved in osteoclastogenesis and bone resorption in the spheroids. The expression of OC and OPN at the mRNA level was stimulated by vitamin K2, and even more so by the combination of vitamins. In addition, the combination induced the same spheroid flexibility as K2 alone, despite an increase in mineralization.

Paper III

Osteoblasts in a perfusion flow bioreactor – tissue engineered constructs of TiO_2 scaffolds and cells for improved clinical performance.
Schroeder M, Reseland JE, Haugen HJ.

3D porous TiO_2 scaffolds were seeded with the mouse pre-osteoblastic cell line MC3T3-E1 or primary human osteoblasts and cultured for 21 days in a perfusion flow bioreactor to induce an *in vivo* 'bone-like' tissue construct. Scaffolds cultured under flow were compared to static controls (no flow). Perfusion flow culture induced an increase in cell growth after 21 days, as indicated by confocal laser scanning microscopy (CLSM) and quantification of DNA content of the constructs. Moreover, perfusion flow culture enhanced the relative mRNA expression of genes associated with the osteoblast phenotype (collagen Type I and OPN) of the cell line osteoblasts, as well as the release of factors beneficial for angiogenesis (monocyte chemoattractant protein-1 (MCP-1) and vascular endothelial growth factor (VEGF)) and bone remodelling (IL-6, interleukin-8 (IL-8), DKK-1, OPG) from primary human osteoblasts after 21 days.

4. DISCUSSION

The implementation of this thesis involved several experimental methods, both well established and new, and there are several challenges and limitations that must be considered before a discussion, of whether the results in this thesis have fulfilled the research objectives and the hypothesis, can be made.

4.1 Methodological considerations

This chapter aims to provide an overview of the applied experimental techniques in this thesis and to discuss their strengths, limitations, and possible alternatives. First the chosen cell cultures and culture techniques to create scaffold-free and scaffold-based 3D *in vitro* models are addressed, then some of the analytical methods, applied to characterize the models, are described. More detailed descriptions of equipment and parameters for each method and technique are available in the individual publications (papers I-III).

4.1.1 Cell cultures and techniques

The aim of paper I and II was to create a clinically relevant scaffold-free 3D *in vitro* model mimicking the cellular structures in soft and hard tissues. Hence, the methodological considerations included cell sourcing, stimulation of tissue-specific ECM production and cellular organization (124). For this approach, primary cell cultures of PDL fibroblasts (paper I) and osteoblasts (paper II) were chosen as the respective cell source for the fabrication of 3D spheroids in a liquid low-shear stress RCCS.

Primary cells are directly cultured from human or animal tissue and hence best resemble the characteristics of the tissue from which they were isolated. Given the right conditions, primary cells are capable of a few cell divisions *in vitro* before they stop dividing or senescence. Moreover, primary cells demonstrate some heterogeneity in culture (239).

In paper I, commercially available primary human PDL fibroblasts, isolated from the ligament that fastens the molars to the jawbone, were used. When culturing PDL fibroblasts, several factors need to be considered regarding the interpretation of study results and the transfer of this data to the clinic (240). Firstly, differences in gene expression and expression levels were observed upon transfer of fibroblasts from the *in vivo* tooth-PDL environment to an *in vitro* setting. These include, among others, reduced expression of ALP, periostin and bone sialoprotein, and selective expression of several growth factors when compared to fresh PDL tissue (241). Since the *in vitro* findings in paper I were not validated in an *in vivo* model, it cannot be ruled out that the aforementioned changes affected the results of paper I. Moreover,

donor-specific factors like age and systemic health status may affect the behaviour of cultured PDL fibroblasts (240), since donor age is associated with the *in vitro* life span (242) and biological activity (243). In paper I, two PDL fibroblast donors, aged 18 and 20 years, both male, were used. In retrospect, a larger selection of donors, spanning different genders and age groups, may have been more physiologically relevant. Stoddart *et al.* recommended to perform *in vitro* experiments using primary human cells with a minimum of three donors (244). Lastly, it is important to also consider tooth-specific-factors (developmental stage, mechanical forces, occlusion) and tooth-health status as effectors of PDL fibroblast behaviour *in vitro* (240).

In paper II, commercially available primary human osteoblasts from two different donors, both aged 32 years, one from the distal femur and one from the tibia, respectively, were used. Several *in vitro* cell culture models are available for bone research, including primary osteoblasts isolated from human donors or other species (*e.g.* mouse, rat, bovine, ovine, rabbit), induced osteoblasts from pluripotent MSCs and osteoblast cell lines (the most studied are MC3T3-E1, SaOs-2, MG-63 and hFOB) (245, 246). The selection of an appropriate and relevant osteoblast *in vitro* model depends on the specific research aim (245). We choose primary human osteoblasts as cell source for fabricating a clinically relevant 3D tissue model mimicking bone (paper II), since these cells most closely resemble the *in vivo* situation in bone and are not influenced by interspecies differences as are primary animal cells or cell lines. In addition, cultured primary human osteoblasts maintain important markers and function (245). However, the cell isolation method, donor age and gender, and skeletal site from which they were extracted, can influence various properties of these cells, including cellular proliferation and the expression of genes and proteins associated with the osteoblast phenotype (247-251).

Spheroids were chosen as scaffold-free 3D *in vitro* model of soft and hard tissues in paper I and II. An advantage of this model is that it does not require the presence of exogenous, foreign materials (122) that could interfere with *e.g.* mechanical testing. However, a limitation is that these spheroids required large cell numbers. This was challenging to achieve in combination with primary cell cultures in paper I and II.

We choose to fabricate and culture the spheroids using the clinostat technology (rotational bioreactor). In this approach, a single cell suspension is placed in a culture chamber (bioreactor), which is then attached to a rotor. Through slow rotation around a horizontal axis the cells are prevented from adhering to the walls of the bioreactor chamber and instead are forced to interact with each other and form aggregates (132, 252). The clinostat method was chosen over other methods to generate and culture spheroids (*e.g.* static plate-based techniques

like low-adhesion plates, trans well culture or hanging drop) since it enables a dynamic culture environment (128). Medium flow around a spheroid reduces the 'oxygen diffusion depleted zone' around constructs with larger radii and assists transporting nutrients to and waste products from the spheroid (148). In addition, the bioreactor technology allows for readily controllable culture conditions (*e.g.* easy access to change the culture medium). These factors make it possible to obtain bigger spheroids with significantly higher biomass and establish long-term cultures (128, 132). An advantage of the bigger spheroids was that all analyses in paper I and II (mechanical testing, histology, gene expression analysis) could be done on the same sample, minimizing experimental variation. Moreover, another advantage of the rotary bioreactor is that it provides very low shear stress to the cells (estimated as ca. 0.01 Pa at 20 rpm for constructs in suspension ('free-fall') in a theoretical model (253)). However, there are also drawbacks to the use of rotary bioreactors. Special equipment and a trained experimenter are needed, in contrast to plate-based approaches or gel embedding, to generate 3D spheroids. These other techniques may be simpler and more cost-effective to implement and allow for an easy transition from 2D to 3D experiments (128, 132). Another issue is that the spheroid size, geometry and distribution in rotary bioreactor systems is not controllable (when injecting a single cell suspension) (132). This was also observed for the spheroids in paper I and II. In these papers, spheroids treated with vitamins were compared to a control group and among each other. Upon consideration, low-adhesion plates might have generated a more homogenous representative spheroid population (132) for the vitamin testing.

The clinostat bioreactor system from the company CelVivo was chosen as rotational culture system in this thesis (Figure 6) (254). The system is an adaption of the RCCS designed by

Figure 6. Rotary cell culture system from CelVivo used to produce spheroids (255).

NASA in 1992 (256). The advantages of the CelVivo system are that the culture vessel is equipped with a humidification chamber, which prevents dehydration of the cells during incubation. Hence, the culture conditions are more stable. Also, the closure mechanism of the

CelVivo system is specially designed to prevent the occurrence of air bubbles, which are typically seen in the NASA RCCS, and can potentially damage the spheroids. Lastly, the culture vessel of the CelVivo system provides easy access to the samples since it can be opened like a petri dish (257).

The fabrication and culture conditions (number of cells initially seeded, rotation speed of the vessel) to obtain stable spheroids of primary human osteoblasts and/or co-cultures of osteoblasts and osteoclasts have been previously described for the NASA RCCS (258, 259). However, adaptions in the rotation speed and culture mode of the spheroids (lower rotation speed, formation and culture of the spheroids at the bottom of the culture vessel instead of in free fall like in the NASA RCCS (258)) had to be made in the CelVivo RCCS. Moreover, the culture conditions had to be further modified for the culture of the PDL fibroblasts in the CelVivo RCCS (shorter overall cultivation time of the PDL fibroblast spheroids in the RCCS compared to the osteoblast spheroids, details in paper I).

Paper III aimed to create a scaffold-based 3D tissue model mimicking the dynamic 3D environment within bone. 3D porous TiO_2 scaffolds were combined with a perfusion flow bioreactor system. In addition to primary human osteoblasts, the mouse pre-osteoblastic cell line MC3T3-E1 was chosen as an osteoblast model system in this paper. In contrast to primary cultures, immortalized or finite cell lines have been modified to proliferate indefinitely or can be continually passaged before senescence, respectively. Cell lines are easy to culture and demonstrate phenotypic stability even with increasing passage numbers, resulting in higher reproducibility of results. However, the characteristics of the original tissue are less closely represented (260, 261). The MC3T3-E1 cell line, derived from primary cells of newborn mouse calvaria (262), is an established bone cell model for mechano-transduction research (263-265) and is frequently used in cell-material interaction studies (245). Furthermore, the cells have been shown to undergo a similar temporal developmental sequence of proliferation and differentiation as during *in vivo* bone formation (266). This makes them an interesting and alternative *in vitro* bone cell model for bone formation and remodelling in relation to primary human osteoblasts (245).

A perfusion flow bioreactor system was chosen in paper III to provide fluid flow-derived shear forces to osteoblasts seeded on porous TiO_2 scaffolds. Details on the design and experimental set-up of the flow bioreactor system are given in Figure 7a-c.

The inlet velocity in paper III was applied as suggested in Zhang *et al.*'s in silico modelling (34 μm/s) (267), corresponding to a flow rate of 0.16 ml/min. Moreover, a lower inlet velocity

(17 μm/s), corresponding to a flow rate of 0.08 ml/min, was also tested. However, pilot studies demonstrated no effect of the perfusion flow bioreactor system on growth, distribution, and differentiation of osteoblasts, compared to constructs cultured in well-plates (no flow). Bancroft *et al.* (268) proposed that one of the requirements for a successful flow perfusion system is to deliver the flow through the scaffolds, minimizing the nonperfusion flow around the cultured constructs. Jansen *et al.* (269) proposed a perfusion chamber containing a basket with a perforated lid and bottom placed in the fluid pathway to ensure that the culture medium was evenly distributed over the surface and within the constructs (270). We implemented this concept for our perfusion flow bioreactor by placing a grid in front of the fluid pathway of each porous TiO$_2$ scaffold.
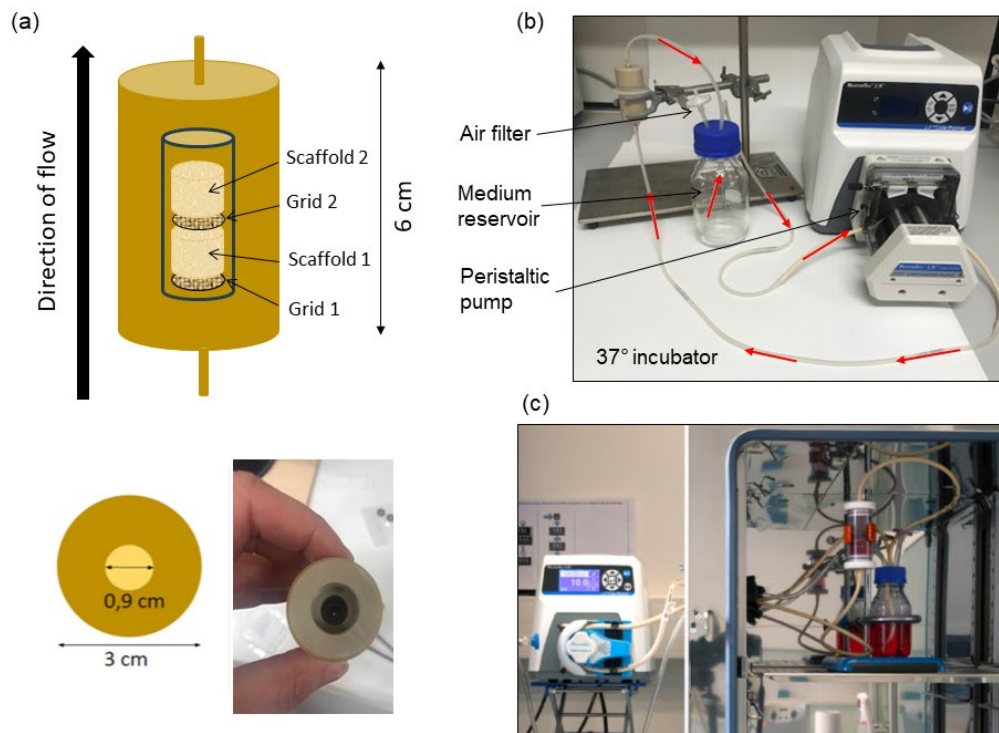
Figure 7. Design and experimental set-up of the flow bioreactor system. (a) Tubular perfusion chamber (height: 6 cm, diameter: 3 cm) that could house up to two porous TiO$_2$ scaffolds (height: 8 mm, diameter: 9 mm) in a loose fit. The chamber contained a single flow inlet at the bottom and a flow outlet at the top. A tubular perfusion chamber with an individual tubing circuit for each chamber was chosen over a block or round perfusion chamber with multiple scaffold chambers feed by one tubing circuit (for review of such systems please see (270)) to avoid an inhomogeneous flow distribution between the scaffold chambers. A round grid (diameter: 0.9 cm; hole diameter: 0.1 cm) was placed in front of each scaffold to ensure a homogenous distribution of flow through the porous construct. (b) The system was designed as closed loop system (recirculating culture medium). A peristaltic pump generated the medium flow from the reservoir to the bottom inlet of the perfusion chamber, exiting through the hole in upper part of the chamber and back to the reservoir (indicated by red arrows). (c) Tubular flow bioreactor system by Chabanon (271) which served as the inspiration for the design of the applied flow bioreactor system in this thesis.

Prior to culture in the perfusion flow bioreactor system, a static pre-culture time of 24h was implemented to ensure sufficient cellular attachment. In most experimental studies, bioreactor culture is initiated within 24-72 h after static pre-culture (272-274). In retrospect, direct seeding of the scaffolds with the cells in the perfusion bioreactor system, as demonstrated by others (269, 275, 276), would have made the approach more clinically relevant (270).

Besides perfusion bioreactors, other systems exist which can provide fluid flow-derived shear forces in combination with 3D porous bone scaffolds. These include spinner flasks (Figure 8a), rotating wall vessels (RWVs) (Figure 8b) and biaxial rotating (BXR) bioreactors (Figure 8c) (277-279).

In spinner flasks, scaffolds are anchored to the cap of the culture chamber and continuous stirring of the medium ensures efficient mixing at the construct surface, which may furthermore enhance the nutrient transport into the pores (280, 281). However, mixing of the medium causes turbulent shear forces at the surface of the scaffolds (280, 282), which have been shown to be detrimental for cell growth and ECM/tissue formation (279, 283).

In contrast to spinner flask, scaffolds or microcarriers in RWV bioreactors are usually free-floating in the culture medium, which is achieved by horizontal rotation of the culture vessel at a certain speed (281, 284). However, a limitation of this approach comes from random collisions of the 3D constructs with the vessel wall as these tumble during culture in the RWV. This phenomenon is driven by density differences between the culture medium and the constructs and can be detrimental for cell growth and tissue formation (283, 285). During our studies, pilot experiments, using TiO_2 scaffolds (2 mm x 2 mm) in the CelVivo RCCS, were conducted using a rotation speed of 60-70 rpm to keep the scaffolds in suspension. This approach resulted in large cell detachment from the scaffolds, possibly due to the turbulence and shear stress generated by the high rotation speed (data not shown here). We also tested a lower rotation speed (0.3–3 rpm). In this approach, the scaffolds were kept at the bottom edge of the culture vessel. However, no observable improvement of this approach was discerned (data not shown).

The fourth system, the BXR bioreactor combines the features of RWVs and perfusion bioreactors. In this approach, the scaffolds are fixated in the culture chamber which rotates in two perpendicular axes simultaneously, generating a more homogenous medium flow than with uni-axial rotation. Moreover, the integrated perfusion system provides circulation of the medium between the culture chamber and the reservoir, leading to enhanced mass transport at low shear stress (279, 286) The BXR bioreactor would have been interesting to test in

combination with our scaffolds and osteoblasts, however, the equipment was not available at the laboratory.
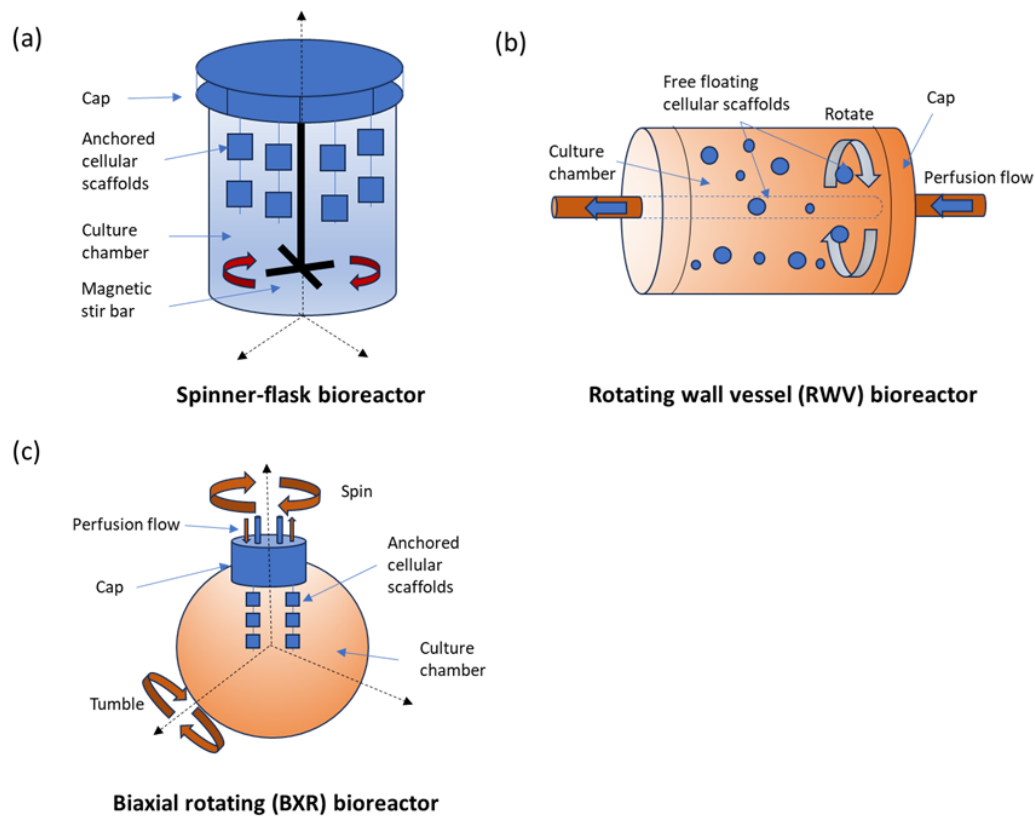
Figure 8. Bioreactor systems that can provide fluid flow-derived shear forces in combination with porous scaffolds. (a) Spinner flask bioreactor. (b) Rotating wall vessel bioreactor. (c) Biaxial rotating bioreactor. Figure adapted from (279).

4.1.2 Analytical methods

4.1.2.1 Mechanical testing

Spheroids of PDL fibroblasts (paper I) and osteoblasts (paper II) were subjected to mechanical testing by nano-indentation. Before testing, the methodological considerations concerned the storage and preservation of the samples without altering their mechanical properties. Bone samples are usually either placed in a fixative for preservation or frozen until mechanical testing is performed (287, 288). Vesper *et al.* proposed that bone samples should be stored frozen and hydrated to preserve their mechanical properties. They also concluded that long-term ethanol storage should be avoided as it increases samples stiffness (288). The freezing of soft tissue samples (*e.g.* ligaments) in combination with mechanical testing is controversial in the literature (289, 290). Hence, PDL fibroblast spheroids were stored in 70% ethanol and spheroids of human osteoblasts were kept in phosphate buffered saline at -80°C until the mechanical testing.

Before testing, spheroids were thawed overnight and then allowed to dry for 24-48 hours at room temperature. However, drying has been reported to increase the hardness of bone samples (291, 292). Nano-indentation, using a Hysitron TriboIndenter nanomechanical test instrument, was used to characterize the mechanical properties of the spheroids. Nano-indentation is a well-established method for determining the mechanical properties of bone at the tissue level (293-295). During conventional nano-indentation, a sharp intender is employed to penetrate a flat surface and the indentation load and displacement are recorded simultaneously (296). In paper I and II, a modified version of this approach, a so-called nano-indentation-based flat punch method, using a diamond flat punch instead of a sharp intender (297), was applied to cope with the irregular geometry of the spheroids. With this approach, the deformation measurement accuracy was ± 0.1 nm for displacement and ± 1 μN for force. However, with the test protocol employed in our studies (details in paper II), the measured magnitudes were significantly greater than these variations estimates, resulting in any potential measurement inaccuracies as to be negligible.

Notably, the data in paper I and II demonstrates that nano-indentation, using the flat punch approach, seems suitable as method to verify the effects of the different vitamin treatments on the mechanical properties of the spheroids, however, it can be questioned whether the method is suitable to verify the spheroid model against biology. The young's modulus of the human PDL *e.g.* has been found to vary upon several orders of magnitude (ranging from 0.01-1750 MPa) depending on the method/approach (experimental, *in vivo*, *in vitro*, finite element analysis) applied to measure it (298). The stiffness of the PDL fibroblast spheroids in paper I was found to range between 29.9 – 12.4 MPa, considerably higher than the stiffness of the osteoblast spheroids in paper II. As mentioned before, the prolonged storage of the PDL fibroblast spheroids in 70% ethanol may have contributed to their increased stiffness. On the other hand, it can be questioned, if we can expect the stiffness of the PDL fibroblast spheroids to match those of human PDL or bone. As elaborated before, the mechanical properties of the PDL are determined by the interaction of the viscose fluid phase with the 3D fibrous collagen network, in which also other cells, nerves and blood vessels are integrated (13-15). This is not represented in our PDL fibroblast spheroid model which consists of one cell type only, which is embedded in a self-generated ECM.

4.1.2.2 Gene expression analyses

Reverse transcription quantitative polymerase chain reaction (RT-qPCR), using messenger RNA (mRNA) (paper I/II) or total RNA (paper III), was used to analyse cellular gene expression profiles in this thesis. The technique is based on the reverse transcription of RNA into complementary DNA (cDNA), amplification of the cDNA by PCR, and detection and measurement of the PCR products in real-time (299, 300). mRNA for RT-qPCR was isolated directly from cell lysates of PDL fibroblast- and osteoblast spheroids using magnetic beads. This method relies upon the fact that eukaryotic mRNA can be separated from other cellular RNA via its poly-adenosine tail at the 3'-termini, which hybridizes with short chains of poly-thymidine nucleotides that are coupled to the beads (301). In contrast, total RNA was isolated in paper III using guanidinium-thiocyanate-phenol extraction (302) since direct mRNA isolation was unsuccessful. An advantage of this method is that it results in high yields (303), however, it requires handling of hazardous chemicals such as chloroform and phenol (302). Another disadvantage is that residual phenol may interfere with RT-qPCR (304). Moreover, higher sensitivity of detection may be achieved using mRNA as template for reverse transcription (305).

In paper I, RT-qPCR was used to clarify the differential effects of the two vitamin D forms $25(OH)D_3$ and $1,25(OH)_2D_3$ in the PDL fibroblast spheroids by analysing the expression level of 1α-hydroxylase, converting $25(OH)D_3$ to $1,25(OH)_2D_3$ (201), and of the endocytotic receptors cubilin and megalin, controlling cellular uptake of $25(OH)D_3$ (306, 307). In paper II, genes related to the mineralized ECM, osteoblast phenotype and bone metabolism (collagen type I alpha I (*COL1A1*), periostin (*POSTN*), alkaline phosphatase (*ALPL*), osteocalcin (*BGLAP*), osteopontin (*SPP1*), *OPG*, *RANKL* were accessed (308) to understand the impact of vitamin supplementation on the mechanical and biological properties of the osteoblast spheroids. The gene expression analyses in paper II were complemented by determining the spheroid's protein levels in the culture medium (chapter 4.1.2.3) and by immunofluorescence (chapter 4.1.2.4) since RT-qPCR data relates to cellular mRNA levels at a given timepoint, however, not to the biological consequences (protein levels) as the half-lives of transcripts and their resultant proteins can often be significantly different (299).

It is worth noting that the spheroids were processed (lysed) as one sample for the gene expression analysis. However, unlike 2D cultures, spheroids do not have a homogenous cell population (309) and may comprise cells at different stages, depending on their location within the spheroid (147, 310). Spatial transcriptomics has emerged as new technique to assess gene transcription while retaining the positional information in a tissue section (for review see (311)).

This approach could have given a more complete picture of the gene expression levels of the whole spheroid population in paper I and II.

Finally, RT-qPCR was also used in paper III to detect changes in osteoblast marker gene expression (*COL1A1*, *ALPL*, *BSP*, *SPP1*, *BGLAP*, *osterix/sp7*) (44, 308) on TiO2 scaffolds induced by the fluid flow, as this would indicate a beneficial effect on bone regeneration.

4.1.2.3 Detection of proteins in the culture medium - Multiplex bead array assay and colorimetric alkaline phosphatase activity

Multiplex bead array assay (MBAA), using the Luminex multi-analyte profiling (xMAP) technology (312, 313), was used in papers I-III to measure the secretion of bone-related proteins and cytokines/chemokines into the culture medium. The assay is based on fluorescent beads (internally dyed to a mixture gradient of red and infrared fluorescence dyes) which are coupled to a capture antibody specific for a potential analyte in the sample. Upon mixing of the sample and beads, the sample analytes bind to their respective capture antibodies, then a fluorescent reporter antibody is added. Subsequently, the beads are injected into a flow chamber which allows one bead at a time to flow through. There the beads and fluorescent dye on the reporter antibody are excited with a red and green laser, upon which they emit light at a specific wavelength, allowing the microsphere set and analyte of interest to be identified and the binding event to be quantified, respectively (313). MBAAs were developed from the traditional enzyme-linked immunoassay (ELISA), which uses enzyme amplification of a colourimetric substrate as a reporter system instead of fluorescence (314). Both assays demonstrate good correlation and similar quantitative values when the same capture and reporting antibody pair is used (314). The MBAA technology enables the parallel quantification of multiple different analytes within the same sample at a small sample size. This is a clear advantage over ELISA assays (313). However, individual analytes with very low or high concentration in the sample may fall out of the dynamic range of the MBAA. Another concern with multiplex immunoassays is the matrix effect, leading to cross-reactivity of antibodies (304, 314).

In paper I, MBAA was used to analyse if vitamins D and K2 may have a beneficial effect on the secretion of factors involved in tissue healing/repair of tissues like the PDL and bone from PDL fibroblast spheroids. Likewise, the effect of vitamin supplementation on the secretion of proteins involved in the mechanical and biological function of bone from osteoblast spheroids was investigated using MBAA in paper II. Prior to analysis, two-thirds of the culture medium was removed from the rotational bioreactors housing the spheroids, then an aliquot of 25 µl was applied in the MBAA. Notably, the protein secretion from the spheroids stems from the cells

residing in the outer proliferating rim of the spheroids only. Hence, the MBAA results are not representative of the whole spheroid cell population. In addition, some factors might not be secreted but rather be trapped within the spheroids (*e.g.* the concentration of osteocalcin in the culture medium was below the detection limit of the standard curve in papers I and II). Measuring the protein concentrations in lysates of the spheroids would have given a more complete picture. Also, immunoblotting of lysates could have been performed to detect specific proteins within the spheroids. However, although immunoblotting is sensitive enough to detect even very low protein concentrations in samples, it only represents a semi-quantitative approach (315).

In paper III, MBAA was used to analyze if fluid flow-derived shear forces may have an effect on the secretion of proteins involved in bone remodeling/repair from osteoblasts on TiO$_2$ scaffolds. A limitation of this approach was that the culture medium volume of the scaffolds cultured under flow was much larger (200 ml) compared to scaffolds cultured without flow (500 µl), resulting in a more diluted protein concentration. To compensate for this, the medium of the dynamic scaffolds was concentrated using centrifugal filters with 3 kDa cut off.

The secretion of soluble ALP to the culture medium of the PDL fibroblast and osteoblast spheroids (paper I/II) was measured using a colourimetric assay based on the hydrolysis of p-nitrophenyl phosphate. ALP is an ectoenzyme which is covalently bound to the outer side of the cell membrane by a glycan-phosphatidylinositol anchor. It can be released in a membrane-bound and soluble form (316, 317). The tissue-nonspecific isozyme is strongly expressed in bone, liver and kidney and is suggested to be involved in bone calcification (318, 319). ALP catalyses the hydrolysis of the chromogenic substrate p-nitrophenyl phosphate to p-nitrophenol, which's absorbance can be measured spectrophotometrically at a wavelength of 405 nm (320).

4.1.2.4 Histology, immunofluorescence and confocal laser scanning microscopy

Spheroid sections for histology, immunofluorescence and CLSM (paper I/II) were prepared following the protocol of Kusumbe *et al.* for high-resolution 3D imaging of skeletal tissue sections (321) with some modifications. In brief, the samples were fixated, cryoprotected, embedded in frozen sectioning medium, snap frozen in liquid nitrogen, and sectioned at a thickness of 10 µm using a cryotome. Due to the low level of mineralization in the spheroids, decalcification was not performed. Frozen sections were chosen over paraffin sections for this sample type since paraffin embedding of tissues may destroy antigen binding sites. On the other hand, cryo-sectioning has been reported to compromise cell- and tissue morphology (322). Nevertheless, frozen spheroid sections demonstrated good antigenicity, preservation of cellular

structures and sample integrity, and were applicable for both histology and confocal microscopy.

One of the aims of both papers I and II was to characterize the (mineralized) ECM in the spheroids. First, primary antibodies against Type I collagen and periostin were applied in standard immunofluorescence staining protocols and sections were imaged by CLSM. Both PDL fibroblasts and osteoblasts in spheroids expressed Type I collagen and periostin. Interestingly, the expression of these proteins partially overlapped. As reported in the literature, periostin can form a complex with Type I collagen (78), although its binding site on collagens has not yet been identified (323). Still, it is worth nothing that co-localization or assembly of the two proteins could have mask some of the antibody-binding epitopes (324) in the spheroid sections, giving false negative staining results.

Since the PDL appears to have a distinct 3D collagen architecture (1, 8), frozen section of PDL fibroblast spheroids were in addition to staining with an antibody against Type I collagen also stained with a collagen hybridization peptide (5-FAM conjugate, 3Helix), which detects unorganized (not organized into the collagen triple helix, actively remodelled) collagen (325, 326). However, these experiments are not enough to conclude whether the complex 3D network of collagen fibres within the PDL was recapitulated in the spheroid model. Transmission electron microscopy could have been applied to further characterise the collagen matrix (*e.g.* collagen fibre orientation, maturation of collagen) in the PDL fibroblast spheroids. This method was previously established on spheroid sections of primary human osteoblasts by Munir *et al.* (327).

CLSM was used in both papers I and II since it is capable of high-resolution imaging of samples. In contrast to conventional fluorescence microscopy, CLMS isolates and collects light only from the focal plane within a sample, rejecting out-of-focus light from the detector and hence reducing blur which may affect image resolution (328).

Von Kossa (329) and Goldner's trichrome staining (330) were used to evaluate mineral deposition within PDL fibroblast and osteoblast spheroid sections, respectively. Von Kossa reacts with the anionic portion of phosphates and carbonates of calcium salts (329). It is based on incubation of tissue sections with a silver nitrate solution in the presence of strong or ultraviolet light. Calcium depositions in the sample are then reduced and replaced with black or brown silver depositions (331). This method was applied in paper I to investigate if the culture conditions in the RCCS could promote the osteoblast-like properties of the PDL fibroblasts with regard to inducing differentiation and the deposition of mineralized nodules. However, without the presence of osteogenic inducers in the culture medium, mineralization

within PDL fibroblast spheroids did not occur within 14 days of culture in the RCCS. It is possible that mineralisation was delayed in this system and might have occurred later. Alizarin Red S, which binds to calcium salts and forms a chelate (332), could have been used as an alternative stain to visualize mineral deposits. However, the staining resulted in an orange-red background even in the negative control and was hence not applied. In paper II, Goldner's trichrome staining (330) was applied to analyse the presence and distribution of mineralized and not yet mineralized bone matrix (osteoid) with embedded osteoblasts within the spheroids. This was valuable information with regard to the mechanical properties of the bone spheroids. Goldner's trichrome staining is recognized as an excellent stain for undecalcified bone due to the fine differentiation between mature, mineralized bone matrix, stained green, and the immature, new bone matrix (osteoid), stained red. Furthermore, the stain provides good visualization of osteoblasts through the haematoxylin component, which stains the cell nuclei blue/black (333). Goldner's trichrome staining of osteospheres was found to vary along the spheroid sections with the peripheral staining being much stronger. This may be explained in part by diffusion limitations as the spheroids had large (~ 2 mm) diameters (paper II).

To obtain confirmatory data on mineral and osteoid (collagen) localization in the bone spheroids, we co-stained sections with a collagen type I antibody and the calcium-chelating fluorophore xylenol-orange, previously applied to visualized mineralized nodules in primary calvarial osteoblast cultures (334). However, the two staining procedures were not compatible, most likely because the chelating effect of xylenol-orange is highly dependent on the pH (335). Another aim in paper II was to determine the nature of the mineral depositions in the bone spheroids by applying a fluorescent osteoImaging staining reagent (Lonza), which specifically binds to hydroxyapatite. However, the staining could not be verified reliably in consecutive sections. In 3D spheroids, several layers of (mineralized) ECM might be present. Hence, this type of sample might not be optimal to image low levels of mineralization. More advanced techniques such as scanning electron microscopy in combination with energy-dispersive X-ray spectroscopy could have been applied to determine the nature of the mineral in the osteospheres (for details please see (156)).

4.1.2.5 Determination of cell number (DNA quantification) of TiO$_2$ scaffolds

To determine the effect of the perfusion flow bioreactor system on cellular growth of osteoblasts on TiO$_2$ scaffolds in paper III, the concentration of double-stranded DNA (dsDNA) was measured using PicoGreen. The dye exhibits low fluorescence in an unbound state and becomes highly fluorescent by intercalating into the bases of DNA (336, 337). The resulting fluorescence

emission was then measured with a Qubit fluorometer, which converts it into dsDNA concentration referring to DNA standards of known concentration. A clear advantage of this method to determine the concentration of dsDNA in samples is that it is highly specific and not influenced by contaminants like detergents, salts or protein (338). The standard method for measuring the concentration of nuclei acids is UV-absorbance using a spectrophotometer. In this method, light at 260 nm is passed through the sample, is absorbed by the DNA, and detected, however it is not specific for dsDNA. Determining the 260/280 nm and 260/230 nm ratio, the purity of DNA can be defined (339, 340). The accuracy of fluorometric methods and UV absorbance spectroscopy for DNA quantification is discussed in the literature (reviewed in (340)) and a combination of both methods may be recommended for obtaining reliable results (340).

4.2 Discussion of results

This thesis aimed at developing clinically relevant scaffold-free and scaffold-based 3D *in vitro* models, mimicking the cellular structures in soft and hard tissues, and at applying these models to study cellular and molecular mechanism involved in tissue repair and remodelling. In recent years, 3D cell models mimicking tissue structures have emerged as valuable tools to bridge the gap between 2D monolayer cultures and animal models (341). Knowledge of cellular responses and mechanisms in these models may gain insights into disease mechanisms of *e.g.* infectious- and developmental diseases as well as tumours, and promote the development of innovative diagnostics and therapies (342, 343).

4.2.1 Scaffold-free and scaffold-based 3D *in vitro* models mimicking the cellular structures in soft and hard tissues and the effect of fluid flow

In tissues, cells are naturally surrounded by other cells and interact with the ECM in a 3D spatial arrangement (117). ECM and tissue architecture have a profound effect on cell-cell communication and how cells respond to signals from the microenvironment (344-346). Scaffold-free 3D cell cultures in which the cells form aggregates or spheroids, recapitulate the native tissue architecture, promote cell-cell interactions and the formation of a self-assembled ECM (347). In paper I, 3D spheroids of human PDL fibroblasts were fabricated in a liquid low shear stress RCCS to mimic the cellular structures in oral soft tissues like the PDL. PDL fibroblasts in the spheroids expressed periostin and collagen Type I and secreted cytokines and bone-related proteins into the culture medium. Interestingly, a rim of collagen type I-positive cells was observed around the constructs, indicating actively proliferating and/or remodelling cells in this area (348, 349). An increased level of fluid flow-derived shear forces at the surface of the spheroids, present during culture in the RCCS, which is absent from the inside, may have induce this layer-like organization of the cells within the generated spheroids (162). This gradient may have furthermore induced a remodelling stimulus in the outer area of the spheroids (162), explaining the increase in collagen Type I deposition by the cells. Yang *et al.* further characterized the PDL fibroblast model and confirmed the presence of organized cellular structures within the spheroids. They also analysed the gene expression within the PDL fibroblast spheroids and detected the expression of several matrix metalloproteinases, indicating active remodelling of the ECM within the constructs (350).

Our generated PDL fibroblast model has some limitations. First of all, during culture in the RCCS, only fluid flow-derived shear forces are present as mechanical stimuli, while other

stimuli such as strain, tension or compression, or combinations of these, which may affect PDL fibroblasts and other cells of the periodontium *in vivo* (351) are not considered.

Mathes *et al.* created a 3D *in vitro* model applying gingival fibroblasts, collagen sponges, shear forces or/and pressure via a bioreactor system to study oral soft tissue healing (352). They observed a rise in collagen Type I secretion from cultures exposed to fluid flow-derived shear stress in the bioreactor system as compared to static cultures. However, increased tenasin-c expression, indicating active remodelling of the ECM by the fibroblasts, was only observed when pressure forces were applied as well. Mathes *et al.* concluded that both stimuli were needed in the *in vitro* model to mimic the clinical situation during soft tissue healing (352).

In addition, our model only focused on PDL fibroblasts and did not consider the cellular crosstalk *e.g.* between MSCs and endothelial cells or the presence of vascularization, which are both essential components for periodontal regeneration (353). Sano *et al.* created 3D spheroids in micro-well chips using co-cultures of human PDL MSCs and endothelial cells. They found that paracrine-derived factors like VEGF, produced by the endothelial cells, influenced the regenerative potential of the PDL MSCs in the spheroids (354). Moreover, Pandula *et al.* fabricated 3D cell-sheets from PDL stem cells and endothelial cells and observed vascular network initiation within the constructs (355), another component which is lacking in our model.

Notably, although the organized 3D network of collagen fibres may not be recapitulated in our PDL fibroblast spheroid model, the characteristic production of ECM components and protein secretion of our tissue model may be used as measurable markers to test the effect of drugs or other therapeutic interventions targeting *e.g.* periodontitis or bone regeneration. The composition and mechanical properties of the ECM play a key role in determining cellular behaviour, controlling tissue homeostasis and the response to drugs (349, 356-358). Cell-ECM interactions, mediated by integrins, have been shown to have a profound effect on cellular drug response (359, 360). Dynamic changes in ECM composition, structure or stiffness may contribute to disease development and progression (349).

The culture of PDL fibroblasts in spheroids stimulated the cells to form their own ECM in which they became entrapped (paper I). The ECM of the human PDL is made up of several different types of collagens, proteoglycans (*e.g.* decorin, lumican, fibromodulin and versican) and glycoproteins (*e.g.* fibronectin, tenascin and periostin) (361, 362). In addition, a large amount of collagen/ECM modifying proteins/enzymes (*e.g.* matrix metalloproteinases, prolyl-hydroxylase, collagenases) can be found in the PDL (363). Remodeling of the PDL is essential to maintain tissue homeostasis, however, excessive matrix breakdown, indicated by high

expression of matrix metalloproteinases, tissue inhibitors of matrix metalloproteinases or other collagen catabolic enzymes, may be associated with the progression of periodontitis (364). Hence, targets for drug responses or diseases progression in our PDL fibroblast spheroid model may be changes in these ECM components, in ECM remodelling or in the integrin-mediated signalling. In addition, the gene expression and protein secretion (markers of inflammation, angiogenesis, bone regeneration and the RANKL/OPG ratio) in the PDL spheroid model could be used as markers to assess the effect of a drug or therapeutic intervention on periodontal/bone regeneration (discussed in detail in paper I).

In paper II and III, we aimed to mimic the dynamic 3D bone microenvironment with primary human osteoblasts in a scaffold-free model (RCCS spheroids) and in a scaffold-based approach in combination with a perfusion flow bioreactor, respectively. Primary human osteoblasts appeared organized within the 3D spheroids, with osteoblasts entrapped within osteoid in the spheroids' outer rim and osteoblasts (or may be even osteocytes) embedded within mineralized matrix in the spheroids' inner area (paper II). This is in line with studies from Clarke *et al.* and Penolazzi *et al.* which co-cultured primary human osteoblasts and osteoclasts in spheroids and observed that the cells underwent spatial organization within the constructs in response to the fluid flow-induced shear forces generated during culture in the RCCS (162, 163). Notably, the 3D bone model of Clarke *et al.* (162) closely resembles the cellular structures and organization within bone, with a central mineralized core which contains osteocytes embedded into trabecula-like structures, and a distinct zone surrounding the core containing active osteoblasts and osteoclasts, as indicative by OC and tartrate-resistant acid phosphatase (TRAP) expression, respectively. A clear advantage of this model is that it allows for the study of the bone remodelling/repair process, as well as the effect of various drugs or stimuli on these processes, without the inclusion of any scaffolding material that may interfere with unravelling the actual sequence of cellular events during remodelling/repair (235).

Moreover, a recent study by Munir *et al.* demonstrated some correlation between the maturation of the mineralized collagen matrix and the development of different cellular structures and phenotypes in spheroids of primary human osteoblasts cultured in an RCCS (327). 21-day-old osteospheres grown in the presence of vitamin A, C and D exhibited areas with bone-like structures containing embedded cells in collagen-rich matrix next to the rim of the constructs. Densely packed, organized collagen fibrils along with needle shaped mineral crystals were observed within these structures. In addition, adjacent to the bone-like structures, areas of loosely organized (less mature) collagen were identified. Transmission electron microscopy

indicated that the cells within the dense, more mature collagen seem to be morphologically more osteocyte-like cells, as shown by the presence of stellate shaped cells with extensions radiating from the cell body, than within the loose collagen. Immunostaining using early and late osteocyte markers demonstrated also more osteocyte-like cells surrounded by mature collagen within the center of the spheroids (327).

It is worth noting that the inclusion of other cells, including those of the vascular network, may have further influenced the development of our osteospheres. The interaction of osteoblasts with endothelial cells may promote the formation of the mineralized bone matrix in the osteospheres (365). Furthermore, the coculture of osteoblasts, microvascular endothelial cells and fibroblasts may increase cell viability and proliferation and promote the formation of intrinsic microvascular networks within the osteospheres (366).

Previously, several studies have fabricated 3D co-culture models of osteoblasts and osteoclasts in combination with scaffolds to study bone remodelling/repair and/or the effect of drugs targeting bone-related diseases (164, 367-370). Taking this approach one step further, Papadimitropoulos *et al.* (371) generated a dynamic 3D *in vitro* model of the bone microenvironment by co-culturing human adipose tissue-derived stromal vascular fraction cells, able to commit to the osteoblastic and endothelial lineage, with human monocytes on porous hydroxyapatite/beta-tricalcium phosphate ceramic scaffolds in a perfusion bioreactor. After 21 days, the scaffolds contained mesenchymal, osteoblastic, osteoclastic and endothelial cells in association with bone-like matrix deposition and resorption, potentially enabling the study of drugs targeting bone homeostasis or the remodelling capacity of bone substitutes (371). Moreover, Beskardes *et al.* (275) co-cultured human MSC-derived osteoblasts and THP-1 (human acute monocytic leukemia cell line)-derived osteoclasts on chitosan-hydroxyapatite superporous hydrogels in a perfusion flow bioreactor under bidirectional flow. They detected increased gene expression of osteoblast and osteoclast markers (ALP, bone-sialoprotein, collagen Type I, osteonectin, TRAP) and ECM deposition in the model in response to the fluid flow-derived mechanical stimuli, which may indicate an enhanced bone regeneration potential of the engineered constructs. (372). Although our scaffold-based 3D bone model just contained osteoblasts, we observed an increase in the expression of genes associated with the osteoblast phenotype (collagen Type I and OPN) and the release of factors beneficial for angiogenesis (MCP-1 and VEGF) and bone remodelling (IL-6, IL-8, DKK-1, OPG) by the fluid flow-derived shear forces in the perfusion bioreactor system (paper III), which is in line with the study from Beskardes *et al.* (372).

It is worth noting that we observed differences in the cellular responses from cells exposed to fluid flow-derived shear forces in scaffolds compared to RCCS spheroids. As mentioned earlier, the shear forces in the RCCS mainly work on the outside of the spheroids (162), while in the perfusion flow bioreactor the medium is directly perfused through the porous scaffolds and all cells experience the wall shear stress (279). In the scaffold-based model, the fluid flow-derived shear forces (or the convection) enhanced cellular growth (paper III). We did not analyse cellular growth in the spheroid models; however, it can be assumed that the growth is much slowed down as cells in a 3D 'tissue like' environment usually reach a dynamic equilibrium (119). Moreover, in both models we observed an increase in cellular differentiation by the fluid flow. The simulation by Zhang *et al*. demonstrated a homogenous distribution of fluid flow-derived shear forces within the porous TiO_2 scaffolds (267), indicating that all cells might undergo differentiation within the scaffold-based model. However, this simulation was conducted in the absence of cells, which may change the pore diameters of the scaffolds upon proliferation and hence might induce a gradient of shear forces at some point during culture. Another factor to consider is the influence of the grid that was placed in front of the fluid path of the bioreactor to ensure a homogenous distribution of the flow through the scaffolds. The effect of the grid on the distribution of flow within the scaffolds needs to be clarified in further studies. In contrast, only a subset of cells might undergo differentiation in the spheroid model, which is more representative of the *in vivo* tissue situation.

4.2.2 Effect of stimulatory factors in 3D *in vitro* models mimicking soft and hard tissues

Tissue models in this thesis were generated by considering the 3D cell configuration *in vivo*, the inclusion of materials, as well as the application of fluid flow, to induce a more *in vivo*-like tissue construct. However, another factor to consider is the recapitulation of the cellular biochemical environment in tissues and the body (237). We used predefined culture medium with fetal bovine serum, containing growth factors, proteins, trace elements, hormones and vitamins (A, B-complex, C, E) (373) to cover the range found in the body and promote physiological cell growth and differentiation within the generated models (237). Moreover, in paper II and III, a commercially available osteoblast growth medium was used which contained AA as supplement. However, to stimulate tissue formation, repair and remodelling in 3D *in vitro* models, additional factors may be needed (374). Growth factors (platelet-derived growth factor, transforming growth factor β, fibroblast growth factors, insulin-like growth factors, BMPs), hormones or bioactive molecules are frequently used to guide and promote soft and (375) hard tissue regeneration *in vitro* and in animal models (376-378). Yang *et al*.

supplemented human PDL fibroblast spheroids with recombinant irisin (350), a polypeptide hormone involved in energy metabolism (379) and osteogenesis (380). They observed that irisin treatment enhanced ECM formation, as well as the osteogenic and angiogenic potential of the fibroblasts in the spheroids, crucial parameters for periodontal soft and hard tissue regeneration (350). Moreover, Lambertini $et\ al.$ incubated spheroids of primary human monocytes and osteoblasts with glucosamine (169), which is suggested to have chondroprotective and anti-inflammatory properties (381, 382). They found that glucosamine supplementation exerted anabolic effects in the bone spheroid model, reducing osteoclast activity and stimulating osteoblast properties (169). In contrast, we applied vitamin supplementation in the scaffold-free 3D tissue models of PDL fibroblast and osteoblast spheroids (paper I and II, respectively). Vitamin D and K2 were chosen as stimulatory factors in these models since both vitamins are implicated in bone metabolism (383, 384). Vitamin D is involved in the modulation of immune and inflammatory responses (385, 386) and may have an effect on fracture healing, bone density and remodelling (203, 387). Vitamin K2 is known for its protective role against bone loss and fractures (388, 389).

In the PDL fibroblast spheroids, vitamin D had an effect on the secretion of factors beneficial for tissue healing (IL-6 (390), IL-8, interleukin-1β (391), FGF-2) (392, 393) and bone remodelling/repair (OPG, DKK-1, ALP) (394). Notably, the biologically most active vitamin D metabolite, $1,25(OH)_2D_3$, produced by 1α-hydroxylation in the kidneys (385), was less effective in promoting these effects than the circulating vitamin D form $25(OH)D_3$. This finding is interesting as it implies that $25(OH)D_3$, at physiological doses (50 – 250 nM (395)), may be considered as an active supplement for (periodontal) bone regeneration.

We verified the expression of several genes (vitamin D receptor, 24-hydroxylase, 1α-hydroxylase) in the PDL fibroblast spheroids which indicates the presence of an active vitamin D metabolism in the cells (paper I). However, the regulation of these mechanisms, which could explain the limited conversion of $25(OH)D_3$ to $1,25(OH)_2D_3$ by 1α-hydroxylase, (396) and the independent effects of $25(OH)D_3$, remains unknown and needs to be analysed in further studies. Unravelling the molecular mechanisms regulating local vitamin D metabolism in periodontal soft and hard tissue cells may open the door to new treatments for periodontitis and strategies to periodontal tissue regeneration (397).

In paper II, $25(OH)D_3$ was chosen as vitamin D form in the osteoblast spheroid model. Interestingly, the effects of $25(OH)D_3$ on factors beneficial for bone remodelling and repair in the soft tissue model were partially mimicked in the osteoblast spheroids. Moreover, vitamin K2 supplementation altered the expression of several components of the bone ECM matrix at

the protein (collagen Type I, periostin) or mRNA level (OC, OPN) and stimulated cellular mechanisms involved in osteoclastogenesis and bone resorption by enhancing RANKL and OPG mRNA expression and the secretion of DKK-1 and G-CSF from the constructs (paper II). Other studies report a beneficial effect of vitamin D or K2 administration on cellular processes involved in bone repair and regeneration in 3D *in vitro* models (398-400). Lee *et al.* supplemented spheroids of human MSCs with vitamin D and observed enhanced differentiation towards the osteogenic lineage within the constructs (398). Vu and Bose fabricated 3D calcium phosphate scaffolds loaded with vitamin D and observed that the release enabled osteoblast proliferation while inhibiting osteoclast activity, indicating enhanced bone healing (399). Mandatori *et al.* supplemented spheroids of human MSCs from amniotic fluid and osteoclast precursors with vitamin K2 and observed a negative effect on osteoclastogenesis while the mineralized matrix deposition and expression of osteogenic markers were enhanced (400).

In summary, stimulatory factors may play an important role to guide and promote tissue remodelling and repair within 3D *in vitro* models. Vitamin supplementation (D and K2) enhanced cellular and molecular mechanisms involved in soft and hard tissue regeneration within the generated 3D spheroids. Vitamins C, K2 and D play an essential role for bone remodelling and repair (186). This may be due to fact that vitamin C promotes osteoblast growth and the induction of genes associated with the osteoblast phenotype (collagen Type I, ALP, osteocalcin) (401-404), vitamin K2 enhances collagen accumulation, its accumulation in the bone matrix and bone matrix quality (221, 405, 406) and vitamin D osteoblast differentiation and matrix mineralization (407, 408). In addition, additive and synergistic effects of vitamins D and K2 on osteoblast differentiation and matrix mineralization *in vitro* (409-411), bone mineral density and fracture reduction *in vivo* (412-416) have been reported in the literature. However, to the best of our knowledge, our study is the first to show that the combination of vitamin D and K2 has various effects on soft tissue cells like PDL fibroblasts. This finding is interesting as it implies that combined D and K2 supplementation may be more effective promoting (periodontal) bone regeneration.

5. CONCLUDING REMARKS AND FUTURE PERSPECTIVES

In conclusion, the developed 3D scaffold-free and scaffold-based *in vitro* models mimicked to some extent the cellular structures in soft and hard tissues. Moreover, the models have provided valuable insights into cellular and molecular tissue repair and remodelling mechanisms.

Special emphasis was placed on the inclusion of fluid flow-derived shear forces in the models. The research demonstrated that these stimuli had an effect on cellular organization and remodelling/repair processes in the generated models. In conclusion, this highlights the need to consider dynamic forces in designing 3D *in vitro* models and points out the importance of fluid flow-derived shear forces in scaffold-free and scaffold-based *in vitro* models to mimic *in vivo* conditions. Future work could dive deeper into the specific effects of fluid flow in the models, exploring different flow rates, patterns, and durations to optimize tissue growth, organization, and functionality. In addition, integrating advanced imaging techniques, such as high-resolution microscopy and live-cell imaging could provide real-time insights into the cellular responses to fluid flow.

Furthermore, the research demonstrated that vitamin supplementation, notably vitamins D and K2, enhanced cellular mechanisms associated with tissue remodelling and repair in the scaffold-free 3D tissue models. This finding highlights the potential of using stimulatory factors to promote tissue regeneration *in vitro*. Future work, using advanced omics technologies, such as transcriptomics and proteomics, could unravel the underlying molecular pathways and signalling cascades mediating the effects of vitamin D and K2. This may allow for the development of targeted approaches to optimise tissue regeneration and novel therapeutic interventions for the treatment of diseases like osteoporosis and periodontitis.

Finally, while the developed 3D tissue models have shown promise in mimicking tissue structures and studying cellular responses, the models need to be further characterized, refined, and standardized to ensure their clinical translation. One aim would be to closer mimic the tissue environment and niche PDL fibroblasts and osteoblasts reside in.
Within the spheroid tissue models, future studies may focus on characterizing the (mineralized) ECM and on refining the culture conditions to closer mimic the composition, 3D architecture and ECM\tissue stiffness within the human PDL and bone. Moreover, future studies may include additional cell types such as MSCs and endothelial cells to enhance the relevance and functionality of the spheroid tissue models.

By accurately replicating the native tissue environment of human PDL and bone, the spheroid tissue models may be suitable candidates for the discovery and testing of novel drugs and other treatments targeting periodontitis and other bone-related diseases, hence reducing the need for animal experiments in the preclinical phase and the failure rate in drug discovery.

The designed perfusion flow bioreactor system holds potential to improve the clinical translation of synthetic bone scaffolds by pre-seeding the scaffold with the patient's own differentiated bone cells before implantation. This approach could significantly enhance the healing process of large bone defects by promoting a more uniform cell distribution and faster tissue regeneration. However, translating these findings into clinical practice is not without challenges. Issues such as the scalability of scaffold production and, subsequently, cell harvesting and seeding. Furthermore, the integration into existing clinical workflows needs to be addressed. Another benefit of the perfusion flow bioreactor system is its capacity to identify less favourable scaffold pore morphologies. If a bone scaffold exhibits suboptimal pore structure, the perfusion system could be instrumental in the early detection of these disadvantages, thereby contributing to the refinement of scaffold designs. This detection capability is crucial, as it optimises scaffold properties to ensure efficient fluid flow, which is pivotal for nutrient delivery and waste removal in tissue engineering applications.

Fluid flow inside the TiO_2 scaffold affected cell differentiation; however, the addition of external dynamic stimuli to the bone scaffold presents an exciting opportunity for enhancing the differentiation of bone cells. However, applying dynamic loading to brittle scaffolds, such as those made of ceramics, which are prone to cracking and fracturing, is challenging. A potential solution could involve the modification of ceramic scaffolds with a polymeric layer, thereby increasing their elastic modulus and making them more amenable to mechanical loading. Investigating the effects of uniaxial or biaxial loading on scaffolds could simulate various physiological conditions, providing insights into how different mechanical environments influence bone regeneration. An interdisciplinary approach combining materials science, biomechanics, and cellular biology knowledge will be crucial in determining how these mechanical stimuli can synergistically work with perfusion flow to optimise scaffold performance.

6. REFERENCES

1.   Nanci A, Bosshardt DD. Structure of periodontal tissues in health and disease. Periodontol 2000. 2006;40:11-28.
2.   Melcher AH. On the Repair Potential of Periodontal Tissues. J Periodontol. 1976;47(5):256-60.
3.   Cho YD, Kim KH, Lee YM, Ku Y, Seol YJ. Periodontal Wound Healing and Tissue Regeneration: A Narrative Review. Pharmaceuticals (Basel). 2021;14(5).
4.   Coolidge ED. The Thickness of the Human Periodontal Membrane. The Journal of the American Dental Association and The Dental Cosmos. 1937;24(8):1260-70.
5.   Beertsen W, McCulloch CAG, Sodek J. The periodontal ligament: a unique, multifunctional connective tissue. Periodontol 2000. 1997;13(1):20-40.
6.   Yang L, Yang Y, Wang S, Li Y, Zhao Z. In vitro mechanical loading models for periodontal ligament cells: from two-dimensional to three-dimensional models. Arch Oral Biol. 2015;60(3):416-24.
7.   Roato I, Masante B, Putame G, Massai D, Mussano F. Challenges of Periodontal Tissue Engineering: Increasing Biomimicry through 3D Printing and Controlled Dynamic Environment. Nanomaterials. 2022;12(21):3878.
8.   Berkovitz BK. Periodontal ligament: structural and clinical correlates. Dent Update. 2004;31(1):46-50, 2, 4.
9.   Butler WT, Birkedal-Hansen H, Beegle WF, Taylor RE, Chung E. Proteins of the periodontium. Identification of collagens with the [alpha1(I)]2alpha2 and [alpha1(III)]3 structures in bovine periodontal ligament. J Biol Chem. 1975;250(23):8907-12.
10.   Karimbux NY, Rosenblum ND, Nishimura I. Site-specific expression of collagen I and XII mRNAs in the rat periodontal ligament at two developmental stages. J Dent Res. 1992;71(7):1355-62.
11.   Lukinmaa PL, Waltimo J. Immunohistochemical localization of types I, V, and VI collagen in human permanent teeth and periodontal ligament. J Dent Res. 1992;71(2):391-7.
12.   Bumann A, Carvalho RS, Schwarzer CL, Yen EH. Collagen synthesis from human PDL cells following orthodontic tooth movement. Eur J Orthod. 1997;19(1):29-37.
13.   Bergomi M, Cugnoni J, Botsis J, Belser UC, Anselm Wiskott HW. The role of the fluid phase in the viscous response of bovine periodontal ligament. Journal of Biomechanics. 2010;43(6):1146-52.
14.   Sanjeevi R, Somanathan N, Ramaswamy D. A viscoelastic model for collagen fibres. J Biomech. 1982;15(3):181-3.
15.   Minns RJ, Soden PD, Jackson DS. The role of the fibrous components and ground substance in the mechanical properties of biological tissues: A preliminary investigation. Journal of Biomechanics. 1973;6(2):153-65.
16.   Ten Cate AR, Mills C, Solomon G. The development of the periodontium. A transplantation and autoradiographic study. Anat Rec. 1971;170(3):365-79.
17.   Groeneveld MC, Everts V, Beertsen W. A Quantitative Enzyme Histochemical Analysis of the Distribution of Alkaline Phosphatase Activity in the Periodontal Ligament of the Rat Incisor. J Dent Res. 1993;72(9):1344-50.
18.   Golub EE, Boesze-Battaglia K. The role of alkaline phosphatase in mineralization. Current Opinion in Orthopaedics. 2007;18(5):444-8.
19.   Groeneveld MC, Everts V, Beertsen W. Formation of Afibrillar Acellular Cementum-like Layers Induced by Alkaline Phosphatase Activity from Periodontal Ligament Explants Maintained in vitro. J Dent Res. 1994;73(10):1588-92.
20.   Ivanovski S, Li H, Haase HR, Bartold PM. Expression of bone associated macromolecules by gingival and periodontal ligament fibroblasts. J Periodontal Res. 2001;36(3):131-41.
21.   Boyko GA, Melcher AH, Brunette DM. Formation of new periodontalligament by periodontal ligament cells implanted in vivo after culture in vitro. J Periodontal Res. 1981;16(1):73-88.

22.   Nyman S, Gottlow J, Karring T, Lindhe J. The regenerative potential of the periodontal ligament. An experimental study in the monkey. J Clin Periodontol. 1982;9(3):257-65.

23.   Sodek J, McKee MD. Molecular and cellular biology of alveolar bone. Periodontol 2000. 2000;24:99-126.

24.   Saffar J-L, Lasfargues J-J, Cherruau M. Alveolar bone and the alveolar process: the socket that is never stable. Periodontol 2000. 1997;13(1):76-90.

25.   Amirazad H, Dadashpour M, Zarghami N. Application of decellularized bone matrix as a bioscaffold in bone tissue engineering. J Biol Eng. 2022;16(1):1.

26.   Erik Fink Eriksen DWA, Flemming Melsen. Bone Histomorphometry Raven Press, New York; 1994.

27.   Marks SC, Odgren PR. Chapter 1 - Structure and Development of the Skeleton. In: Bilezikian JP, Raisz LG, Rodan GA, editors. Principles of Bone Biology (Second Edition). San Diego: Academic Press; 2002. p. 3-15.

28.   Clarke B. Normal bone anatomy and physiology. Clin J Am Soc Nephrol. 2008;3 Suppl 3(Suppl 3):S131-9.

29.   Buckwalter JA, Cooper RR. Bone structure and function. Instr Course Lect. 1987;36:27-48.

30.   Buckwalter JA, Glimcher MJ, Cooper RR, Recker R. Bone Biology. JBJS. 1995;77(8):1256-75.

31.   Sommerfeldt DW, Rubin CT. Biology of bone and how it orchestrates the form and function of the skeleton. Eur Spine J. 2001;10 Suppl 2(Suppl 2):S86-95.

32.   Triffitt JT. The organic matrix of bone tissue. Fundamental and clinical bone physiology. 1980:45-82.

33.   Rossert J, Decrombrugghe B. Type I CollagenStructure, Synthesis, and Regulation. 2002. p. 189-210.

34.   Weiner S, Traub W. Bone structure: from angstroms to microns. FASEB J. 1992;6(3):879-85.

35.   Fratzl P. Mechanical Design of Biomineralized Tissues. Bone and Other Hierarchical Materials. Biomineralization2008. p. 547-75.

36.   Marks SC, Jr., Popoff SN. Bone cell biology: the regulation of development, structure, and function in the skeleton. Am J Anat. 1988;183(1):1-44.

37.   Capulli M, Paone R, Rucci N. Osteoblast and osteocyte: games without frontiers. Arch Biochem Biophys. 2014;561:3-12.

38.   Bonewald LF. The amazing osteocyte. J Bone Miner Res. 2011;26(2):229-38.

39.   Miller SC, de Saint-Georges L, Bowman BM, Jee WS. Bone lining cells: structure and function. Scanning Microsc. 1989;3(3):953-60; discussion 60-1.

40.   Canas F, Terepka AR, Neuman WF. Potassium and milieu intérieur of bone. Am J Physiol. 1969;217(1):117-20.

41.   Talmage RV. Morphological and physiological considerations in a new concept of calcium transport in bone. Am J Anat. 1970;129(4):467-76.

42.   Hauge EM, Qvesel D, Eriksen EF, Mosekilde L, Melsen F. Cancellous Bone Remodeling Occurs in Specialized Compartments Lined by Cells Expressing Osteoblastic Markers. Journal of Bone and Mineral Research. 2001;16(9):1575-82.

43.   Everts V, Delaissé JM, Korper W, Jansen DC, Tigchelaar-Gutter W, Saftig P, Beertsen W. The bone lining cell: its role in cleaning Howship's lacunae and initiating bone formation. J Bone Miner Res. 2002;17(1):77-90.

44.   Lian JB, Stein GS, Javed A, van Wijnen AJ, Stein JL, Montecino M, et al. Networks and hubs for the transcriptional control of osteoblastogenesis. Rev Endocr Metab Disord. 2006;7(1-2):1-16.

45.   Aubin JE. Regulation of osteoblast formation and function. Rev Endocr Metab Disord. 2001;2(1):81-94.

46.   Manolagas SC. Birth and death of bone cells: basic regulatory mechanisms and implications for the pathogenesis and treatment of osteoporosis. Endocr Rev. 2000;21(2):115-37.

47.   Boyce B, Xing L, Jilka R, Bellido T, Weinstein R, Parfitt A, Manolagas S. Apoptosis in Bone Cells. 12002. p. 151-68.

48.   Thomson BM. BONE*. In: Caballero B, editor. Encyclopedia of Human Nutrition (Second Edition). Oxford: Elsevier; 1998. p. 220-5.

49.   Dallas SL, Prideaux M, Bonewald LF. The osteocyte: an endocrine cell ... and more. Endocr Rev. 2013;34(5):658-90.

50.   Schaffler MB, Cheung W-Y, Majeska R, Kennedy O. Osteocytes: Master Orchestrators of Bone. Calcified Tissue International. 2014;94(1):5-24.

51.   Wolff J. The law of bone remodelling: Springer Science & Business Media; 2012.

52.   Frost HM. Bone "mass" and the "mechanostat": A proposal. The Anatomical Record. 1987;219(1):1-9.

53.   Weinbaum S, Cowin SC, Zeng Y. A model for the excitation of osteocytes by mechanical loading-induced bone fluid shear stresses. Journal of Biomechanics. 1994;27(3):339-60.

54.   Yavropoulou MP, Yovos JG. The molecular basis of bone mechanotransduction. J Musculoskelet Neuronal Interact. 2016;16(3):221-36.

55.   Teitelbaum SL. Bone resorption by osteoclasts. Science. 2000;289(5484):1504-8.

56.   Xiong J, Onal M, Jilka RL, Weinstein RS, Manolagas SC, O'Brien CA. Matrix-embedded cells control osteoclast formation. Nat Med. 2011;17(10):1235-41.

57.   Nakashima T, Hayashi M, Fukunaga T, Kurata K, Oh-Hora M, Feng JQ, et al. Evidence for osteocyte regulation of bone homeostasis through RANKL expression. Nat Med. 2011;17(10):1231-4.

58.   Crockett JC, Mellis DJ, Scott DI, Helfrich MH. New knowledge on critical osteoclast formation and activation pathways from study of rare genetic diseases of osteoclasts: focus on the RANK/RANKL axis. Osteoporos Int. 2011;22(1):1-20.

59.   Arai F, Miyamoto T, Ohneda O, Inada T, Sudo T, Brasel K, et al. Commitment and differentiation of osteoclast precursor cells by the sequential expression of c-Fms and receptor activator of nuclear factor kappaB (RANK) receptors. J Exp Med. 1999;190(12):1741-54.

60.   Li J, Sarosi I, Yan XQ, Morony S, Capparelli C, Tan HL, et al. RANK is the intrinsic hematopoietic cell surface receptor that controls osteoclastogenesis and regulation of bone mass and calcium metabolism. Proc Natl Acad Sci U S A. 2000;97(4):1566-71.

61.   Sokos D, Everts V, de Vries TJ. Role of periodontal ligament fibroblasts in osteoclastogenesis: a review. J Periodontal Res. 2015;50(2):152-9.

62.   Simonet WS, Lacey DL, Dunstan CR, Kelley M, Chang MS, Lüthy R, et al. Osteoprotegerin: a novel secreted protein involved in the regulation of bone density. Cell. 1997;89(2):309-19.

63.   Boyce BF, Xing L. Functions of RANKL/RANK/OPG in bone modeling and remodeling. Arch Biochem Biophys. 2008;473(2):139-46.

64.   Frost HM. Tetracycline-based histological analysis of bone remodeling. Calcif Tissue Res. 1969;3(3):211-37.

65.   Parfitt AM. Targeted and Nontargeted Bone Remodeling: Relationship to Basic Multicellular Unit Origination and Progression. Bone. 2002;30:5-7.

66.   Parfitt AM. Osteonal and hemi-osteonal remodeling: the spatial and temporal framework for signal traffic in adult human bone. J Cell Biochem. 1994;55(3):273-86.

67.   Kenkre JS, Bassett J. The bone remodelling cycle. Ann Clin Biochem. 2018;55(3):308-27.

68.   Saunders M, Truesdell S. Bone remodeling platforms: Understanding the need for multicellular lab-on-a-chip systems and predictive agent-based models. Mathematical biosciences and engineering: MBE. 2019;17:1233-52.

69.   Sims NA, Martin TJ. Coupling Signals between the Osteoclast and Osteoblast: How are Messages Transmitted between These Temporary Visitors to the Bone Surface? Front Endocrinol (Lausanne). 2015;6:41.

70.   Burr DB. Targeted and nontargeted remodeling. Bone. 2002;30(1):2-4.

71.   Burger EH, Klein-Nulend J. Mechanotransduction in bone--role of the lacuno-canalicular network. FASEB journal : official publication of the Federation of American Societies for Experimental Biology. 1999;13 Suppl:S101-12.

72.   Burr DB. Bone material properties and mineral matrix contributions to fracture risk or age in women and men. J Musculoskelet Neuronal Interact. 2002;2(3):201-4.

73.   Viguet-Carrin S, Garnero P, Delmas PD. The role of collagen in bone strength. Osteoporos Int. 2006;17(3):319-36.

74.   Turner CH. Bone strength: current concepts. Ann N Y Acad Sci. 2006;1068:429-46.

75.   Garnero P. The Role of Collagen Organization on the Properties of Bone. Calcified tissue international. 2015;97(3):229-40.

76.   Wang X, Bank RA, TeKoppele JM, Agrawal CM. The role of collagen in determining bone mechanical properties. J Orthop Res. 2001;19(6):1021-6.

77.   Horiuchi K, Amizuka N, Takeshita S, Takamatsu H, Katsuura M, Ozawa H, et al. Identification and Characterization of a Novel Protein, Periostin, with Restricted Expression to Periosteum and Periodontal Ligament and Increased Expression by Transforming Growth Factor β. Journal of Bone and Mineral Research. 1999;14(7):1239-49.

78.   Norris RA, Damon B, Mironov V, Kasyanov V, Ramamurthi A, Moreno-Rodriguez R, et al. Periostin regulates collagen fibrillogenesis and the biomechanical properties of connective tissues. Journal of Cellular Biochemistry. 2007;101(3):695-711.

79.   Bonnet N, Gineyts E, Ammann P, Conway SJ, Garnero P, Ferrari S. Periostin deficiency increases bone damage and impairs injury response to fatigue loading in adult mice. PLoS One. 2013;8(10):e78347.

80.   Morgan S, Poundarik AA, Vashishth D. Do Non-collagenous Proteins Affect Skeletal Mechanical Properties? Calcified tissue international. 2015;97(3):281-91.

81.   Loi F, Córdova LA, Pajarinen J, Lin TH, Yao Z, Goodman SB. Inflammation, fracture and bone repair. Bone. 2016;86:119-30.

82.   Marsell R, Einhorn TA. The biology of fracture healing. Injury. 2011;42(6):551-5.

83.   Claes L, Recknagel S, Ignatius A. Fracture healing under healthy and inflammatory conditions. Nat Rev Rheumatol. 2012;8(3):133-43.

84.   Jagodzinski M, Krettek C. Effect of mechanical stability on fracture healing--an update. Injury. 2007;38 Suppl 1:S3-10.

85.   Bahney CS, Zondervan RL, Allison P, Theologis A, Ashley JW, Ahn J, et al. Cellular biology of fracture healing. J Orthop Res. 2019;37(1):35-50.

86.   Maruyama M, Rhee C, Utsunomiya T, Zhang N, Ueno M, Yao Z, Goodman SB. Modulation of the Inflammatory Response and Bone Healing. Front Endocrinol (Lausanne). 2020;11:386.

87.   Dimitriou R, Jones E, McGonagle D, Giannoudis PV. Bone regeneration: current concepts and future directions. BMC Medicine. 2011;9(1):66.

88.   Bauer TW, Muschler GF. Bone graft materials. An overview of the basic science. Clin Orthop Relat Res. 2000(371):10-27.

89.   Khan SN, Cammisa FP, Jr., Sandhu HS, Diwan AD, Girardi FP, Lane JM. The biology of bone grafting. J Am Acad Orthop Surg. 2005;13(1):77-86.

90.   Younger EM, Chapman MW. Morbidity at bone graft donor sites. J Orthop Trauma. 1989;3(3):192-5.

91.   Ehrler DM, Vaccaro AR. The use of allograft bone in lumbar spine surgery. Clin Orthop Relat Res. 2000(371):38-45.

92.   Zimmermann G, Moghaddam A. Allograft bone matrix versus synthetic bone graft substitutes. Injury. 2011;42 Suppl 2:S16-21.

93.   Williams BR, Freking WG, Ridley TJ, Agel J, Swiontkowski MF. The Proportion of Abstracts Presented at the 2010 American Academy of Orthopaedic Surgeons Annual Meeting Ultimately Published. Orthopedics. 2020;43(4):e263-e9.

94.   Henkel J, Woodruff MA, Epari DR, Steck R, Glatt V, Dickinson IC, et al. Bone Regeneration Based on Tissue Engineering Conceptions — A 21st Century Perspective. Bone Research. 2013;1(1):216-48.

95.   Wang W, Yeung KWK. Bone grafts and biomaterials substitutes for bone defect repair: A review. Bioact Mater. 2017;2(4):224-47.

96.   Haugen HJ, Lyngstadaas SP, Rossi F, Perale G. Bone grafts: which is the ideal biomaterial? J Clin Periodontol. 2019;46 Suppl 21:92-102.

97.   Karageorgiou V, Kaplan D. Porosity of 3D biomaterial scaffolds and osteogenesis. Biomaterials. 2005;26(27):5474-91.

98.   Williams DF. On the mechanisms of biocompatibility. Biomaterials. 2008;29(20):2941-53.

99.   Albrektsson T, Johansson C. Osteoinduction, osteoconduction and osseointegration. Eur Spine J. 2001;10 Suppl 2(Suppl 2):S96-101.

100.   Albrektsson T, Brånemark PI, Hansson HA, Lindström J. Osseointegrated titanium implants. Requirements for ensuring a long-lasting, direct bone-to-implant anchorage in man. Acta Orthop Scand. 1981;52(2):155-70.

101.   Giannoudis PV, Dinopoulos H, Tsiridis E. Bone substitutes: an update. Injury. 2005;36 Suppl 3:S20-7.

102.   Zwingenberger S, Nich C, Valladares RD, Yao Z, Stiehler M, Goodman SB. Recommendations and considerations for the use of biologics in orthopedic surgery. BioDrugs. 2012;26(4):245-56.

103.   Baino F, Novajra G, Vitale-Brovarone C. Bioceramics and Scaffolds: A Winning Combination for Tissue Engineering. Front Bioeng Biotechnol. 2015;3:202.

104.   Ginebra MP, Espanol M, Maazouz Y, Bergez V, Pastorino D. Bioceramics and bone healing. EFORT Open Rev. 2018;3(5):173-83.

105.   Tiainen H, Wiedmer D, Haugen HJ. Processing of highly porous TiO2 bone scaffolds with improved compressive strength. Journal of the European Ceramic Society. 2013;33(1):15-24.

106.   Carter DR, Hayes WC. Bone compressive strength: the influence of density and strain rate. Science. 1976;194(4270):1174-6.

107.   Haugen H, Will J, Köhler A, Hopfner U, Aigner J, Wintermantel E. Ceramic TiO2-foams: characterisation of a potential scaffold. Journal of the European Ceramic Society. 2004;24(4):661-8.

108.   Fostad G, Hafell B, Forde A, Dittmann R, Sabetrasekh R, Will J, et al. Loadable TiO2 scaffolds-A correlation study between processing parameters, micro CT analysis and mechanical strength. Journal of the European Ceramic Society. 2009;29:2773-81.

109.   Gomez-Florit M, Rubert M, Ramis J, Haugen H, Tiainen H, Lyngstadaas S, Monjo M. TiO2 Scaffolds Sustain Differentiation of MC3T3-E1 Cells. Journal of Biomaterials and Tissue Engineering. 2012;2:336-44.

110.   Sabetrasekh R, Tiainen H, Lyngstadaas SP, Reseland J, Haugen H. A novel ultra-porous titanium dioxide ceramic with excellent biocompatibility. J Biomater Appl. 2011;25(6):559-80.

111.   Haugen HJ, Monjo M, Rubert M, Verket A, Lyngstadaas SP, Ellingsen JE, et al. Porous ceramic titanium dioxide scaffolds promote bone formation in rabbit peri-implant cortical defect model. Acta Biomaterialia. 2013;9(2):5390-9.

112.   Tiainen H, Wohlfahrt JC, Verket A, Lyngstadaas SP, Haugen HJ. Bone formation in TiO2 bone scaffolds in extraction sockets of minipigs. Acta Biomater. 2012;8(6):2384-91.

113.   Le Thieu MK, Homayouni A, Hæren LR, Tiainen H, Verket A, Ellingsen JE, et al. Impact of simultaneous placement of implant and block bone graft substitute: an in vivo peri-implant defect model. Biomaterials Research. 2021;25(1):43.

114.   Thieu MKL, Haugen HJ, Sanz-Esporrin J, Sanz M, Lyngstadaas SP, Verket A. Guided bone regeneration of chronic non-contained bone defects using a volume stable porous block TiO2 scaffold: An experimental in vivo study. Clin Oral Implants Res. 2021;32(3):369-81.

115.   Nygren H, Tengvall P, Lundström I. The initial reactions of TiO2 with blood. J Biomed Mater Res. 1997;34(4):487-92.

116.   Jokinen M, Pätsi M, Rahiala H, Peltola T, Ritala M, Rosenholm JB. Influence of sol and surface properties on in vitro bioactivity of sol-gel-derived TiO2 and TiO2-SiO2 films deposited by dip-coating method. J Biomed Mater Res. 1998;42(2):295-302.

117.   Edmondson R, Broglie JJ, Adcock AF, Yang L. Three-dimensional cell culture systems and their applications in drug discovery and cell-based biosensors. Assay Drug Dev Technol. 2014;12(4):207-18.

118.   Li XJ, Valadez AV, Zuo P, Nie Z. Microfluidic 3D cell culture: potential application for tissue-based bioassays. Bioanalysis. 2012;4(12):1509-25.

119.   Wrzesinski K, Rogowska-Wrzesinska A, Kanlaya R, Borkowski K, Schwämmle V, Dai J, et al. The cultural divide: exponential growth in classical 2D and metabolic equilibrium in 3D environments. PLoS One. 2014;9(9):e106973.

120.   Calitz C, Hamman JH, Viljoen AM, Fey SJ, Wrzesinski K, Gouws C. Toxicity and anti-prolific properties of Xysmalobium undulatum water extract during short-term exposure to two-dimensional and three-dimensional spheroid cell cultures. Toxicology Mechanisms and Methods. 2018;28(9):641-52.

121.   Anthon SG, Valente KP. Vascularization Strategies in 3D Cell Culture Models: From Scaffold-Free Models to 3D Bioprinting. International Journal of Molecular Sciences. 2022;23(23):14582.

122.   Ovsianikov A, Khademhosseini A, Mironov V. The Synergy of Scaffold-Based and Scaffold-Free Tissue Engineering Strategies. Trends Biotechnol. 2018;36(4):348-57.

123.   Athanasiou KA, Eswaramoorthy R, Hadidi P, Hu JC. Self-organization and the self-assembling process in tissue engineering. Annu Rev Biomed Eng. 2013;15:115-36.

124.   DuRaine GD, Brown WE, Hu JC, Athanasiou KA. Emergence of scaffold-free approaches for tissue engineering musculoskeletal cartilages. Ann Biomed Eng. 2015;43(3):543-54.

125.   Kobayashi J, Akiyama Y, Yamato M, Shimizu T, Okano T. Design of Temperature-Responsive Cell Culture Surfaces for Cell Sheet-Based Regenerative Therapy and 3D Tissue Fabrication. In: Chun HJ, Park CH, Kwon IK, Khang G, editors. Cutting-Edge Enabling Technologies for Regenerative Medicine. Singapore: Springer Singapore; 2018. p. 371-93.

126.   Elloumi-Hannachi I, Yamato M, Okano T. Cell sheet engineering: a unique nanotechnology for scaffold-free tissue reconstruction with clinical applications in regenerative medicine. Journal of Internal Medicine. 2010;267(1):54-70.

127.   Ryu NE, Lee SH, Park H. Spheroid Culture System Methods and Applications for Mesenchymal Stem Cells. Cells. 2019;8(12).

128.   Frandsen HS. Overview of six 3D culture techniques: CelVivo; 2022 [Available from: https://www.linkedin.com/pulse/overview-six-3d-cell-culture-techniques-celvivo/?trackingId=ELiRBxsqpSkz3Pz5HWJLGg%3D%3D.

129.   Costa EC, de Melo-Diogo D, Moreira AF, Carvalho MP, Correia IJ. Spheroids Formation on Non-Adhesive Surfaces by Liquid Overlay Technique: Considerations and Practical Approaches. Biotechnol J. 2018;13(1).

130.   Gunti S, Hoke ATK, Vu KP, London NR, Jr. Organoid and Spheroid Tumor Models: Techniques and Applications. Cancers (Basel). 2021;13(4).

131.   Timmins NE, Nielsen LK. Generation of multicellular tumor spheroids by the hanging-drop method. Methods Mol Med. 2007;140:141-51.

132.   Breslin S, O'Driscoll L. Three-dimensional cell culture: the missing link in drug discovery. Drug discovery today. 2013;18(5-6):240-9.

133.   Langhans SA. Three-Dimensional in Vitro Cell Culture Models in Drug Discovery and Drug Repositioning. Frontiers in Pharmacology. 2018;9.

134.   Cheema U. Position Paper Progress in the development of biomimetic engineered human tissues. J Tissue Eng. 2023;14:20417314221145663.

135.   Cheema U, Brown RA. Rapid Fabrication of Living Tissue Models by Collagen Plastic Compression: Understanding Three-Dimensional Cell Matrix Repair In Vitro. Adv Wound Care (New Rochelle). 2013;2(4):176-84.

136.   Tibbitt MW, Anseth KS. Hydrogels as extracellular matrix mimics for 3D cell culture. Biotechnol Bioeng. 2009;103(4):655-63.

137.   Nezhad-Mokhtari P, Ghorbani M, Roshangar L, Soleimani Rad J. A review on the construction of hydrogel scaffolds by various chemically techniques for tissue engineering. European Polymer Journal. 2019;117:64-76.

138.   Giancotti FG, Ruoslahti E. Integrin Signaling. Science. 1999;285(5430):1028-33.

139.   Morwood AJ, El-Karim IA, Clarke SA, Lundy FT. The Role of Extracellular Matrix (ECM) Adhesion Motifs in Functionalised Hydrogels. Molecules. 2023;28(12).

140. Pape J, Emberton M, Cheema U. 3D Cancer Models: The Need for a Complex Stroma, Compartmentalization and Stiffness. Frontiers in Bioengineering and Biotechnology. 2021;9.

141. Zhang B, Korolj A, Lai BFL, Radisic M. Advances in organ-on-a-chip engineering. Nature Reviews Materials. 2018;3(8):257-78.

142. Cheema U, Rong Z, Kirresh O, Macrobert AJ, Vadgama P, Brown RA. Oxygen diffusion through collagen scaffolds at defined densities: implications for cell survival in tissue models. J Tissue Eng Regen Med. 2012;6(1):77-84.

143. Franko AJ, Sutherland RM. Oxygen Diffusion Distance and Development of Necrosis in Multicell Spheroids. Radiation Research. 1979;79(3):439-53.

144. Cheema U, Brown RA, Alp B, MacRobert AJ. Spatially defined oxygen gradients and vascular endothelial growth factor expression in an engineered 3D cell model. Cell Mol Life Sci. 2008;65(1):177-86.

145. Mueller-Klieser WF, Sutherland RM. Oxygen consumption and oxygen diffusion properties of multicellular spheroids from two different cell lines. Adv Exp Med Biol. 1984;180:311-21.

146. Streeter I, Cheema U. Oxygen consumption rate of cells in 3D culture: The use of experiment and simulation to measure kinetic parameters and optimise culture conditions. Analyst. 2011;136(19):4013-9.

147. Mehta G, Hsiao AY, Ingram M, Luker GD, Takayama S. Opportunities and challenges for use of tumor spheroids as models to test drug delivery and efficacy. Journal of controlled release : official journal of the Controlled Release Society. 2012;164(2):192-204.

148. Wrzesinski K, Fey SJ. Metabolic Reprogramming and the Recovery of Physiological Functionality in 3D Cultures in Micro-Bioreactors. Bioengineering (Basel). 2018;5(1).

149. Dmitriev RI, Zhdanov AV, Nolan YM, Papkovsky DB. Imaging of neurosphere oxygenation with phosphorescent probes. Biomaterials. 2013;34(37):9307-17.

150. Stamati K, Mudera V, Cheema U. Evolution of oxygen utilization in multicellular organisms and implications for cell signalling in tissue engineering. J Tissue Eng. 2011;2(1):2041731411432365.

151. Johnson RW, Sowder ME, Giaccia AJ. Hypoxia and Bone Metastatic Disease. Curr Osteoporos Rep. 2017;15(4):231-8.

152. Pilz M, Kwapiszewska K, Kalwarczyk T, Bubak G, Nowis D, Hołyst R. Transport of nanoprobes in multicellular spheroids. Nanoscale. 2020;12(38):19880-7.

153. Al Hosni R, Bozec L, Roberts SJ, Cheema U. Reprogramming bone progenitor identity and potency through control of collagen density and oxygen tension. iScience. 2022;25(4):104059.

154. Pavlou M, Shah M, Gikas P, Briggs T, Roberts SJ, Cheema U. Osteomimetic matrix components alter cell migration and drug response in a 3D tumour-engineered osteosarcoma model. Acta Biomater. 2019;96:247-57.

155. Winer JP, Janmey PA, McCormick ME, Funaki M. Bone marrow-derived human mesenchymal stem cells become quiescent on soft substrates but remain responsive to chemical or mechanical stimuli. Tissue Eng Part A. 2009;15(1):147-54.

156. Koblenzer M, Weiler M, Fragoulis A, Rütten S, Pufe T, Jahr H. Physiological Mineralization during In Vitro Osteogenesis in a Biomimetic Spheroid Culture Model. Cells. 2022;11(17):2702.

157. Bessot A, Gunter J, Waugh D, Clements JA, Hutmacher DW, McGovern J, Bock N. GelMA and Biomimetic Culture Allow the Engineering of Mineralized, Adipose, and Tumor Tissue Human Microenvironments for the Study of Advanced Prostate Cancer In Vitro and In Vivo. Adv Healthc Mater. 2023;12(14):e2201701.

158. Cheema U, Alekseeva T, Abou-Neel EA, Brown RA. Switching off angiogenic signalling: creating channelled constructs for adequate oxygen delivery in tissue engineered constructs. Eur Cell Mater. 2010;20:274-80; discussion 80-1.

159. Sayin E, Baran ET, Elsheikh A, Mudera V, Cheema U, Hasirci V. Evaluating Oxygen Tensions Related to Bone Marrow and Matrix for MSC Differentiation in 2D and 3D Biomimetic Lamellar Scaffolds. Int J Mol Sci. 2021;22(8).

160. Barralet J, Drager J, Harvey EJ. Hypoxia signalling manipulation for bone regeneration. Expert Reviews in Molecular Medicine. 2015;17:e6.

161. Wirsig K, Kilian D, von Witzleben M, Gelinsky M, Bernhardt A. Impact of Sr(2+) and hypoxia on 3D triple cultures of primary human osteoblasts, osteocytes and osteoclasts. Eur J Cell Biol. 2022;101(3):151256.

162. Clarke MS, Sundaresan A, Vanderburg CR, Banigan MG, Pellis NR. A three-dimensional tissue culture model of bone formation utilizing rotational co-culture of human adult osteoblasts and osteoclasts. Acta Biomater. 2013;9(8):7908-16.

163. Penolazzi L, Lolli A, Sardelli L, Angelozzi M, Lambertini E, Trombelli L, et al. Establishment of a 3D-dynamic osteoblasts-osteoclasts co-culture model to simulate the jawbone microenvironment in vitro. Life Sci. 2016;152:82-93.

164. Domaschke H, Gelinsky M, Burmeister B, Fleig R, Hanke T, Reinstorf A, et al. In vitro ossification and remodeling of mineralized collagen I scaffolds. Tissue engineering. 2006;12(4):949-58.

165. Burmeister B, Domaschke H, Gelinsky M, Rösen-Wolff A, Pompe W. Co-culture of osteoblasts and osteoclasts on resorbable mineralised collagen scaffolds: Establishment of an in vitro model of bone remodeling. Eur Cell Mater. 2003;5.

166. Vermeulen S, Knoops K, Duimel H, Parvizifard M, van Beurden D, López-Iglesias C, et al. An in vitro model system based on calcium- and phosphate ion-induced hMSC spheroid mineralization. Materials Today Bio. 2023;23:100844.

167. Bakkalci D, Jay A, Rezaei A, Howard CA, Haugen HJ, Pape J, et al. Bioengineering the ameloblastoma tumour to study its effect on bone nodule formation. Sci Rep. 2021;11(1):24088.

168. Mandatori D, Penolazzi L, Pelusi L, Lambertini E, Michelucci F, Porreca A, et al. Three-Dimensional Co-Culture System of Human Osteoblasts and Osteoclast Precursors from Osteoporotic Patients as an Innovative Model to Study the Role of Nutrients: Focus on Vitamin K2. Nutrients. 2021;13(8).

169. Lambertini E, Penolazzi L, Pandolfi A, Mandatori D, Sollazzo V, Piva R. Human osteoclasts/osteoblasts 3D dynamic co-culture system to study the beneficial effects of glucosamine on bone microenvironment. Int J Mol Med. 2021;47(4).

170. Haugen S, He J, Sundaresan A, Stunes AK, Aasarød KM, Tiainen H, et al. Adiponectin Reduces Bone Stiffness: Verified in a Three-Dimensional Artificial Human Bone Model In Vitro. Frontiers in endocrinology. 2018;9:236-.

171. Galván-Chacón VP, Zampouka A, Hesse B, Bohner M, Habibovic P, Barata D. Bone-on-a-Chip: A Microscale 3D Biomimetic Model to Study Bone Regeneration. Advanced Engineering Materials. 2022;24(7):2101467.

172. Bernhardt A, Skottke J, von Witzleben M, Gelinsky M. Triple Culture of Primary Human Osteoblasts, Osteoclasts and Osteocytes as an In Vitro Bone Model. Int J Mol Sci. 2021;22(14).

173. Kuttenberger J, Polska E, Schaefer BM. A novel three-dimensional bone chip organ culture. Clin Oral Investig. 2013;17(6):1547-55.

174. Jusoh N, Oh S, Kim S, Kim J, Jeon NL. Microfluidic vascularized bone tissue model with hydroxyapatite-incorporated extracellular matrix. Lab on a Chip. 2015;15(20):3984-8.

175. Boehrs J, Zaharias RS, Laffoon J, Ko YJ, Schneider GB. Three-dimensional culture environments enhance osteoblast differentiation. J Prosthodont. 2008;17(7):517-21.

176. Jähn K, Richards RG, Archer CW, Stoddart MJ. Pellet culture model for human primary osteoblasts. European cells & materials. 2010;20:149-61.

177. Kim J, Adachi T. Cell Condensation Triggers the Differentiation of Osteoblast Precursor Cells to Osteocyte-Like Cells. Frontiers in Bioengineering and Biotechnology. 2019;7.

178. Haugen S, He J, Sundaresan A, Stunes AK, Aasarød KM, Tiainen H, et al. Adiponectin Reduces Bone Stiffness: Verified in a Three-Dimensional Artificial Human Bone Model In Vitro. Front Endocrinol (Lausanne). 2018;9:236.

179. Restle L, Costa-Silva D, Lourenço ES, Bachinski RF, Batista AC, Linhares ABR, Alves GG. A 3D Osteoblast In Vitro Model for the Evaluation of Biomedical Materials. Advances in Materials Science and Engineering. 2015;2015:268930.

180. Gaitán-Salvatella I, López-Villegas EO, González-Alva P, Susate-Olmos F, Álvarez-Pérez MA. Case Report: Formation of 3D Osteoblast Spheroid Under Magnetic Levitation for Bone Tissue Engineering. Front Mol Biosci. 2021;8:672518.

181. Facer SR, Zaharias RS, Andracki ME, Lafoon J, Hunter SK, Schneider GB. Rotary culture enhances pre-osteoblast aggregation and mineralization. J Dent Res. 2005;84(6):542-7.

182. Heo DN, Hospodiuk M, Ozbolat IT. Synergistic interplay between human MSCs and HUVECs in 3D spheroids laden in collagen/fibrin hydrogels for bone tissue engineering. Acta Biomaterialia. 2019;95:348-56.

183. Russell L. The importance of patients' nutritional status in wound healing. Br J Nurs. 2001;10(6 Suppl):S42, s4-9.

184. Chow O, Barbul A. Immunonutrition: Role in Wound Healing and Tissue Regeneration. Advances in wound care. 2014;3 1:46-53.

185. Barchitta M, Maugeri A, Favara G, Magnano San Lio R, Evola G, Agodi A, Basile G. Nutrition and Wound Healing: An Overview Focusing on the Beneficial Effects of Curcumin. Int J Mol Sci. 2019;20(5).

186. Ahmadieh H, Arabi A. Vitamins and bone health: beyond calcium and vitamin D. Nutr Rev. 2011;69(10):584-98.

187. Najeeb S, Zafar MS, Khurshid Z, Zohaib S, Almas K. The Role of Nutrition in Periodontal Health: An Update. Nutrients. 2016;8(9).

188. Mohd Fairulnizal Md N, Rathi Devi Nair G, Suraiami M. Vitamin A in Health and Disease. In: Leila Queiroz Z, Veridiana Vera de R, Eduardo J-L, editors. Vitamin A. Rijeka: IntechOpen; 2019. p. Ch. 2.

189. Zinder R, Cooley R, Vlad LG, Molnar JA. Vitamin A and Wound Healing. Nutrition in Clinical Practice. 2019;34(6):839-49.

190. Hunt TK, Ehrlich HP, Garcia JA, Dunphy JE. Effect of vitamin A on reversing the inhibitory effect of cortisone on healing of open wounds in animals and man. Ann Surg. 1969;170(4):633-41.

191. Yee MMF, Chin KY, Ima-Nirwana S, Wong SK. Vitamin A and Bone Health: A Review on Current Evidence. Molecules. 2021;26(6).

192. Reynolds TM. The future of nutrition and wound healing. J Tissue Viability. 2001;11(1):5-13.

193. Alvarez OM, Gilbreath RL. Thiamine influence on collagen during the granulation of skin wounds. Journal of Surgical Research. 1982;32(1):24-31.

194. Neiva RF, Al-Shammari K, Nociti FH, Jr., Soehren S, Wang HL. Effects of vitamin-B complex supplementation on periodontal wound healing. J Periodontol. 2005;76(7):1084-91.

195. Sherman AR, Barkley M. Nutrition and wound healing. J Wound Care. 2011;20(8):357-8, 60, 62-7.

196. Padayatty SJ, Katz A, Wang Y, Eck P, Kwon O, Lee J-H, et al. Vitamin C as an Antioxidant: Evaluation of Its Role in Disease Prevention. Journal of the American College of Nutrition. 2003;22(1):18-35.

197. Maxfield L, Crane JS. Vitamin C Deficiency. StatPearls. Treasure Island (FL): StatPearls Publishing Copyright © 2022, StatPearls Publishing LLC.; 2022.

198. Barrios-Garay K, Toledano-Serrabona J, Gay-Escoda C, Sánchez-Garcés M. Clinical effect of vitamin C supplementation on bone healing: A systematic review. Med Oral Patol Oral Cir Bucal. 2022;27(3):e205-e15.

199. Abrahmsohn GM, Halberstein RA, Fregeolle S. Vitamin C and dental healing: testing and placebo effect. Gen Dent. 1993;41(6):523-7; quiz 9-30.

200. Pisalsitsakul N, Pinnoi C, Sutanthavibul N, Kamolratanakul P. Taking 200 mg Vitamin C Three Times per Day Improved Extraction Socket Wound Healing Parameters: A Randomized Clinical Trial. Int J Dent. 2022;2022:6437200.

201. Jones G, Strugnell SA, DeLuca HF. Current Understanding of the Molecular Actions of Vitamin D. Physiological Reviews. 1998;78(4):1193-231.

202. Brumbaugh PF, Speer DP, Pitt MJ. 1 alpha, 25-Dihydroxyvitamin D3 a metabolite of vitamin D that promotes bone repair. Am J Pathol. 1982;106(2):171-9.

203.   Gorter EA, Hamdy NA, Appelman-Dijkstra NM, Schipper IB. The role of vitamin D in human fracture healing: a systematic review of the literature. Bone. 2014;64:288-97.

204.   Haussler MR, Whitfield GK, Kaneko I, Haussler CA, Hsieh D, Hsieh J-C, Jurutka PW. Molecular Mechanisms of Vitamin D Action. Calcified Tissue International. 2013;92(2):77-98.

205.   Dietrich T, Joshipura KJ, Dawson-Hughes B, Bischoff-Ferrari HA. Association between serum concentrations of 25-hydroxyvitamin D3 and periodontal disease in the US population. The American Journal of Clinical Nutrition. 2004;80(1):108-13.

206.   Bonnet C, Rabbani R, Moffatt ME, Kelekis-Cholakis A, Schroth RJ. The relation between periodontal disease and vitamin D. J Can Dent Assoc. 2019;85(j4):1488-2159.

207.   Bashutski JD, Eber RM, Kinney JS, Benavides E, Maitra S, Braun TM, et al. The impact of vitamin D status on periodontal surgery outcomes. J Dent Res. 2011;90(8):1007-12.

208.   Hobson R. Vitamin E and wound healing: an evidence-based review. Int Wound J. 2016;13(3):331-5.

209.   Galeano M, Torre V, Deodato B, Campo GM, Colonna M, Sturiale A, et al. Raxofelast, a hydrophilic vitamin E-like antioxidant, stimulates wound healing in genetically diabetic mice. Surgery. 2001;129(4):467-77.

210.   Kim JE, Shklar G. The effect of vitamin E on the healing of gingival wounds in rats. J Periodontol. 1983;54(5):305-8.

211.   Wong SK, Mohamad NV, Ibrahim N, Chin KY, Shuid AN, Ima-Nirwana S. The Molecular Mechanism of Vitamin E as a Bone-Protecting Agent: A Review on Current Evidence. Int J Mol Sci. 2019;20(6).

212.   Dodington DW, Fritz PC, Sullivan PJ, Ward WE. Higher Intakes of Fruits and Vegetables, β-Carotene, Vitamin C, α-Tocopherol, EPA, and DHA Are Positively Associated with Periodontal Healing after Nonsurgical Periodontal Therapy in Nonsmokers but Not in Smokers. The Journal of Nutrition. 2015;145(11):2512-9.

213.   Dam H, Schønheyder F. The occurrence and chemical nature of vitamin K. Biochem J. 1936;30(5):897-901.

214.   Dam H. The antihaemorrhagic vitamin of the chick. Biochem J. 1935;29(6):1273-85.

215.   Shearer MJ, Newman P. Metabolism and cell biology of vitamin K. Thrombosis and Haemostasis. 2008;100:530 - 47.

216.   Krueger T, Westenfeld R, Schurgers L, Brandenburg V. Coagulation meets calcification: the vitamin K system. Int J Artif Organs. 2009;32(2):67-74.

217.   Thijssen HH, Drittij-Reijnders MJ. Vitamin K status in human tissues: tissue-specific accumulation of phylloquinone and menaquinone-4. Br J Nutr. 1996;75(1):121-7.

218.   Halder M, Petsophonsakul P, Akbulut AC, Pavlic A, Bohan F, Anderson E, et al. Vitamin K: Double Bonds beyond Coagulation Insights into Differences between Vitamin K1 and K2 in Health and Disease. Int J Mol Sci. 2019;20(4).

219.   Willems BA, Vermeer C, Reutelingsperger CP, Schurgers LJ. The realm of vitamin K dependent proteins: shifting from coagulation toward calcification. Mol Nutr Food Res. 2014;58(8):1620-35.

220.   Ichikawa T, Horie-Inoue K, Ikeda K, Blumberg B, Inoue S. Vitamin K-2 induces phosphorylation of protein kinase A and expression of novel target genes in osteoblastic cells. Journal of molecular endocrinology. 2007;39:239-47.

221.   Ichikawa T, Horie-Inoue K, Ikeda K, Blumberg B, Inoue S. Steroid and xenobiotic receptor SXR mediates vitamin K2-activated transcription of extracellular matrix-related genes and collagen accumulation in osteoblastic cells. J Biol Chem. 2006;281(25):16927-34.

222.   Katsuyama H, Saijoh K, Otsuki T, Tomita M, Fukunaga M, Sunami S. Menaquinone-7 regulates gene expression in osteoblastic MC3T3E1 cells. Int J Mol Med. 2007;19(2):279-84.

223.   Urayama S, Kawakami A, Nakashima T, Tsuboi M, Yamasaki S, Hida A, et al. Effect of vitamin K2 on osteoblast apoptosis: Vitamin K2 inhibits apoptotic cell death of human osteoblasts induced by Fas, proteasome inhibitor, etoposide, and staurosporine. Journal of Laboratory and Clinical Medicine. 2000;136(3):181-93.

224.	Kameda T, Miyazawa K, Mori Y, Yuasa T, Shiokawa M, Nakamaru Y, et al. Vitamin K2 inhibits osteoclastic bone resorption by inducing osteoclast apoptosis. Biochem Biophys Res Commun. 1996;220(3):515-9.

225.	Koshihara Y, Hoshi K, Okawara R, Ishibashi H, Yamamoto S. Vitamin K stimulates osteoblastogenesis and inhibits osteoclastogenesis in human bone marrow cell culture. J Endocrinol. 2003;176(3):339-48.

226.	Könönen E, Gursoy M, Gursoy UK. Periodontitis: A Multifaceted Disease of Tooth-Supporting Tissues. J Clin Med. 2019;8(8).

227.	Raisz L. Pathogenesis of osteoporosis: Concepts, conflicts, and prospects. The Journal of clinical investigation. 2006;115:3318-25.

228.	Struillou X, Boutigny H, Soueidan A, Layrolle P. Experimental Animal Models in Periodontology: A Review. The open dentistry journal. 2010;4:37-47.

229.	Kantarci A, Hasturk H, Van Dyke TE. Animal models for periodontal regeneration and peri-implant responses. Periodontol 2000. 2015;68(1):66-82.

230.	Bonucci E, Ballanti P. Osteoporosis—Bone Remodeling and Animal Models. Toxicologic Pathology. 2014;42(6):957-69.

231.	Komori T. Animal models for osteoporosis. Eur J Pharmacol. 2015;759:287-94.

232.	Benam KH, Dauth S, Hassell B, Herland A, Jain A, Jang KJ, et al. Engineered in vitro disease models. Annu Rev Pathol. 2015;10:195-262.

233.	McGonigle P, Ruggeri B. Animal models of human disease: challenges in enabling translation. Biochem Pharmacol. 2014;87(1):162-71.

234.	Aveic S, Craveiro RB, Wolf M, Fischer H. Current Trends in In Vitro Modeling to Mimic Cellular Crosstalk in Periodontal Tissue. Adv Healthc Mater. 2021;10(1):e2001269.

235.	Owen R, Reilly GC. In vitro Models of Bone Remodelling and Associated Disorders. Front Bioeng Biotechnol. 2018;6:134.

236.	Tan SY, Leung Z, Wu AR. Recreating Physiological Environments In Vitro: Design Rules for Microfluidic-Based Vascularized Tissue Constructs. Small. 2020;16(9):1905055.

237.	Moysidou C-M, Barberio C, Owens RM. Advances in Engineering Human Tissue Models. Frontiers in Bioengineering and Biotechnology. 2021;8.

238.	De Pieri A, Rochev Y, Zeugolis DI. Scaffold-free cell-based tissue engineering therapies: advances, shortfalls and forecast. npj Regenerative Medicine. 2021;6(1):18.

239.	Mitry RR, Hughes RD. Human Cell Culture Protocols: Humana Press; 2016.

240.	Marchesan JT, Scanlon CS, Soehren S, Matsuo M, Kapila YL. Implications of cultured periodontal ligament cells for the clinical and experimental setting: a review. Arch Oral Biol. 2011;56(10):933-43.

241.	Lallier TE, Spencer A. Use of microarrays to find novel regulators of periodontal ligament fibroblast differentiation. Cell Tissue Res. 2007;327(1):93-109.

242.	Sawa Y, Phillips A, Hollard J, Yoshida S, Braithwaite MW. The in vitro life-span of human periodontal ligament fibroblasts. Tissue Cell. 2000;32(2):163-70.

243.	Sawa Y, Yamaoka Y, Kuroshima S, Yoshida S. Reduction of alkaline phosphatase activity in aged human osteogenic periodontal ligament fibroblasts exhibiting short telomeres. Cell Tissue Res. 2004;315(3):331-7.

244.	Stoddart MJ, Richards RG, Alini M. In vitro experiments with primary mammalian cells: to pool or not to pool? Eur Cell Mater. 2012;24:i-ii.

245.	Czekanska EM, Stoddart MJ, Richards RG, Hayes JS. In search of an osteoblast cell model for in vitro research. Eur Cell Mater. 2012;24:1-17.

246.	Kartsogiannis V, Ng KW. Cell lines and primary cell cultures in the study of bone cell biology. Mol Cell Endocrinol. 2004;228(1-2):79-102.

247.	Voegele TJ, Voegele-Kadletz M, Esposito V, Macfelda K, Oberndorfer U, Vecsei V, Schabus R. The effect of different isolation techniques on human osteoblast-like cell growth. Anticancer Res. 2000;20(5b):3575-81.

248. Jonsson KB, Frost A, Nilsson O, Ljunghall S, Ljunggren O. Three isolation techniques for primary culture of human osteoblast-like cells: a comparison. Acta Orthop Scand. 1999;70(4):365-73.

249. Martínez ME, del Campo MT, Medina S, Sánchez M, Sánchez-Cabezudo MJ, Esbrit P, et al. Influence of skeletal site of origin and donor age on osteoblastic cell growth and differentiation. Calcif Tissue Int. 1999;64(4):280-6.

250. Kasperk C, Wergedal J, Strong D, Farley J, Wangerin K, Gropp H, et al. Human bone cell phenotypes differ depending on their skeletal site of origin. J Clin Endocrinol Metab. 1995;80(8):2511-7.

251. Katzburg S, Lieberherr M, Ornoy A, Klein BY, Hendel D, Somjen D. Isolation and hormonal responsiveness of primary cultures of human bone-derived cells: gender and age differences. Bone. 1999;25(6):667-73.

252. Hammond TG, Hammond JM. Optimized suspension culture: the rotating-wall vessel. Am J Physiol Renal Physiol. 2001;281(1):F12-25.

253. Cinbiz MN, Tığlı RS, Beşkardeş IG, Gümüşderelioğlu M, Çolak Ü. Computational fluid dynamics modeling of momentum transport in rotating wall perfused bioreactor for cartilage tissue engineering. Journal of Biotechnology. 2010;150(3):389-95.

254. Krzysztof W, Søren A, Hans HJ, Karoline M, Torsten DB, Julie SV, et al. A Purpose-Built System for Culturing Cells as In Vivo Mimetic 3D Structures. In: Ziyad SH, Ibrokhim YA, Abdelwahed B, editors. Biomechanics and Functional Tissue Engineering. Rijeka: IntechOpen; 2021. p. Ch. 7.

255. Wrzesinski K. 3D spheroid culture - advanced user course. Lecture 4. Preparation for microgravity bioreacor handling. CelVivo IVS. 2019.

256. Schwarz RP, Goodwin TJ, Wolf DA. Cell culture for three-dimensional modeling in rotating-wall vessels: an application of simulated microgravity. J Tissue Cult Methods. 1992;14(2):51-7.

257. Fey S, Wrzesinski K, inventors; Drugmode Aps, Hoersholm (DK), assignee. Bioreactor with lid for easy access to incubation cavity. United States2013.

258. Clarke M, Sundaresan A, Vanderburg C, Banigan M, Pellis N. A Three-Dimensional Tissue Culture Model of Bone Formation Utilizing Rotational Co-Culture Of Human Adult Osteoblasts and Osteoclasts. Acta biomaterialia. 2013;9.

259. Penolazzi L, Lolli A, Sardelli L, Angelozzi M, Lambertini E, Trombelli L, et al. Establishment of a 3D-dynamic osteoblasts–osteoclasts co-culture model to simulate the jawbone microenvironment in vitro. Life Sciences. 2016;152.

260. Kaur G, Dufour JM. Cell lines: Valuable tools or useless artifacts. Spermatogenesis. 2012;2(1):1-5.

261. Castilho LR, editor Animal Cell Technology: From Biopharmaceuticals to Gene Therapy2009.

262. Kodama H-a, Amagai Y, Sudo H, Kasai S, Yamamoto S. Establishment of a clonal osteogenic cell line from newborn mouse calvaria. Japanese Journal of Oral Biology. 1981;23(4):899-901.

263. Owan I, Burr DB, Turner CH, Qiu J, Tu Y, Onyia JE, Duncan RL. Mechanotransduction in bone: osteoblasts are more responsive to fluid forces than mechanical strain. Am J Physiol. 1997;273(3 Pt 1):C810-5.

264. Genetos DC, Geist DJ, Liu D, Donahue HJ, Duncan RL. Fluid shear-induced ATP secretion mediates prostaglandin release in MC3T3-E1 osteoblasts. J Bone Miner Res. 2005;20(1):41-9.

265. You J, Reilly GC, Zhen X, Yellowley CE, Chen Q, Donahue HJ, Jacobs CR. Osteopontin gene regulation by oscillatory fluid flow via intracellular calcium mobilization and activation of mitogen-activated protein kinase in MC3T3-E1 osteoblasts. J Biol Chem. 2001;276(16):13365-71.

266. Quarles LD, Yohay DA, Lever LW, Caton R, Wenstrup RJ. Distinct proliferative and differentiated stages of murine MC3T3-E1 cells in culture: an in vitro model of osteoblast development. J Bone Miner Res. 1992;7(6):683-92.

267. Zhang X, Tiainen H, Haugen HJ. Comparison of titanium dioxide scaffold with commercial bone graft materials through micro-finite element modelling in flow perfusion. Medical & Biological Engineering & Computing. 2019;57(1):311-24.

268.	Bancroft GN, Sikavitsas VI, Mikos AG. Design of a flow perfusion bioreactor system for bone tissue-engineering applications. Tissue Eng. 2003;9(3):549-54.
269.	Janssen FW, Hofland I, van Oorschot A, Oostra J, Peters H, van Blitterswijk CA. Online measurement of oxygen consumption by goat bone marrow stromal cells in a combined cell-seeding and proliferation perfusion bioreactor. Journal of biomedical materials research Part A. 2006;79(2):338-48.
270.	Gaspar DA, Gomide V, Monteiro FJ. The role of perfusion bioreactors in bone tissue engineering. Biomatter. 2012;2(4):167-75.
271.	Chabanon M. Multiscale study of a perfusion bioreactor for bone tissue engineering 2015.
272.	Bancroft GN, Sikavitsas VI, van den Dolder J, Sheffield TL, Ambrose CG, Jansen JA, Mikos AG. Fluid flow increases mineralized matrix deposition in 3D perfusion culture of marrow stromal osteoblasts in a dose-dependent manner. Proceedings of the National Academy of Sciences. 2002;99(20):12600-5.
273.	Yamada S, Yassin MA, Schwarz T, Hansmann J, Mustafa K. Induction of osteogenic differentiation of bone marrow stromal cells on 3D polyester-based scaffolds solely by subphysiological fluidic stimulation in a laminar flow bioreactor. Journal of Tissue Engineering. 2021;12:20417314211019375.
274.	Bjerre L, Bünger CE, Kassem M, Mygind T. Flow perfusion culture of human mesenchymal stem cells on silicate-substituted tricalcium phosphate scaffolds. Biomaterials. 2008;29(17):2616-27.
275.	Beşkardeş IG, Aydın G, Bektaş Ş, Cengiz A, Gümüşderelioğlu M. A systematic study for optimal cell seeding and culture conditions in a perfusion mode bone-tissue bioreactor. Biochemical Engineering Journal. 2018;132:100-11.
276.	Wendt D, Marsano A, Jakob M, Heberer M, Martin I. Oscillating perfusion of cell suspensions through three-dimensional scaffolds enhances cell seeding efficiency and uniformity. Biotechnology and Bioengineering. 2003;84(2):205-14.
277.	Rauh J, Milan F, Günther KP, Stiehler M. Bioreactor systems for bone tissue engineering. Tissue Eng Part B Rev. 2011;17(4):263-80.
278.	Yeatts AB, Fisher JP. Bone tissue engineering bioreactors: dynamic culture and the influence of shear stress. Bone. 2011;48(2):171-81.
279.	Zhang ZY, Teoh SH, Teo EY, Khoon Chong MS, Shin CW, Tien FT, et al. A comparison of bioreactors for culture of fetal mesenchymal stem cells for bone tissue engineering. Biomaterials. 2010;31(33):8684-95.
280.	Sucosky P, Osorio DF, Brown JB, Neitzel GP. Fluid mechanics of a spinner-flask bioreactor. Biotechnology and bioengineering. 2004;85(1):34-46.
281.	Goldstein AS, Juarez TM, Helmke CD, Gustin MC, Mikos AG. Effect of convection on osteoblastic cell growth and function in biodegradable polymer foam scaffolds. Biomaterials. 2001;22(11):1279-88.
282.	Meinel L, Karageorgiou V, Fajardo R, Snyder B, Shinde-Patil V, Zichner L, et al. Bone tissue engineering using human mesenchymal stem cells: effects of scaffold material and medium flow. Annals of biomedical engineering. 2004;32(1):112-22.
283.	Sikavitsas VI, Bancroft GN, Mikos AG. Formation of three-dimensional cell/polymer constructs for bone tissue engineering in a spinner flask and a rotating wall vessel bioreactor. Journal of biomedical materials research. 2002;62(1):136-48.
284.	Granet C, Laroche N, Vico L, Alexandre C, Lafage-Proust MH. Rotating-wall vessels, promising bioreactors for osteoblastic cell culture: comparison with other 3D conditions. Medical and Biological Engineering and Computing. 1998;36(4):513-9.
285.	Gao H, Ayyaswamy PS, Ducheyne P. Dynamics of a microcarrier particle in the simulated microgravity environment of a rotating-wall vessel. Microgravity Sci Technol. 1997;10(3):154-65.
286.	Singh H, Teoh SH, Low HT, Hutmacher DW. Flow modelling within a scaffold under the influence of uni-axial and bi-axial bioreactor rotation. J Biotechnol. 2005;119(2):181-96.
287.	Linde F, Sørensen HC. The effect of different storage methods on the mechanical properties of trabecular bone. J Biomech. 1993;26(10):1249-52.

288.   Vesper EO, Hammond MA, Allen MR, Wallace JM. Even with rehydration, preservation in ethanol influences the mechanical properties of bone and how bone responds to experimental manipulation. Bone. 2017;97:49-53.

289.   Dorlot J-M, Ait Ba Sidi M, Tremblay GM, Drouin G. Load Elongation Behavior of the Canine Anterior Cruciate Ligament. Journal of Biomechanical Engineering. 1980;102(3):190-3.

290.   Woo SL, Orlando CA, Camp JF, Akeson WH. Effects of postmortem storage by freezing on ligament tensile behavior. J Biomech. 1986;19(5):399-404.

291.   Rho JY, Pharr GM. Effects of drying on the mechanical properties of bovine femur measured by nanoindentation. J Mater Sci Mater Med. 1999;10(8):485-8.

292.   Nyman JS, Roy A, Shen X, Acuna RL, Tyler JH, Wang X. The influence of water removal on the strength and toughness of cortical bone. J Biomech. 2006;39(5):931-8.

293.   Zysset PK, Guo XE, Hoffler CE, Moore KE, Goldstein SA. Elastic modulus and hardness of cortical and trabecular bone lamellae measured by nanoindentation in the human femur. J Biomech. 1999;32(10):1005-12.

294.   Rho JY, Roy ME, 2nd, Tsui TY, Pharr GM. Elastic properties of microstructural components of human bone tissue as measured by nanoindentation. J Biomed Mater Res. 1999;45(1):48-54.

295.   Hoffler CE, Moore KE, Kozloff K, Zysset PK, Brown MB, Goldstein SA. Heterogeneity of bone lamellar-level elastic moduli. Bone. 2000;26(6):603-9.

296.   Rodriguez-Florez N, Oyen ML, Shefelbine SJ. Insight into differences in nanoindentation properties of bone. Journal of the Mechanical Behavior of Biomedical Materials. 2013;18:90-9.

297.   He JY, Zhang ZL, Kristiansen H. Nanomechanical characterization of single micron-sized polymer particles. Journal of Applied Polymer Science. 2009;113(3):1398-405.

298.   Fill TS, Carey JP, Toogood RW, Major PW. Experimentally determined mechanical properties of, and models for, the periodontal ligament: critical review of current literature. J Dent Biomech. 2011;2011:312980.

299.   Nolan T, Hands RE, Bustin SA. Quantification of mRNA using real-time RT-PCR. Nature Protocols. 2006;1(3):1559-82.

300.   Ginzinger DG. Gene quantification using real-time quantitative PCR: an emerging technology hits the mainstream. Exp Hematol. 2002;30(6):503-12.

301.   Green MR, Sambrook J. Isolation of Poly(A)(+) Messenger RNA Using Magnetic Oligo(dT) Beads. Cold Spring Harb Protoc. 2019;2019(10).

302.   Chomczynski P, Sacchi N. Single-step method of RNA isolation by acid guanidinium thiocyanate-phenol-chloroform extraction. Analytical Biochemistry. 1987;162(1):156-9.

303.   Ali N, Rampazzo RCP, Costa ADT, Krieger MA. Current Nucleic Acid Extraction Methods and Their Implications to Point-of-Care Diagnostics. Biomed Res Int. 2017;2017:9306564.

304.   Juncker D, Bergeron S, Laforte V, Li H. Cross-reactivity in antibody microarrays and multiplexed sandwich assays: shedding light on the dark side of multiplexing. Current Opinion in Chemical Biology. 2014;18:29-37.

305.   Wendisch VF, Zimmer DP, Khodursky A, Peter B, Cozzarelli N, Kustu S. Isolation of Escherichia coli mRNA and comparison of expression using mRNA and total RNA on DNA microarrays. Anal Biochem. 2001;290(2):205-13.

306.   Nykjaer A, Dragun D, Walther D, Vorum H, Jacobsen C, Herz J, et al. An endocytic pathway essential for renal uptake and activation of the steroid 25-(OH) vitamin D3. Cell. 1999;96(4):507-15.

307.   Nykjaer A, Fyfe JC, Kozyraki R, Leheste JR, Jacobsen C, Nielsen MS, et al. Cubilin dysfunction causes abnormal metabolism of the steroid hormone 25(OH) vitamin D(3). Proc Natl Acad Sci U S A. 2001;98(24):13895-900.

308.   Lian JB, Stein GS. Concepts of osteoblast growth and differentiation: basis for modulation of bone cell development and tissue formation. Crit Rev Oral Biol Med. 1992;3(3):269-305.

309.   Lin RZ, Chang HY. Recent advances in three-dimensional multicellular spheroid culture for biomedical research. Biotechnol J. 2008;3(9-10):1172-84.

310.   Khaitan D, Chandna S, Arya MB, Dwarakanath BS. Establishment and characterization of multicellular spheroids from a human glioma cell line; Implications for tumor therapy. Journal of translational medicine. 2006;4:12-.

311.   Williams CG, Lee HJ, Asatsuma T, Vento-Tormo R, Haque A. An introduction to spatial transcriptomics for biomedical research. Genome Medicine. 2022;14(1):68.

312.   Leng SX, McElhaney JE, Walston JD, Xie D, Fedarko NS, Kuchel GA. ELISA and multiplex technologies for cytokine measurement in inflammation and aging research. J Gerontol A Biol Sci Med Sci. 2008;63(8):879-84.

313.   Khalifian S, Raimondi G, Brandacher G. The use of luminex assays to measure cytokines. J Invest Dermatol. 2015;135(4):1-5.

314.   Elshal M, McCoy J. Multiplex Bead Array Assays: Performance Evaluation and Comparison of Sensitivity to ELISA. Methods (San Diego, Calif). 2006;38:317-23.

315.   Costa E, Moreira A, de Melo-Diogo D, Gaspar V, Carvalho M, Correia I. 3D tumor spheroids: an overview on the tools and techniques used for their analysis. Biotechnology Advances. 2016;34.

316.   Moss DW. Perspectives in alkaline phosphatase research. Clin Chem. 1992;38(12):2486-92.

317.   Fishman WH. Alkaline phosphatase isozymes: recent progress. Clin Biochem. 1990;23(2):99-104.

318.   Vimalraj S. Alkaline phosphatase: Structure, expression and its function in bone mineralization. Gene. 2020;754:144855.

319.   Sharma U, Pal D, Prasad R. Alkaline phosphatase: an overview. Indian J Clin Biochem. 2014;29(3):269-78.

320.   Lorenz U. Protein Tyrosine Phosphatase Assays. Current Protocols in Immunology. 2011;93(1):11.7.1-.7.2.

321.   Kusumbe AP, Ramasamy SK, Starsichova A, Adams RH. Sample preparation for high-resolution 3D confocal imaging of mouse skeletal tissue. Nature Protocols. 2015;10(12):1904-14.

322.   Stein H, Gatter KC, Heryet A, Mason DY. Freeze-dried paraffin-embedded human tissue for antigen labelling with monoclonal antibodies. Lancet. 1984;2(8394):71-3.

323.   Kudo A, Kii I. Periostin function in communication with extracellular matrices. J Cell Commun Signal. 2018;12(1):301-8.

324.   Pullisaar H, Colaianni G, Lian AM, Vandevska-Radunovic V, Grano M, Reseland JE. Irisin promotes growth, migration and matrix formation in human periodontal ligament cells. Arch Oral Biol. 2020;111:104635.

325.   Li Y, Yu SM. Targeting and mimicking collagens via triple helical peptide assembly. Curr Opin Chem Biol. 2013;17(6):968-75.

326.   Hwang J, Huang Y, Burwell TJ, Peterson NC, Connor J, Weiss SJ, et al. In Situ Imaging of Tissue Remodeling with Collagen Hybridizing Peptides. ACS Nano. 2017;11(10):9825-35.

327.   Munir A, Reseland JE, Tiainen H, Haugen HJ, Sikorski P, Christiansen EF, et al. Osteocyte-Like Cells Differentiated From Primary Osteoblasts in an Artificial Human Bone Tissue Model. JBMR Plus. 2023;7(9):e10792.

328.   Elliott AD. Confocal Microscopy: Principles and Modern Practices. Curr Protoc Cytom. 2020;92(1):e68.

329.   Bills CE, Eisenberg H, Pallante SL. Complexes of organic acids with calcium phosphate: the von Kossa stain as a clue to the composition of bone mineral. Johns Hopkins Med J. 1971;128(4):194-207.

330.   Luna LG. Histopathologic Methods and Color Atlas of Special Stains and Tissue Artifacts: American Histolabs; 1992.

331.   Sheehan DC, Hrapchak BB. Theory and practice of histotechnology: Mosby; 1980.

332.   Puchtler H, Meloan SN, Terry MS. On the history and mechanism of alizarin and alizarin red S stains for calcium. Journal of Histochemistry & Cytochemistry. 1969;17(2):110-24.

333.   Gruber HE. Adaptations of Goldner's Masson trichrome stain for the study of undecalcified plastic embedded bone. Biotech Histochem. 1992;67(1):30-4.

334.	Wang Y-H, Liu Y, Maye P, Rowe DW. Examination of mineralized nodule formation in living osteoblastic cultures using fluorescent dyes. Biotechnology progress. 2006;22(6):1697-701.

335.	Barge A, Cravotto G, Gianolio E, Fedeli F. How to determine free Gd and free ligand in solution of Gd chelates. A technical note. Contrast Media Mol Imaging. 2006;1(5):184-8.

336.	Schweitzer C, Scaiano JC. Selective binding and local photophysics of the fluorescent cyanine dye PicoGreen in double-stranded and single-stranded DNA. Physical Chemistry Chemical Physics. 2003;5(21):4911-7.

337.	Dragan AI, Casas-Finet JR, Bishop ES, Strouse RJ, Schenerman MA, Geddes CD. Characterization of PicoGreen interaction with dsDNA and the origin of its fluorescence enhancement upon binding. Biophys J. 2010;99(9):3010-9.

338.	Singer VL, Jones LJ, Yue ST, Haugland RP. Characterization of PicoGreen Reagent and Development of a Fluorescence-Based Solution Assay for Double-Stranded DNA Quantitation. Analytical Biochemistry. 1997;249(2):228-38.

339.	O'neill M, McPartlin J, Arthure K, Riedel S, McMillan N, editors. Comparison of the TLDA with the Nanodrop and the reference Qubit system. Journal of Physics: Conference Series; 2011: IOP Publishing.

340.	Bruijns B, Hoekema T, Oomens L, Tiggelaar R, Gardeniers H. Performance of Spectrophotometric and Fluorometric DNA Quantification Methods. Analytica. 2022;3(3):371-84.

341.	Yamada KM, Cukierman E. Modeling Tissue Morphogenesis and Cancer in 3D. Cell. 2007;130(4):601-10.

342.	Fatehullah A, Tan SH, Barker N. Organoids as an in vitro model of human development and disease. Nature Cell Biology. 2016;18(3):246-54.

343.	Wu X, Su J, Wei J, Jiang N, Ge X. Recent Advances in Three-Dimensional Stem Cell Culture Systems and Applications. Stem Cells Int. 2021;2021:9477332.

344.	Bissell MJ, Rizki A, Mian IS. Tissue architecture: the ultimate regulator of breast epithelial function. Curr Opin Cell Biol. 2003;15(6):753-62.

345.	Roskelley CD, Desprez PY, Bissell MJ. Extracellular matrix-dependent tissue-specific gene expression in mammary epithelial cells requires both physical and biochemical signal transduction. Proc Natl Acad Sci U S A. 1994;91(26):12378-82.

346.	Weaver VM, Petersen OW, Wang F, Larabell CA, Briand P, Damsky C, Bissell MJ. Reversion of the malignant phenotype of human breast cells in three-dimensional culture and in vivo by integrin blocking antibodies. J Cell Biol. 1997;137(1):231-45.

347.	Fennema E, Rivron N, Rouwkema J, van Blitterswijk C, de Boer J. Spheroid culture as a tool for creating 3D complex tissues. Trends in biotechnology. 2013;31(2):108-15.

348.	Jensen C, Teng Y. Is It Time to Start Transitioning From 2D to 3D Cell Culture? Front Mol Biosci. 2020;7:33.

349.	Bonnans C, Chou J, Werb Z. Remodelling the extracellular matrix in development and disease. Nat Rev Mol Cell Biol. 2014;15(12):786-801.

350.	Yang Y, Geng T, Samara A, Olstad OK, He J, Agger AE, et al. Recombinant irisin enhances the extracellular matrix formation, remodeling potential, and differentiation of human periodontal ligament cells cultured in 3D. J Periodontal Res. 2023;58(2):336-49.

351.	Chukkapalli SS, Lele TP. Periodontal cell mechanotransduction. Open Biol. 2018;8(9).

352.	Mathes SH, Wohlwend L, Uebersax L, von Mentlen R, Thoma DS, Jung RE, et al. A bioreactor test system to mimic the biological and mechanical environment of oral soft tissues and to evaluate substitutes for connective tissue grafts. Biotechnol Bioeng. 2010;107(6):1029-39.

353.	Baru O, Nutu A, Braicu C, Cismaru CA, Berindan-Neagoe I, Buduru S, Badea M. Angiogenesis in Regenerative Dentistry: Are We Far Enough for Therapy? Int J Mol Sci. 2021;22(2).

354.	Sano K, Usui M, Moritani Y, Nakazawa K, Hanatani T, Kondo H, et al. Co-cultured spheroids of human periodontal ligament mesenchymal stem cells and vascular endothelial cells enhance periodontal tissue regeneration. Regen Ther. 2020;14:59-71.

355.   Pandula PK, Samaranayake LP, Jin LJ, Zhang CF. Human umbilical vein endothelial cells synergize osteo/odontogenic differentiation of periodontal ligament stem cells in 3D cell sheets. J Periodontal Res. 2014;49(3):299-306.

356.   Handorf AM, Zhou Y, Halanski MA, Li WJ. Tissue stiffness dictates development, homeostasis, and disease progression. Organogenesis. 2015;11(1):1-15.

357.   Kular JK, Basu S, Sharma RI. The extracellular matrix: Structure, composition, age-related differences, tools for analysis and applications for tissue engineering. J Tissue Eng. 2014;5:2041731414557112.

358.   Sebens S, Schafer H. The tumor stroma as mediator of drug resistance--a potential target to improve cancer therapy? Curr Pharm Biotechnol. 2012;13(11):2259-72.

359.   Dickreuter E, Cordes N. The cancer cell adhesion resistome: mechanisms, targeting and translational approaches. Biol Chem. 2017;398(7):721-35.

360.   Holle AW, Young JL, Spatz JP. In vitro cancer cell-ECM interactions inform in vivo cancer treatment. Adv Drug Deliv Rev. 2016;97:270-9.

361.   Barczyk M, Bolstad AI, Gullberg D. Role of integrins in the periodontal ligament: organizers and facilitators. Periodontol 2000. 2013;63(1):29-47.

362.   Dangaria SJ, Ito Y, Walker C, Druzinsky R, Luan X, Diekwisch TG. Extracellular matrix-mediated differentiation of periodontal progenitor cells. Differentiation. 2009;78(2-3):79-90.

363.   Kaku M, Yamauchi M. Mechano-regulation of collagen biosynthesis in periodontal ligament. J Prosthodont Res. 2014;58(4):193-207.

364.   Checchi V, Maravic T, Bellini P, Generali L, Consolo U, Breschi L, Mazzoni A. The Role of Matrix Metalloproteinases in Periodontal Disease. Int J Environ Res Public Health. 2020;17(14).

365.   Dariima T, Jin GZ, Lee EJ, Wall IB, Kim HW. Cooperation between osteoblastic cells and endothelial cells enhances their phenotypic responses and improves osteoblast function. Biotechnol Lett. 2013;35(7):1135-43.

366.   Walser R, Metzger W, Görg A, Pohlemann T, Menger MD, Laschke MW. Generation of co-culture spheroids as vascularisation units for bone tissue engineering. Eur Cell Mater. 2013;26:222-33.

367.   Hayden RS, Vollrath M, Kaplan DL. Effects of clodronate and alendronate on osteoclast and osteoblast co-cultures on silk-hydroxyapatite films. Acta Biomater. 2014;10(1):486-93.

368.   Jones GL, Motta A, Marshall MJ, El Haj AJ, Cartmell SH. Osteoblast: osteoclast co-cultures on silk fibroin, chitosan and PLLA films. Biomaterials. 2009;30(29):5376-84.

369.   Heinemann C, Heinemann S, Worch H, Hanke T. Development of an osteoblast/osteoclast co-culture derived by human bone marrow stromal cells and human monocytes for biomaterials testing. Eur Cell Mater. 2011;21:80-93.

370.   Schmid FV, Kleinhans C, Schmid FF, Kluger PJ. Osteoclast Formation within a Human Co-Culture System on Bone Material as an In Vitro Model for Bone Remodeling Processes. Journal of Functional Morphology and Kinesiology. 2018;3(1):17.

371.   Papadimitropoulos A, Scherberich A, Güven S, Theilgaard N, Crooijmans HJ, Santini F, et al. A 3D in vitro bone organ model using human progenitor cells. European cells & materials. 2011;21:445-58; discussion 58.

372.   Beşkardeş IG, Hayden RS, Glettig DL, Kaplan DL, Gümüşderelioğlu M. Bone tissue engineering with scaffold-supported perfusion co-cultures of human stem cell-derived osteoblasts and cell line-derived osteoclasts. Process Biochemistry. 2017;59:303-11.

373.   Lee DY, Lee SY, Yun SH, Jeong JW, Kim JH, Kim HW, et al. Review of the Current Research on Fetal Bovine Serum and the Development of Cultured Meat. Food Sci Anim Resour. 2022;42(5):775-99.

374.   Nam K-H, Smith AST, Lone S, Kwon S, Kim D-H. Biomimetic 3D Tissue Models for Advanced High-Throughput Drug Screening. SLAS Technology. 2015;20(3):201-15.

375.   Li Y, Zhou M, Zheng W, Yang J, Jiang N. Scaffold-based tissue engineering strategies for soft–hard interface regeneration. Regenerative Biomaterials. 2022;10.

376.   Giannobile WV. Periodontal tissue engineering by growth factors. Bone. 1996;19(1, Supplement 1):S23-S37.

377.   ten Dijke P, Iwata KK. Growth Factors For Wound Healing. Bio/Technology. 1989;7(8):793-8.

378.   Azevedo HS, Pashkuleva I. Biomimetic supramolecular designs for the controlled release of growth factors in bone regeneration. Advanced Drug Delivery Reviews. 2015;94:63-76.

379.   Chen N, Li Q, Liu J, Jia S. Irisin, an exercise-induced myokine as a metabolic regulator: an updated narrative review. Diabetes Metab Res Rev. 2016;32(1):51-9.

380.   Colaianni G, Cuscito C, Mongelli T, Pignataro P, Buccoliero C, Liu P, et al. The myokine irisin increases cortical bone mass. Proceedings of the National Academy of Sciences. 2015;112(39):12157-62.

381.   Nagaoka I, Igarashi M, Hua J, Ju Y, Yomogida S, Sakamoto K. Recent aspects of the anti-inflammatory actions of glucosamine. Carbohydrate Polymers. 2011;84(2):825-30.

382.   Nagaoka I, Tsuruta A, Yoshimura M. Chondroprotective action of glucosamine, a chitosan monomer, on the joint health of athletes. Int J Biol Macromol. 2019;132:795-800.

383.   Bikle DD. Vitamin D and bone. Curr Osteoporos Rep. 2012;10(2):151-9.

384.   Akbari S, Rasouli-Ghahroudi AA. Vitamin K and Bone Metabolism: A Review of the Latest Evidence in Preclinical Studies. Biomed Res Int. 2018;2018:4629383.

385.   Hewison M. Vitamin D and innate and adaptive immunity. Vitam Horm. 2011;86:23-62.

386.   Yin K, Agrawal DK. Vitamin D and inflammatory diseases. J Inflamm Res. 2014;7:69-87.

387.   Lips P, van Schoor NM. The effect of vitamin D on bone and osteoporosis. Best Practice & Research Clinical Endocrinology & Metabolism. 2011;25(4):585-91.

388.   Iwamoto J. Vitamin K_2 therapy for postmenopausal osteoporosis. Nutrients. 2014;6(5):1971-80.

389.   Salma, Ahmad SS, Karim S, Ibrahim IM, Alkreathy HM, Alsieni M, Khan MA. Effect of Vitamin K on Bone Mineral Density and Fracture Risk in Adults: Systematic Review and Meta-Analysis. Biomedicines. 2022;10(5).

390.   Johnson BZ, Stevenson AW, Prêle CM, Fear MW, Wood FM. The Role of IL-6 in Skin Fibrosis and Cutaneous Wound Healing. Biomedicines. 2020;8(5).

391.   Macleod T, Berekmeri A, Bridgewood C, Stacey M, McGonagle D, Wittmann M. The Immunological Impact of IL-1 Family Cytokines on the Epidermal Barrier. Frontiers in Immunology. 2021;12.

392.   Prudovsky I. Cellular Mechanisms of FGF-Stimulated Tissue Repair. Cells. 2021;10(7).

393.   Charoenlarp P, Rajendran AK, Iseki S. Role of fibroblast growth factors in bone regeneration. Inflammation and regeneration. 2017;37:10.

394.   Jorde R, Stunes AK, Kubiak J, Joakimsen R, Grimnes G, Thorsby PM, Syversen U. Effects of vitamin D supplementation on bone turnover markers and other bone-related substances in subjects with vitamin D deficiency. Bone. 2019;124:7-13.

395.   Holick MF. Vitamin D deficiency. N Engl J Med. 2007;357(3):266-81.

396.   Liu K, Meng H, Hou J. Characterization of the Autocrine/Paracrine Function of Vitamin D in Human Gingival Fibroblasts and Periodontal Ligament Cells. PLOS ONE. 2012;7(6):e39878.

397.   Andrukhov O, Blufstein A, Behm C, Moritz A, Rausch-Fan X. Vitamin D3 and Dental Mesenchymal Stromal Cells. Applied Sciences. 2020;10(13):4527.

398.   Lee HJ, Song YM, Baek S, Park YH, Park JB. Vitamin D Enhanced the Osteogenic Differentiation of Cell Spheroids Composed of Bone Marrow Stem Cells. Medicina (Kaunas). 2021;57(11).

399.   Vu AA, Bose S. Effects of vitamin D3 release from 3D printed calcium phosphate scaffolds on osteoblast and osteoclast cell proliferation for bone tissue engineering. RSC Advances. 2019;9(60):34847-53.

400.   Mandatori D, Penolazzi L, Pipino C, Di Tomo P, Di Silvestre S, Di Pietro N, et al. Menaquinone-4 enhances osteogenic potential of human amniotic fluid mesenchymal stem cells cultured in 2D and 3D dynamic culture systems. Journal of tissue engineering and regenerative medicine. 2018;12(2):447-59.

401.	Harada S, Matsumoto T, Ogata E. Role of ascorbic acid in the regulation of proliferation in osteoblast-like MC3T3-E1 cells. J Bone Miner Res. 1991;6(9):903-8.

402.	Franceschi RT, Iyer BS. Relationship between collagen synthesis and expression of the osteoblast phenotype in MC3T3-E1 cells. J Bone Miner Res. 1992;7(2):235-46.

403.	Xiao G, Cui Y, Ducy P, Karsenty G, Franceschi RT. Ascorbic acid-dependent activation of the osteocalcin promoter in MC3T3-E1 preosteoblasts: requirement for collagen matrix synthesis and the presence of an intact OSE2 sequence. Mol Endocrinol. 1997;11(8):1103-13.

404.	Urban K, Höhling HJ, Lüttenberg B, Szuwart T, Plate U. An in vitro study of osteoblast vitality influenced by the vitamins C and E. Head Face Med. 2012;8:25.

405.	Sato T, Inaba N, Yamashita T. MK-7 and Its Effects on Bone Quality and Strength. Nutrients. 2020;12(4).

406.	Sato T. Vitamin K2 and Bone Quality. Vitamins & Minerals. 2013;s6.

407.	Woeckel VJ, Alves RD, Swagemakers SM, Eijken M, Chiba H, van der Eerden BC, van Leeuwen JP. 1Alpha,25-(OH)2D3 acts in the early phase of osteoblast differentiation to enhance mineralization via accelerated production of mature matrix vesicles. J Cell Physiol. 2010;225(2):593-600.

408.	van Driel M, Koedam M, Buurman CJ, Roelse M, Weyts F, Chiba H, et al. Evidence that both 1alpha,25-dihydroxyvitamin D3 and 24-hydroxylated D3 enhance human osteoblast differentiation and mineralization. Journal of cellular biochemistry. 2006;99(3):922-35.

409.	Koshihara Y, Hoshi K, Ishibashi H, Shiraki M. Vitamin K2 promotes 1alpha,25(OH)2 vitamin D3-induced mineralization in human periosteal osteoblasts. Calcified tissue international. 1996;59(6):466-73.

410.	Poon CC, Li RW, Seto SW, Kong SK, Ho HP, Hoi MP, et al. In vitro vitamin K(2) and 1α,25-dihydroxyvitamin D(3) combination enhances osteoblasts anabolism of diabetic mice. Eur J Pharmacol. 2015;767:30-40.

411.	Lancaster C, Harrison R. Effects of Vitamin D, K1, and K2 Supplementation on Bone Formation by Osteoblasts In Vitro: A Meta-analysis. Journal of Biometrics & Biostatistics. 2017;08.

412.	Kidd PM. Vitamins D and K as pleiotropic nutrients: clinical importance to the skeletal and cardiovascular systems and preliminary evidence for synergy. Altern Med Rev. 2010;15(3):199-222.

413.	van Ballegooijen AJ, Pilz S, Tomaschitz A, Grübler MR, Verheyen N. The Synergistic Interplay between Vitamins D and K for Bone and Cardiovascular Health: A Narrative Review. Int J Endocrinol. 2017;2017:7454376.

414.	Ushiroyama T, Ikeda A, Ueki M. Effect of continuous combined therapy with vitamin K(2) and vitamin D(3) on bone mineral density and coagulofibrinolysis function in postmenopausal women. Maturitas. 2002;41(3):211-21.

415.	Iwamoto J, Takeda T, Ichimura S. Effect of combined administration of vitamin D3 and vitamin K2 on bone mineral density of the lumbar spine in postmenopausal women with osteoporosis. J Orthop Sci. 2000;5(6):546-51.

416.	Kuang X, Liu C, Guo X, Li K, Deng Q, Li D. The combination effect of vitamin K and vitamin D on human bone quality: a meta-analysis of randomized controlled trials. Food Funct. 2020;11(4):3280-97.

I

II

ORIGINAL ARTICLE

Vitamin K2 Modulates Vitamin D-Induced Mechanical Properties of Human 3D Bone Spheroids In Vitro

Maria Schröder,[1] Elisabeth Aurstad Riksen,[1] Jianying He,[2] Bjørn Helge Skallerud,[2] Mona Elisabeth Møller,[3] Aina-Mari Lian,[4] Unni Syversen,[4,5,6] and Janne Elin Reseland[1]

[1]Department of Biomaterials, University of Oslo, Oslo, Norway
[2]Department of Structural Engineering, Faculty of Engineering, Norwegian University of Science and Technology (NTNU), Trondheim, Norway
[3]Axial Vita AS, Oslo, Norway
[4]Oral Research Laboratory, Institute for Clinical Dentistry, University of Oslo, Oslo, Norway
[5]Department of Clinical and Molecular Medicine, NTNU, Trondheim, Norway
[6]Department of Endocrinology, Clinic of Medicine, St. Olavs Hospital, Trondheim University Hospital, Trondheim, Norway

ABSTRACT

Rotational culture promotes primary human osteoblasts (hOBs) to form three-dimensional (3D) multicellular spheroids with bone tissue-like structure without any scaffolding material. Cell-based bone models enable us to investigate the effect of different agents on the mechanical strength of bone. Given that low dietary intake of both vitamin D and K is negatively associated with fracture risk, we aimed to assess the effect of these vitamins in this system. Osteospheres of hOBs were generated with menaquinone-4 (MK-4; 10μM) and 25-hydroxyvitamin D_3 [25(OH)D_3; 0.01μM], alone and in combination, or without vitamins. The mechanical properties were tested by nanoindentation using a flat-punch compression method, and the mineralized extracellular bone matrix was characterized by microscopy. The in vitro response of hOBs to MK-4 and 25(OH)D_3 was further evaluated in two-dimensional (2D) cultures and in the 3D bone constructs applying gene expression analysis and multiplex immunoassays. Mechanical testing revealed that 25(OH)D_3 induced a stiffer and MK-4 a softer or more flexible osteosphere compared with control. Combined vitamin conditions induced the same flexibility as MK-4 alone. Enhanced levels of periostin ($p < 0.001$) and altered distribution of collagen type I (COL-1) were found in osteospheres supplemented with MK-4. In contrast, 25(OH)D_3 reduced COL-1, both at the mRNA and protein levels, increased alkaline phosphatase, and stimulated mineral deposition in the osteospheres. With the two vitamins in combination, enhanced gene expression of periostin and COL-1 was seen, as well as extended osteoid formation into the central region and increased mineral deposition all over the area. Moreover, we observed enhanced levels of osteocalcin in 2D and osteopontin in 3D cultures exposed to 25(OH)D_3 alone and combined with MK-4. In conclusion, the two vitamins seem to affect bone mechanical properties differently: vitamin D enhancing stiffness and K2 conveying flexibility to bone. These effects may translate to increased fracture resistance in vivo. © 2020 The Authors. *JBMR Plus* published by Wiley Periodicals LLC on behalf of American Society for Bone and Mineral Research.

KEY WORDS: BONE STIFFNESS; OSTEOBLASTS; OSTEOSPHERES; VITAMIN D; VITAMIN K2

Introduction

Three-dimendional (3D) bone spheroids, also referred to as osteospheres, represent new in vitro models to study the molecular mechanisms of bone remodeling,[1] as well as the pathophysiology of bone diseases and healing.[2] Slow horizontal clinorotation promotes aggregation and differentiation of bone cells into bone tissue-like structures without the inclusion of any scaffold material.[1,3–5] Under these culture conditions, primary human osteoblasts (hOBs) form a self-assembled mineralized extracellular matrix within the 3D bone spheroids.[1] We

have previously shown that these spheroids represent a suitable model for assessment of the effect of various stimuli on the biomechanical properties of bone.[6]

Vitamin D stimulates the absorption of calcium and phosphate from the intestine. Low serum vitamin D levels induce secondary hyperparathyroidism, leading to increased bone resorption, decreased BMD, and a higher fracture incidence.[7] Vitamin D is mainly synthesized in the skin after exposure to sunlight, but is also obtained from dietary sources. Vitamin D is metabolized to 25-hydroxyvitamin D_3 [25(OH)D_3] in the liver, and to 1,25-dihydroxyvitamin D_3 [1,25(OH)$_2D_3$] in the kidneys

by the enzyme 1α-hydroxylase.[8] 1,25(OH)$_2$D$_3$ is the biologically active form,[9] whereas 25(OH)D$_3$ levels are used as a measure of vitamin D status.[10] 1α-hydroxylase, as well as the vitamin D receptor, is also expressed in osteoblasts.[11–15] For studies of the effect of vitamin D on osteoblasts in vitro, 25(OH)D$_3$ is preferred over 1,25(OH)$_2$D$_3$ because of its longer half-life time.[16]

Menaquinones, referred to as vitamin K2, are a family of molecules consisting of a 2-methyl-1,4-naphthoquinone structure with a variable number of 3′-substituted isoprene units.[17] The main dietary menaquinones are MK-4 to MK-10, which are found in fermented food and animal products.[18,19] Vitamin K-dependent proteins have been isolated in bone, cartilage, kidney, and vascular and soft tissues.[20] These proteins include, among others, osteocalcin (OC) and periostin.[21] OC gene expression is regulated by 1,25(OH)$_2$D$_3$,[22] whereas the protein's capability to bind to calcium relies on the vitamin K-dependent gamma-carboxylation of three glutamic acid residues in the molecule.[23] Periostin is a matricellular protein involved in the regulation of collagen fibril diameter and cross-linking.[24] Vitamin K2 also exerts direct effects on bone cells, stimulating osteoblastogenesis[25–27] and inhibiting the osteoclast differentiation.[25,27] Vitamin K2 has been reported to bind to the steroid and xenobiotic receptor (SXR), resulting in enhanced expression of several components of the bone matrix.[26] Low vitamin K intake, as well as high levels of undercarboxylated OC (unOC), is associated with an increased risk of bone fragility concomitant with hip fractures in elderly patients.[28–30]

The vitamin K2 synthetic form MK-4 is approved in antiosteoporosis therapy in Japan and is frequently used in combination with bisphosphonates.[31] However, the effect of MK-4 on BMD and fracture risk remains a controversy.[32] Combined administration of vitamin D and K is suggested to have synergistic positive effects on calcium homeostasis and bone and cardiovascular health.[33] Vitamin D enhances vitamin K-dependent bone protein production.[34,35] Both vitamin D and K have been demonstrated to be cofactors in the gamma-carboxylation of OC.[36,37] An increasing number of randomized controlled trials have also evaluated the combined treatment of vitamin K2 and D with different outcomes.[38–40]

Both vitamins D and K play important roles in bone health; however, their combined effects on mechanical properties of 3D bone spheroids have, to our knowledge, not been studied before. Therefore, we wanted to investigate the in vitro effects of vitamin D and K, alone and in combination on the biomechanical properties of 3D bone spheroids of primary hOBs. To elucidate the molecular mechanisms, we aimed at identifying the effect of these vitamins on the gene expression and secretion of proteins and cytokines involved in the biological and mechanical functions of bone in both 2D cell cultures of primary hOBs and in 3D bone constructs.

Materials and Methods

2D Cell cultures

Commercially available primary hOBs (NHOst cell system; Lonza, Walkersville, MD, USA) were grown in osteoblast growth medium (OGM; Lonza) at 37°C in a humidified atmosphere of 95% air and 5% CO$_2$. The medium was changed three times weekly, and the cells were subcultured and seeded in 24-well-plates. At confluence, synthetic vitamin K2, MK-4 (at 1μM and 10μM; gift from Kappa Biosciences, Oslo, Norway), and 25(OH)D$_3$ (0.01μM; Calcifediol CRS; European Pharacopoeia Reference Standard, EDQM, Strasbourg,

France) were added alone or in combination to the culture medium. Cells cultured with regular OGM were used as control. Cell culture media were harvested after 1, 7, 14, and 20 days of incubation.

Generation of 3D osteospheres

Primary hOBs (Lonza) were cultured in OGM (PromoCell, Heidelberg, Germany) with supplement mix (PromoCell) and 100 U mL^{-1} penicillin and 100 μg/mL^{-1} streptomycin (PAA Laboratories GmbH, Pasching, Austria). hOBs (>3 × 10^6 cells) were inoculated into CelVivo 10-mL bioreactors (Cat. no. DM 010; CelVivo, Blommenslyst, Denmark), and osteospheres were generated in the BioArray Matrix drive BAM v4 (CelVivo) in a humidified atmosphere with 5% CO$_2$ at 37°C at a rotation speed of 4 rpm. On culture day 7, the medium was supplemented with 10mM β-glycerophosphate, 50 μg/mL^{-1} ascorbic acid, and 200nM hydrocortisone-21-hemisuccinate (Sigma-Aldrich, St. Louis, MO, USA). MK-4 (10μM) (gift from Kappa Biosciences) and 25(OH)D$_3$ (0.01μM; EDQM) were added alone or in combination. Cell medium without vitamins (untreated) was used as control. Culture medium was changed every 3 days. Osteospheres (approximately 2 mm in diameter) were harvested after 21 days and divided into two halves with a scalpel. One half was stored in −80°C until the mechanical testing. The other half was fixed, sectioned, and evaluated by confocal microscopy.

Mechanical testing of osteospheres

The semispheres were thawed overnight and dried for 24 to 48 hours at room temperature in air. The main global geometry, ie, the surface at the equatorial plane and the height of the samples, was established with a microscope. μCT scanning was not applicable because of the low density of the immature bone tissue. Based on the size of a pixel in the microscope image, the size of the surface was transformed into real size. Assuming an elliptical cross section, a section area was determined and used to calculate the equivalent circular cross section with an equivalent radius. The average cross-section radius and the height of the samples were applied in finding stress and strain measures from the measured global force and displacement in the mechanical testing of the semiosteospheres. The mechanical response of the osteospheres at room temperature was characterized by nanoindentation using a Hysitron TI950 TriboIndenter (Hysitron, Minneapolis, MN, USA). Because of the irregular geometry of the samples, conventional nanoindentation was not applicable. Instead, a so-called flat-punch method for a compression test of the particle-like materials was used.[41] The semispheres were placed on a silicon chip and compressed with a diamond flat punch with a diameter of 1.08 mm, comparable with sample size, as previously illustrated in Haugen and colleagues.[6] A sketch of the compression test set-up is given in Fig. 1. The predefined loading function consisted of one cycle with a small load sequence of maximum 50 mN with a 2-s hold time at load peak. Then, a 10-cycle sequence leading up to a 50-mN maximum load, and finally a 10-cycle sequence of increasing load up to 200 mN were applied. The cyclic load–displacement response was done stepwise with the load protocol increasing in 10 steps to 200 mN with partial unloadings, as a viscous effect evolves when the peak load is held constant. A nominal measure of tangential stiffness can be estimated by connecting the 10 points corresponding to each load increase. This leads to the response curves, as shown in Fig. 2A. To remove some of the geometrical influences of the semispheres on the
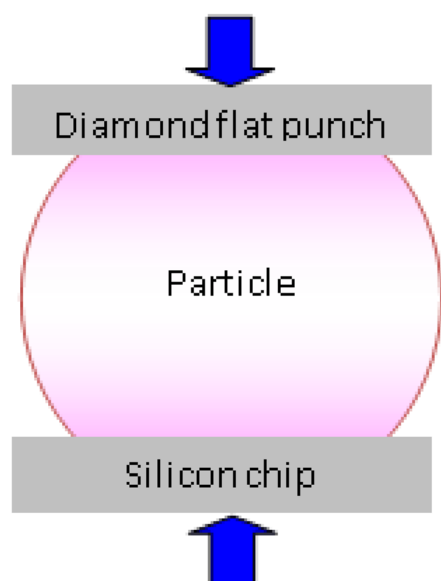
Fig 1. Schematic illustration of the flat-punch method used for compression test of particle-like materials.

response, the curves in Fig. 2A are mapped into nominal stress and strain. The global load was divided by the equivalent semi-circular equatorial cross-section area to get a stress measure (ie, stress = punch force/πr^2, where r is the radius of the semicircular equatorial cross section). The resultant global displacement was divided by the height of the sample to obtain a strain measure (ie, strain = global displacement/height of the semisphere).

Microscopy analysis of osteospheres

Osteospheres were washed in sterile PBS, fixed with 4% paraformaldehyde, embedded in OCT frozen sectioning medium (VWR

International BVBA, Leuven, Belgium), and sectioned at a thickness of 10 μm using a CryoStar NX70 cryostat (Thermo Fisher Scientific, Waltham, MA, USA). For immunofluorescence characterization, sections were stained with a modified version of Goldner's trichrome method.[42] Weigert's hematoxylin solution, chromotrop 2R, fuchsine acid, orange G, tungstophosphoric acid, and fast green powder, as well as Entellan mounting medium were purchased from Merck KGaA (Merck, Darmstadt, Germany). In brief, sections were incubated in Bouin's solution (Sigma-Aldrich) for 1 hour at 50°C, washed in tap water, stained with Weigert's hematoxylin for 5 min, and washed again. After incubation with chromotrope 2R/fuchsine acid for 15 min, sections were washed in 1% acetic acid, stained with orange G for 7 min, washed in 1% acetic acid, stained with fast green for 10 min, and washed in 1% acetic acid again. After dehydration, the sections were mounted with entellan and imaged with a Leica DM RBE microscope (Leica, Wetzlar, Germany) with a digital camera. Prior to confocal microscopy, the sections were immunostained with primary antibodies against periostin and collagen type I (COL-1). Antigen retrieval was performed in 10mM citrate buffer, pH 6.0, with 0.05% Tween 20 at 60°C overnight. Sections were cooled to room temperature, washed with PBS, permeabilized with 0.1% triton X-100 for 10 min, washed with PBS, and blocked in 10% normal goat serum (NGS; Abcam, Cambridge, UK) for 1 hour at room temperature. Sections were then incubated with rabbit antiperiostin (ab14041; Abcam) and mouse COL-1 (ab90395; Abcam) antibody at a 1:300 dilution in 2% NGS, overnight at 4°C, and washed three times with PBS. Alexa Fluor 488 goat anti-rabbit (Thermo Fisher Scientific) and Alexa Fluor 568 goat anti-mouse (Thermo Fisher Scientific) secondary antibodies were used at a 1:500 dilution in 4% NGS for 1 hour at room temperature, sections were washed three times with PBS, counterstained with Hoechst 33342 (1 μg/mL; Sigma-Aldrich) for 30 min and mounted. Sections were imaged with Leica SP8 confocal microscope (Leica Microsystems CMS GmbH, Mannheim, Germany) using 405-, 488-, and 552-nm excitation, and 420- to 480-nm, 500- to 550-nm, and 580- to 630-nm emission filters for Hoechst 33342, Alexa Fluor 488, and Alexa Fluor 568, respectively. Confocal images were processed with ImageJ
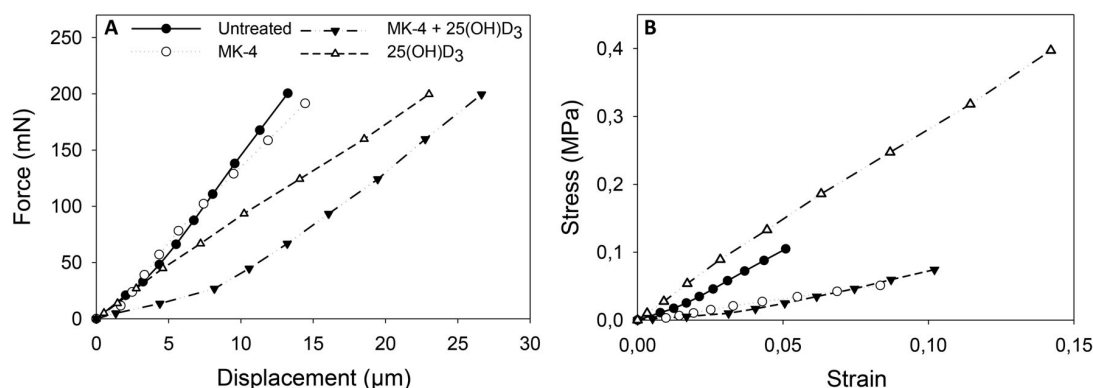

Fig 2. Compression force-displacement curves and stress–strain relationship from osteospheres of primary human osteoblasts without treatment and treated with 10μM menaquinone-4 (MK-4) or 0.01μM 25-hydroxyvitamin D$_3$ [25(OH)D$_3$], alone and in combination. (A) Shows the global response of the spheres, ie, nanoindentation force versus displacement, the corresponding nominal stress-strain response is illustrated in (B). Notable differences in the stiffness of the vitamin supplemented osteospheres compared with the untreated sample were observed as the tangent stiffness of the 25(OH)D$_3$-treated sample was considerably higher and of the MK-4 and MK-4 + 25(OH)D$_3$-treated sample lower than under untreated conditions.

software (NIH, Bethesda, MD, USA; https://imagej.nih.gov/ij/). For each image, random ROIs ($n = 5$) on each section were selected and quantified for their mean intensity. Five ROIs were also selected in the image areas containing no section (background), quantified for their mean intensity, averaged, and subtracted from the section mean intensities. 5-bromo-4-chloro-3-indolyl phosphate/nitro blue tetrazolium (Sigma-Aldrich) was applied for detection of alkaline phosphatase (ALP) in frozen sections of osteospheres as previously described by Brauer and colleagues.[43]

Alkaline phosphatase activity assay

ALP activity in the cell culture media of the 3D osteospheres after 1, 3, 7, and 14 days of culture was determined by measuring the hydrolysis of p-nitrophenyl phosphate (pNPP) (Sigma-Aldrich) into the yellow end-product p-nitrophenol, which absorbs at 405 nm. Prior to analysis, aliquots of the cell culture media were concentrated fivefold using MicrosepTM centrifugal tubes with 3 KDa cut-off from Pall Life Science (Ann Arbor, MI, USA). There was 25 μL of each concentrated sample incubated with 100-μL pNPP for 30 min in the dark at room temperature; then, the reaction was stopped by adding 50 μL of 3M NaOH. The absorbance was measured at 405 nm in a plate reader (ELX800; BioTek, Winooski, VT, USA) and the ALP activity was quantified using a standard curve based on calf intestinal ALP (Promega, Madison, WI, USA).

Quantification of proteins secreted in the cell culture medium

Multianalyte profiling of protein levels in the culture media of the 2D cultures and of the osteospheres was performed on the Luminex 200 system employing xMAP technology (Luminex Corp., Austin, TX, USA). Acquired fluorescence data were analyzed by the xPONENT 3.1 software (Luminex). Prior to analysis, aliquots of the cell culture media from the 2D experiment were concentrated 10-fold using MicrosepTM centrifugal tubes (Pall Life Science) with 3 KDa cut-off . Analyses were performed using the Milliplex Human Bone Panel kit (EMD Millipore, Billerica, MA, USA). For the 2D cultures, the effect of MK-4 and 25(OH)D$_3$, alone and in combination, on the secretion of cytokines and proteins (IL-1b, IL-6, osteoprotegerin [OPG], OC, leptin, osteopontin [OPN], PTH, TNF-α, adrenocorticotropic hormone, adiponectin, and insulin) to the culture medium after 1, 7, 14, and 20 days were measured. The secretion of OC, OPG, OPN, dickkopf-related protein 1, FGF23, IL-6, and sclerostin to the culture medium of the osteospheres was assessed after 1, 3, 7, and 14 days of vitamin treatment. Furthermore, in the 3D experiment, the level of

angiogenic markers was determined using the Milliplex Human Angiogenesis / Growth Factor Panel kit (granulocyte-colony stimulating factor, leptin, VEGF-A, VEGF-C, and VEGF-D). All analyses were performed according to the manufacturer's protocols.

RNA isolation and RT-PCR analysis

Total mRNA from 3D osteospheres and 2D cultures was isolated using the Dynabeads mRNA DIRECT kit (Thermo Fisher Scientific) with some modifications to the manufacturer's protocol. Briefly, the cells were lysed in lysis/binding buffer (100mM Tris–HCl, pH 7.5, 500mM LiCl, 10mM EDTA, pH 8.0, 1% lithium dodecyl sulfate, 5mM dithiothreitol), the lysate was sonicated (UP50H; Hielscher Ultrasonics GmbH, Teltow, Germany) for 10 s and centrifuged for 5 min at 4°C; then the supernatant was collected. mRNA was isolated using magnetic beads [oligo (dT)$_{25}$] as described by the manufacturer. Beads containing mRNA were suspended in 10mM Tris–HCl, pH 7.5, and stored at −80°C until use. Two- step RT-PCR was performed using technical triplicates of total mRNA for the first cDNA Strand Synthesis kit 1612 according to the manufacturer's protocol (Thermo Fisher Scientific). The second step, real-time PCR was carried out in a Bio-Rad CFX 384 (Bio-Rad Laboratories, Hercules, CA, USA), using SYBR green-based assay iQ SYBR supermix (Bio-Rad Laboratories). RT-PCR data were analyzed using the $2^{-\Delta\Delta Ct}$ method 2 [−Delta Delta C(T)].[44] Each treatment was compared with the respective control and normalized against β-actin. The primer sequences are listed in Table 1.

Statistical analysis

Statistical analysis was performed using SigmaPlot software version 14.0 (Systat Software, San Jose, CA, USA). Data obtained by Luminex analysis and RT-PCR ($\Delta\Delta Ct$ values) were compared between the groups by t test or Mann–Whitney U test, depending on their normal distribution. Data are presented as percentage of untreated cells ($= 100\%$) at each time point of observation. Mean intensities from the confocal image analysis ($n = 5$ per sample) were compared between the groups by t test. A probability of ≤0.05 was considered significant.

Results

25(OH)D$_3$ increases and MK-4 reduces the stiffness of osteospheres

The nominal stress–strain response, illustrating potential effects of the vitamin treatment on the mechanical properties of the irregularly shaped osteospheres, is shown in Fig. 2B. The tangent

Table 1. Primer Sequences Used for Real-Time RT-PCR Analysis

| Protein	Gene	Primer sequence (5′ - 3′)
β-Actin	h-ACTB h-ACTB	f CTGGAACGGTGAAGGTGACA r AAGGGACTTCCTGTAACAA
β2-Microglobulin	h-B2M h-B2M	f AGCAAGGACTGGTCTTTCTATCTC r CATGTCTCGATCCCACTTAACTATC
Collagen type I alpha 1	h-COL1A1 h-COL1A1	f CCAAATCCGATGTTTCTGCT r CATCTCCCCTTCGTTTTTGA
Alkaline phosphatase	h-ALPL h-ALPL	f AGACTGCGCCTGGTAGTTGT r GACAAGAAGCCCTTCACTGC
Osteocalcin	h-BGLAP h-BGLAP	f GCTTCACCCTCGAAATGGTA r GCAAGTAGCGCCAATCTAGG
Osteopontin	h-SPP1 h-SPP1	f TGAGGTGATGTCCTCGTCTG r GCCGAGGTGATAGTGTGGTT
Periostin	h-POSTN h-POSTN	f GCCCTGGTTATATGAGAATGGA r ATGCCCAGGTGCCATAAAC
OPG	h-OPG h-OPG	f GTGTCTTGGTCGCCATTTTT r TGGGAGCAGAAGACATTGAA
RANKL	h-RANKL h-RANKL	f GCGCTAGATGACACCCTCTC r CGGGGTGACCTTATGAGAAA
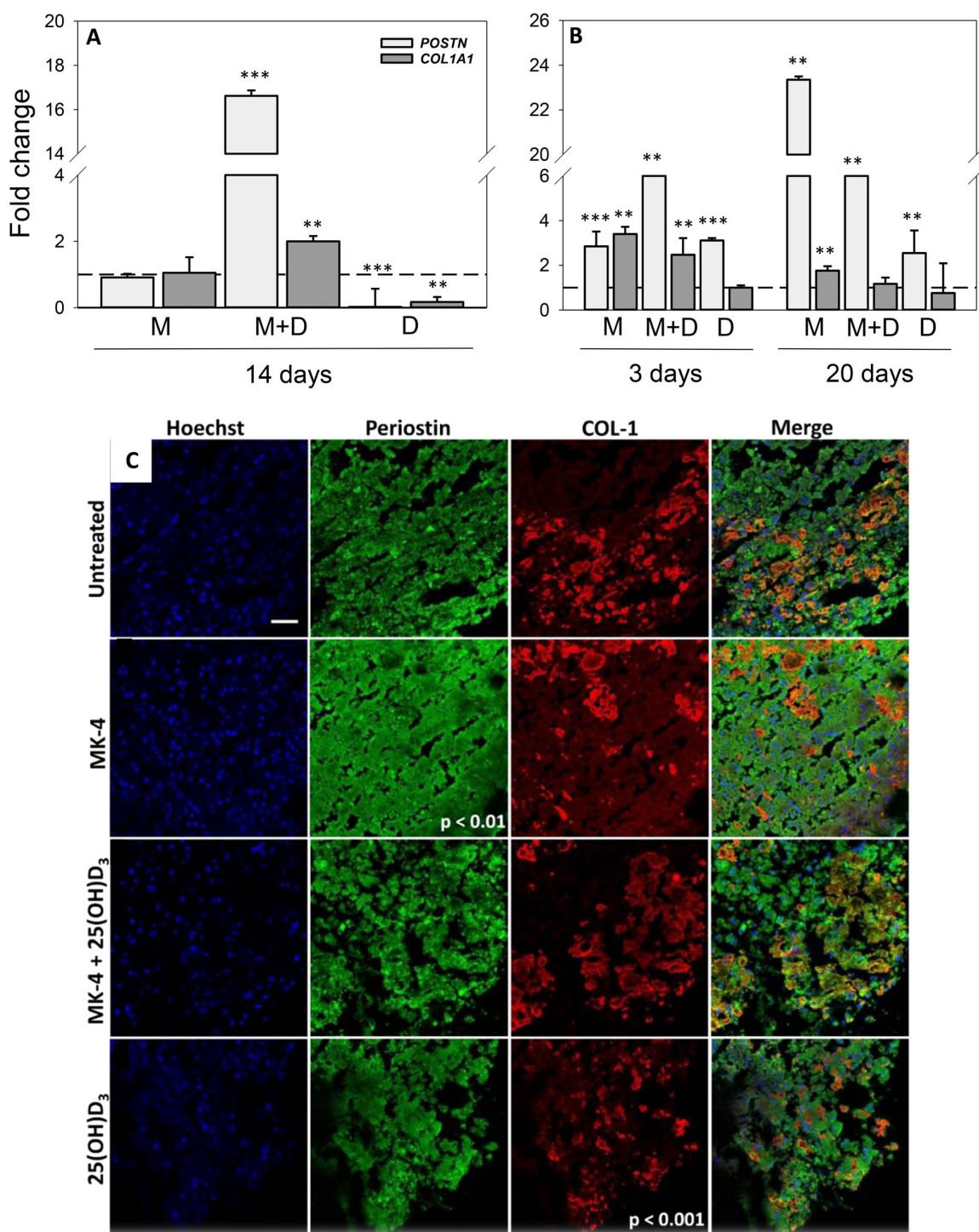
Fig 3. Effect of menaquinone-4 (MK-4) and 25-hydroxyvitamin D₃ [25(OH)D₃], alone and combined, on periostin and collagen type I (COL-1) expression in 3D and 2D cultures of primary human osteoblasts (hOBs): Relative mRNA expression levels for *POSTN* and *COL1A1* in 3D osteospheres (*A*) and 2D cultures of primary hOBs (*B*) cultured with 10μM MK-4 (M) or 0.01μM 25(OH)D₃ (*D*), alone and in combination (MD) at different days after vitamin addition. Relative mRNA expression levels were normalized to reference gene *ACTB* (2D cultures) and *ACTB* and *B2M* (3D cultures) and presented as fold-change relative to unexposed controls. Values represent the mean ± SD. (*C*) Immunofluorescence characterization of cell nuclei (blue), periostin (green), and COL-1 (red) in selected areas of frozen sections of 21-day-old mineralized osteospheres without treatment and treated with 10 μM MK-4, 10μM MK-4 and 0.01 μM 25(OH)D₃, and 0.01μM 25(OH)D₃ (scale bar = 50 μm). Mean intensities were quantified in five random regions of interest in each whole section. Significant differences were analyzed with SigmaPlot *t* test. Significant different from control at $p < 0.05$, $p < 0.01$, and $p < 0.001$.

stiffness was obtained by the line connecting the stress at each cyclic peak on the loading part of the stress–strain curves and found to be 1.93 MPa for the untreated semisphere, 0.61 MPa and 2.83 MPa for MK-4 and 25(OH)D$_3$ treatment alone, respectively, and 0.63 MPa for MK-4 in combination with 25(OH)D$_3$.

MK-4 alters the expression of periostin and COL-1 in 3D osteospheres and enhances *POSTN* and *COL1A1* expression in 2D cultures

Exposure of 3D osteospheres to 25(OH)D$_3$ reduced the mRNA expression of *POSTN* 50-fold ($p < 0.001$) and *COL1A1* more than fivefold ($p < 0.01$) relative to control on day 14. In contrast, the combination of MK-4 and 25(OH)D$_3$ enhanced *POSTN* expression levels more than 16-fold ($p < 0.001$) and *COL1A1* levels twofold ($p < 0.01$; Fig. 3*A*).

In the 2D cultures, the relative *POSTN* expression on day 3 was elevated 13-fold by combined vitamin conditions ($p < 0.01$), threefold by 25(OH)D$_3$ ($p < 0.001$), and more than twofold by MK-4 ($p < 0.001$). On day 20, *POSTN* gene expression was enhanced most by exposure to MK-4 (23-fold; $p < 0.01$), followed by combined vitamin supplementation (sixfold; $p < 0.01$) and 25(OH)D$_3$ (threefold; $p < 0.01$; Fig. 3*B*). Moreover, exposure to MK-4 increased the relative mRNA expression of *COL1A1* in the 2D cultures threefold ($p < 0.01$) on day 3 and twofold ($p < 0.01$) on day 20. In combination with 25(OH)D$_3$, a more than twofold ($p < 0.01$) rise occurred on day 3.

Primary hOBs in frozen sections of 21-day-old mineralized 3D osteospheres expressed periostin and produced COL-1. Interestingly, in the untreated osteospheres, COL-1 was expressed as a stripe-like area in the outer regions of the semiconstructs. Osteospheres treated with MK-4 showed a significant stronger expression of periostin than the control ($p < 0.01$). Additionally, in these osteospheres, COL-1 was expressed in small amounts over the whole area of the semispheres. Combined administration of MK-4 and 25(OH)D$_3$ did not induce significant changes in COL-1 and periostin expression or the COL-1 expression pattern compared with the control. COL-1 in osteospheres treated with 25(OH)D$_3$ alone was expressed at a reduced level ($p < 0.001$), and also all over the area of the semiconstructs compared with the control (Fig. 3*C*).

25(OH)D$_3$ increases the secretion of ALP from 3D osteospheres and enhances *ALPL* expression in 2D cultures

Exposure of 3D osteospheres to 25(OH)D$_3$ reduced the mRNA expression of *ALPL* twofold ($p < 0.001$) relative to control on day 14, whereas no significant differences were observed after exposure to MK-4 or the vitamins in combination (Fig. 4*A*). Conversely, incubation of 2D cultures with 25(OH)D$_3$ increased *ALPL* expression more than 11-fold ($p < 0.01$) on day 3 and eightfold ($p < 0.01$) on day 20. In addition, relative *ALPL* expression was enhanced sixfold ($p < 0.05$) by MK-4 and 25(OH)D$_3$ together on day 3, and more than threefold by both MK-4 alone and the combination on day 20 ($p < 0.01$ for both; Fig. 4*B*).

The levels of membrane-bound ALP in frozen sections of 21-day-old mineralized 3D osteospheres were not affected by any of the vitamins compared with control (data not shown). However, the secretion of ALP to the culture medium from 3D osteospheres was decreased to 70 ± 1.3% ($p < 0.05$) of control
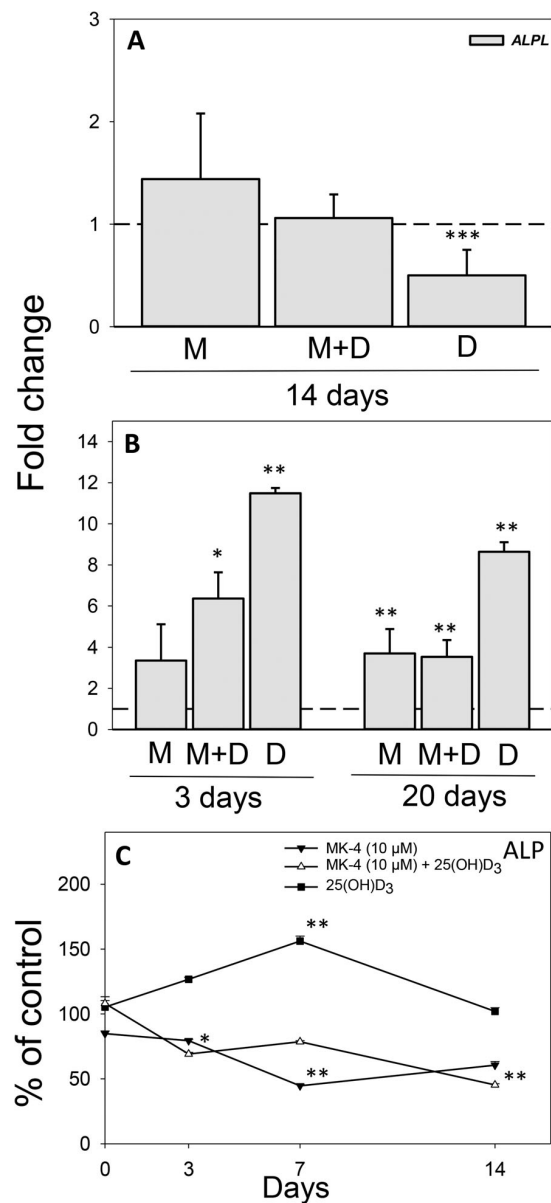

Fig 4. Effect of menaquinone-4 (MK-4) and 25-hydroxyvitamin D$_3$ [25 (OH)D$_3$], alone and combined, on alkaline phosphatase (ALP) in 3D and 2D cultures of primary human osteoblasts (hOBs): Relative mRNA expression levels for *ALPL* in 3D osteospheres (*A*) and 2D cultures of primary hOBs (*B*) cultured with 10 μM MK-4 (M) or 0.01 μM 25(OH)D$_3$ (D), alone and in combination (MD) at different days after vitamin addition. Relative mRNA expression levels were normalized to reference gene *ACTB* (2D cultures) and *ACTB* and *B2M* (3D cultures) and presented as fold-change relative to unexposed controls. (*C*) Secretion of ALP to the culture medium from 3D osteospheres cultured with 10 μM MK-4 or 0.01μM 25(OH)D$_3$, alone and in combination. Spheres were grown for 7 days under untreated conditions, on culture day 8 (= day 0 of comparison to control) vitamins were added to the culture medium. Values represent the mean ± SD. Significant different from control at *$p < 0.05$, **$p < 0.01$, and ***$p < 0.001$.
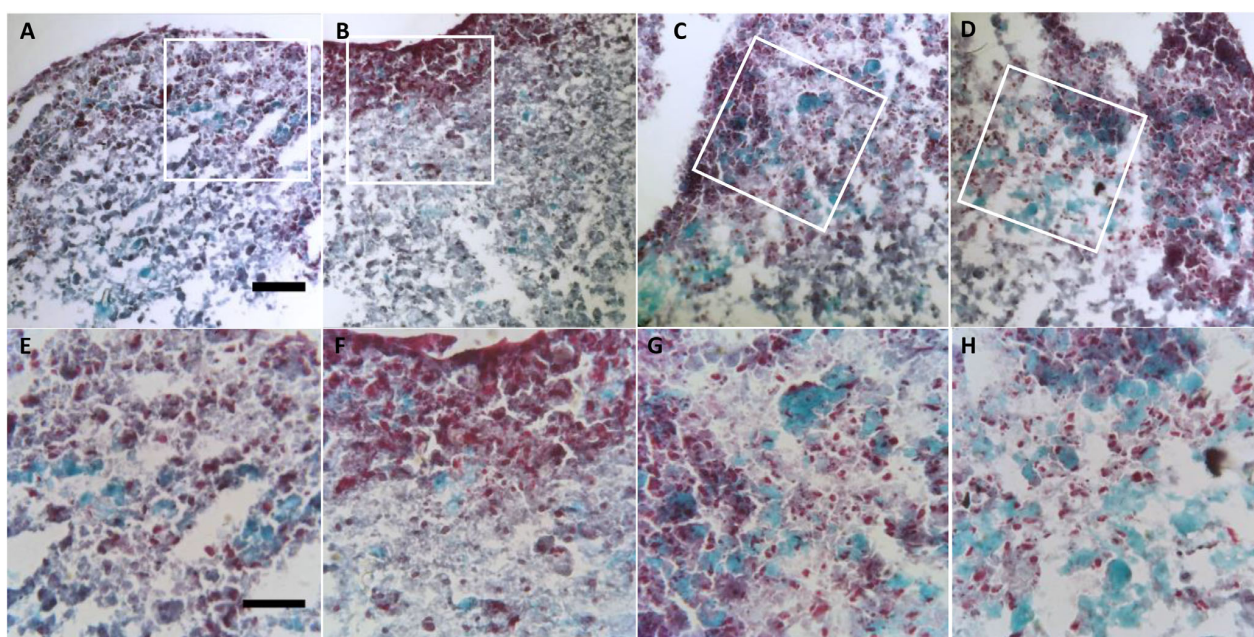
Fig 5. Histochemical characterization of cell nuclei (black), osteoid (red), and mineralized bone (green) stained with Goldner trichrome method in frozen sections of 21-day-old mineralized osteospheres. (*A* to *D*) Show a 10-µm frozen section of a semiosteosphere without treatment (*A*), treated with 10µM MK-4 (*B*), 10µM MK-4 + 0.01µM 25-hydroxyvitamin D$_3$ [25(OH)D$_3$] (*C*), or 0.01µM 25(OH)D$_3$ (*D*) (scale bar = 100 µm). (*E* to *H*) Are high-magnification images (scale bar = 50 µm) of a representative area of semiosteospheres without treatment (*E*), treated with 10µM MK-4 (*F*), 10µM MK-4 + 0.01µM 25(OH)D$_3$ (*G*), or 0.01 µM 25(OH)D$_3$ (*H*).

on day 3 and $45 \pm 0.8\%$ ($p < 0.01$) on day 14 by combined supplementation with MK-4 and 25(OH)D$_3$. Similarly, ALP secretion was reduced to $45 \pm 1\%$ ($p < 0.01$) of control by MK-4 on day 7. In contrast, a rise in ALP secretion to $156 \pm 4\%$ ($p < 0.01$) of control was observed on day 7 after exposure to 25(OH)D$_3$ (Fig. 4*C*).

25(OH)D$_3$ enhances the deposition of mineral in osteospheres

Frozen sections of untreated 21-day-old mineralized bone spheroids showed large osteoid formation in the outer region of the semiconstructs, whereas little deposition of mineral was
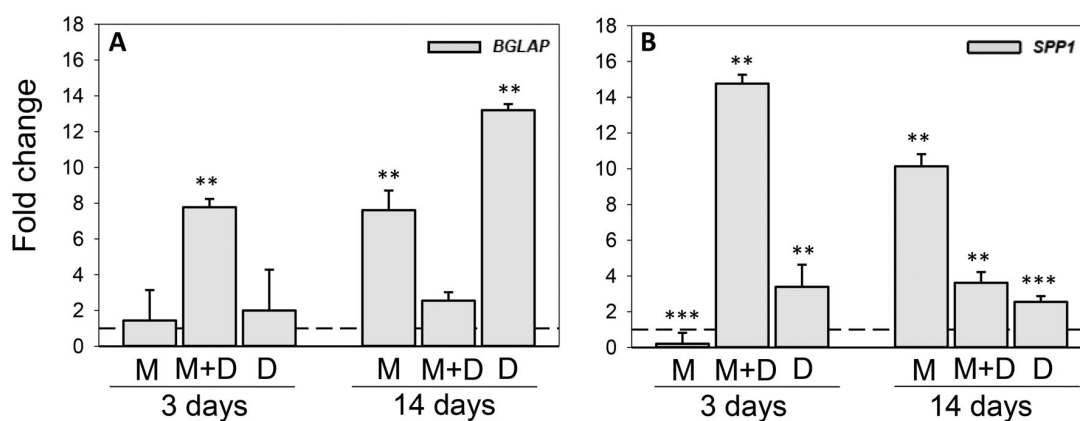

Fig 6. Effect of menaquinone-4 (MK-4) and 25-hydroxyvitamin D$_3$ [25(OH)D$_3$], alone and combined, on osteocalcin (*BGLAP*) and osteopontin (*SPP1*) gene expression in 2D cultures of primary human osteoblasts: Relative mRNA expression levels for *BGLAP* (*A*) and *SPP1* (*B*) in 2D cultures exposed to 10µM MK-4 (M) or 0.01 µM 25(OH)D$_3$ (D), alone and in combination (MD) at days 3 and 20 after vitamin addition. Relative mRNA expression levels were normalized to reference gene *ACTB* and presented as fold-change relative to unexposed controls. Values represent the mean $\pm$ SD. Significant different from control at *$p < 0.05$, **$p < 0.01$, and ***$p < 0.001$.
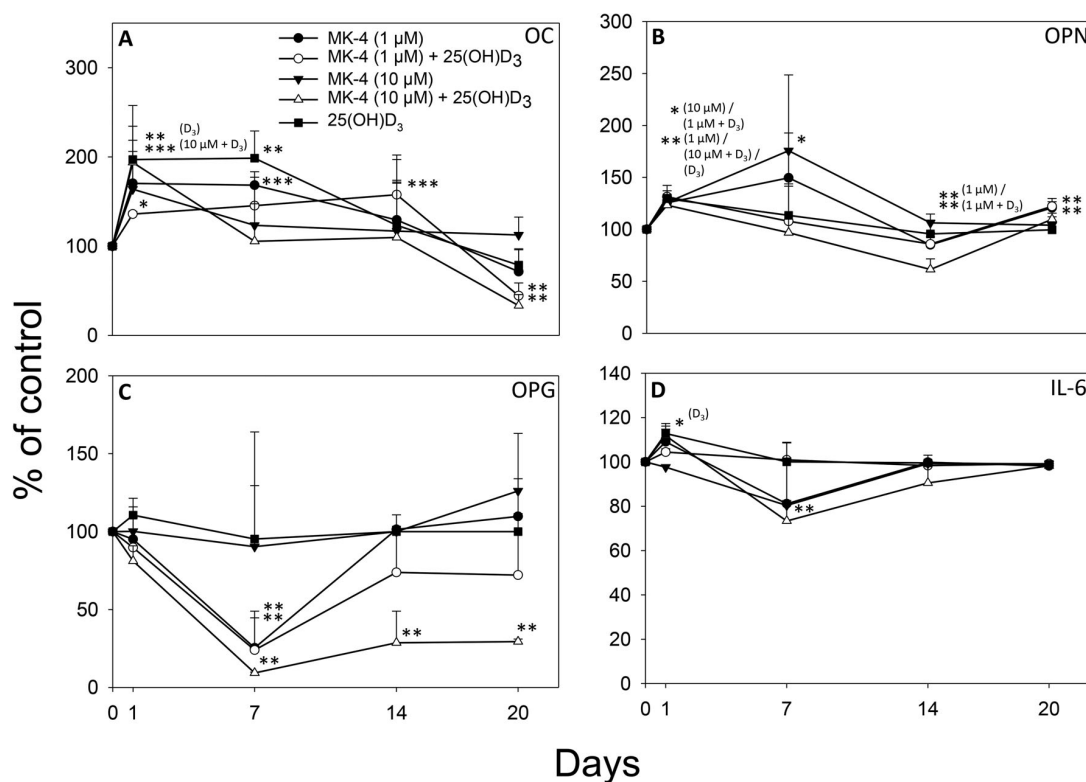
Fig 7. Secretion of osteocalcin (OC) (*A*), osteopontin (OPN) (*B*), osteoprotegrin (OPG) (*C*), and interleukin-6 (IL-6) (*D*) to the culture medium from primary human osteoblasts treated with 1μM menaquinone-4 (MK-4), 10μM MK-4 or 0.01μM 25-hydroxyvitamin D_3 [25(OH)D_3], alone and in combination, is shown in % of control at 1, 7, 14, and 20 days. Values represent the mean $\pm$ SD. Significant different from control at *$p < 0.05$, **$p < 0.01$, and ***$p < 0.001$.

detected within the spheres (Fig. 5*A,E*). MK-4 supplementation did not affect mineralization, but the osteoid appeared to be much more condensed compared with the control (Fig. 5*B,F*). Osteospheres treated with a combination of MK-4 and 25(OH)D_3 showed extended osteoid formation into the central region of the constructs and increased mineral deposition over the whole area compared with the control (Fig. 5*C,G*). In osteospheres treated with 25(OH)D_3 alone, increased mineralization organized as a stripe-like area over the semiconstruct was observed (Fig. 5*D,H*).

25(OH)D_3 alone, or in combination with MK-4 alters the secretion of OC and IL-6 of primary hOBs

In the 2D cultures, combined supplementation with MK-4 (10μM) and 25(OH)D_3 significantly increased the relative mRNA expression of *BGLAP* more than sevenfold ($p < 0.01$) on day 3. Additionally, *BGLAP* expression levels were raised 13-fold ($p < 0.01$) by exposure to 25(OH)D_3 and eightfold ($p < 0.01$) by MK-4 on day 20 (Fig. 6*A*). Relative *SPP1* expression on day 3 was elevated more than 14-fold by combined vitamin conditions ($p < 0.01$) and threefold by 25(OH)D_3 ($p < 0.01$), whereas MK-4 (10μM) reduced the expression fivefold ($p < 0.001$). On day 20, *SPP1* gene expression was enhanced most by exposure to MK-4 (10-fold; $p < 0.01$), followed by combined vitamin supplementation (fourfold; $p < 0.01$) and 25(OH)D_3 (threefold, $p < 0.001$; Fig. 6*B*).

Protein levels of IL-1b, leptin, TNF-α, and adiponectin in the cell culture media of the 2D cultures were below the detection limit for the standard curves and are consequently not presented. Both 25(OH)D_3 alone and in combination with MK-4 (1μM and 10μM) resulted in an acute increased secretion of OC (day 1: 197 $\pm$ 61%, $p < 0.01$; 136 $\pm$ 3%, $p < 0.05$; and 194 $\pm$ 12%, $p < 0.001$, respectively). The OC release was elevated by both 25(OH)D_3 and MK-4 (1μM) alone on day 7 (199 $\pm$ 31%, $p < 0.01\%$ and 168 $\pm$ 1.4%, $p < 0.001$, respectively) and by the combined treatment of MK-4 (1μM) and 25(OH)D_3 on day 14 (158 $\pm$ 16%, $p < 0.001$) compared with control. On day 20, OC levels were reduced to around 40% of control by the combined administration of MK-4 (both 1μM and 10μM) and 25(OH)D_3 ($p < 0.01$ and $p < 0.01$, respectively; Fig. 7*A*). The amount of OPN in the culture medium was increased by 30% over control by all treatments after one day of incubation. After 7 days, OPN levels were only significantly higher for MK-4 (10μM) treatment (176 $\pm$ 17%, $p < 0.05$) and the release was reduced by MK-4 (1μM) alone and in combination with 25(OH)D_3 on day 14 (85 $\pm$ 12% and 86 $\pm$ 7%, respectively: $p < 0.01$ for both; Fig. 7*B*). OPG levels were fourfold reduced by MK-4 (μM) alone ($p < 0.01$) and in combination with 25(OH)D_3 ($p < 0.01$) 7 days after treatment. Combined supplementation of MK-4 (10μM) and 25(OH)D_3 decreased the secretion of OPG to 9 $\pm$ 0.6% at day 7 ($p < 0.01$) and maintained the reduced secretion of OPG to 29 $\pm$ 1.7% of control at day 20 ($p < 0.01$; Fig. 7*C*). The release of IL-6 was significantly enhanced by
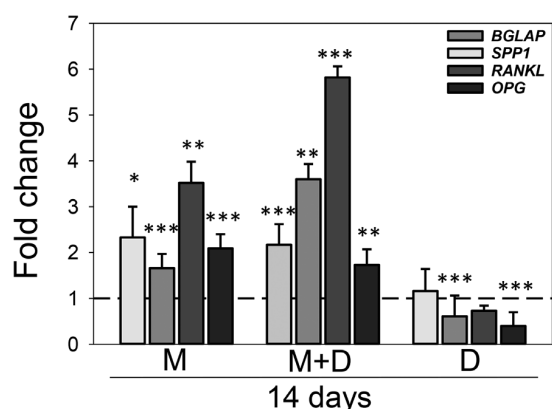
Fig 8. Effect of menaquinone-4 (MK-4) and 25-hydroxyvitamin D_3 [25 (OH)D_3], alone and combined, on osteocalcin (*BGLAP*), osteopontin (*SPP1*), osteoprotegrin (*OPG*), and receptor activator of nuclear factor-κB ligand (RANKL) gene expression in 3D cultures of primary human osteoblasts: Relative mRNA expression levels for, *BGLAP*, *SPP1*, *OPG*, and *RANKL* in 3D osteospheres cultured with 10μM MK-4 (M) or 0.01μM 25(OH)D_3 (D), alone and in combination (MD) at day 14 after vitamin addition. Relative mRNA expression levels were normalized to reference genes *ACTB* and *B2M* and presented as fold-change relative to unexposed controls. Values represent the mean ± SD. Significant different from control at *$p < 0.05$, **$p < 0.01$, and ***$p < 0.001$.

25(OH)D_3 on day 1 (113 ± 4%, $p < 0.05$) and reduced in combination with MK-4 (10μM) on day 7 (73 ± 9%, $p < 0.01$; Fig. 7D).

MK-4 alone, or in combination with 25(OH)D_3, alters the expression of *BGLAP*, *SPP1*, *RANKL*, and *OPG* in 3D osteospheres as compared with 25(OH)D_3 alone

Exposure of 3D osteospheres to 25(OH)D_3 did not significantly change *BGLAP* and *RANKL* gene expression, but reduced *SPP1* expression 1.6-fold ($p < 0.001$) and *OPG* expression 2.5-fold ($p < 0.001$) on day 14. Conversely, treatment with MK-4 increased the relative mRNA expression of *BGLAP* more than twofold ($p < 0.05$), of *SPP1* 1.6-fold ($p < 0.001$), of *RANKL* more than threefold ($p < 0.01$) and of *OPG* more than twofold ($p < 0.001$). Similarly, *BGLAP* expression levels were raised twofold ($p < 0.001$), *SPP1* levels more than threefold ($p < 0.01$), *RANKL* levels more than fivefold ($p < 0.001$), and *OPG* levels 1.7-fold ($p < 0.01$) by combined vitamin conditions (Fig. 8). In addition, the *RANKL/OPG* ratio was significantly downregulated in 3D osteospheres treated with 25(OH)D_3 (1.59, $p < 0.001$), as well as both vitamins in combination (1.80, $p < 0.01$) compared with control (3.05). MK-4 alone did not significantly affect the *RANKL/OPG* ratio (3.36, $p > 0.05$) after 14 days.

MK-4 alone or in combination with 25(OH)D_3 alters the secretion of OPG, VEGF-C, IL-6, and G-CSF from 3D osteospheres as compared with 25(OH)D_3 alone

Protein levels of OC, sclerostin, and FGF23 in the cell culture media from osteospheres were below the detection limit for the standard curves and are consequently not presented. Both 25(OH)D_3 supplementation alone and in combination with

MK-4 (10μM) induced an acute increase in the release of OPN (day 1: 545 ± 67%, $p < 0.001$ and 455 ± 105%, $p < 0.01$, respectively), whereas MK-4 alone had no significant effect compared with untreated control cells. On day 3, OPN levels were reduced to around 20% of control by both single treatments with MK-4 and 25(OH)D_3 ($p < 0.01$ and $p < 0.01$, respectively), and afterwards stabilized to near control levels (Fig. 9A). The secretion of OPG was increased by 25(OH)D_3 alone to approximately 40% of control during the whole culture period. MK-4 (10μM) alone and in combination with 25(OH)D_3 significantly enhanced the OPG release on day 1 ($p < 0.001$) and reduced it on day 14 ($p < 0.01$) by <20% of control (Fig. 9B). Single-vitamin treatments, or the combination, induced only minor changes into the secretion of VEGF-C. VEGF-C levels were 145 ± 9% ($p < 0.01$) for 25(OH)D_3 alone, 117 ± 2% ($p < 0.01$) for combined vitamin conditions, and 108 ± 3% for MK-4 compared with the control after 14 days (Fig. 9C). The administration of 25(OH)D_3 significantly enhanced the IL-6 levels at days 1 and 3 after vitamin treatment (174 ± 10%, $p < 0.001$ and 215 ± 6%, $p < 0.001$, respectively) with peak effect after 7 days (342 ± 11%, $p < 0.001$). MK-4 treatment alone increased the IL-6 release threefold ($p < 0.001$) and in combination with 25(OH)D_3 more than 1.5-fold ($p < 0.001$) by day 7 (Fig. 9D). Significantly higher amounts of DKK-1 in the culture medium were detected for 25(OH)D_3 alone at 3 days (126 ± 11%, $p < 0.05$) and 7 days (119 ± 5%, $p < 0.01$) after incubation, and for both single treatments with 25(OH)D_3 and MK-4 by day 14 (168 ± 5%, $p < 0.001$ and 163 ± 7%, $p < 0.001$, respectively; Fig. 9E). G-CSF levels were more than threefold enhanced at days 1 ($p < 0.001$) and 3 ($p < 0.001$) by treatment with 25(OH)D_3 alone. Combined vitamin conditions enhanced the secretion to 179 ± 4% (day 1, $p < 0.001$) and 160 ± 4% (day 3, $p < 0.001$) compared with control. After 7 days, 25(OH)D_3 administration had peak effect (482 ± 16%, $p < 0.001$), whereas G-CSF release from MK-4-and combined vitamin-treated cells did not increase further compared with days 1 and 3 (331 ± 16%, $p < 0.001$ and 144 ± 8%, $p < 0.01$, respectively; Fig. 9F).

Discussion

We demonstrate the differential effects of vitamin D and K2 on the mechanical properties of human 3D bone spheroids in vitro ÷ exposure to 25(OH)D_3-induced increased stiffness, whereas the synthetic vitamin K2, MK-4, induced softer or more flexible osteospheres compared with untreated spheroids. Osteospheres treated with a combination of 25(OH)D_3 and K2 had the same flexibility as those treated with K2 alone. To the best of our knowledge, this is the first study to show that vitamin K2 modulates vitamin D-induced mechanical properties in a 3D bone model based on hOBs.

Cell-based in vitro models, previously generated by a rotational coculture approach of hOBs and osteoclasts without any exogenous scaffolding material,[1,2,6] enable us to study the bone microenvironment. In contrast to these two cell systems, we produced 3D mineralized tissue constructs from single cultures of primary hOBs. Osteoblasts in our 3D bone spheroids formed mineralized bone matrix similar to Clark and colleagues and Haugen and colleagues,[1,6] and secreted the bone matrix protein OPN as reported by Penolazzi and colleagues.[2] In addition to 3D spheroids, we applied 2D cultures of primary hOBs to assess the effect of MK-4 and 25(OH)D_3 on proteins and cytokines involved in the mechanical and biological function of bone. In
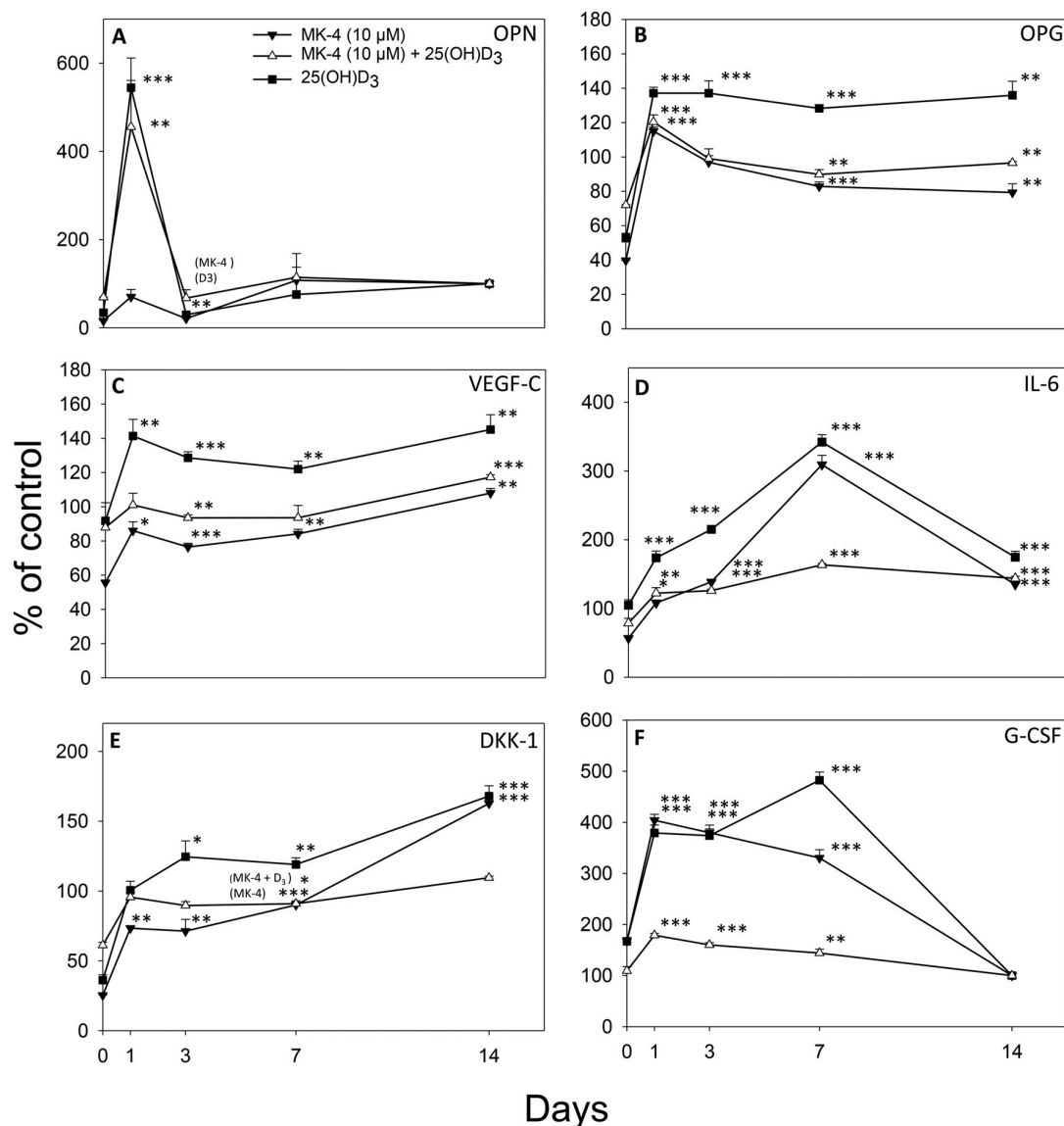
Fig 9. Secretion of osteopontin (OPN) (*A*), osteoprotegrin (OPG) (*B*), vascular endothelial growth factor C (VEGF-C) (*C*), interleukin-6 (IL-6) (*D*), dickkopf-related protein 1 (DKK1) (*E*), and granulocyte-colony stimulating factor (G-CSF) (*F*) to the culture medium from osteospheres of human primary osteoblasts treated with 10μM menaquinone-4 (MK-4) or 0.01μM 25-hydroxyvitamin D$_3$ [25(OH)D$_3$], alone and in combination, is shown in % of control at 1, 3, 7, and 14 days. Spheres were grown for 7 days under untreated conditions, on culture day 8 (= day 0 of comparison to control) vitamins were added to the culture medium. Values represent the mean ± SD. Significant different from control at *p < 0.05, **p < 0.01, and ***p < 0.001.

3D cultures, cellular behavior reflects in vivo tissue functionality more accurately than in monolayer cultures. 3D cultures are thus better suited for the evaluation of cellular responses to various compounds or drugs.[45]

The strength of bone and its ability to resist fracture are dependent on its mass and geometry, but also on the bone material properties,[46] which are determined by, among others, the quality, amount, and orientation of collagen fibers[47]; and degree of mineralization.[48] The mineral phase of bone influences the ability to resist deformation and provides stiffness and strength to the bone structure,[47,48] whereas collagen is

associated with its flexibility (toughness), giving resistance to impact load.[47,49]

We observed an increase in ALP secreted to the culture medium from osteospheres exposed to 25(OH)D$_3$ and in line with this, enhanced mineral deposition, which may, in addition to the reduced expression of COL-1, account for their higher bone stiffness. On the other hand, administration of MK-4 alone reduced the ALP activity in the medium and did not stimulate mineralization, but induced enhanced expression of periostin and altered distribution of COL-1. This was reflected in reduced bone stiffness and higher flexibility in the osteospheres. In

agreement, we found significantly upregulated expression of *POSTN* and *COL1A1* in 2D cultures exposed to MK-4. However, mRNA expression in the osteospheres was not altered. Periostin is a vitamin K-dependent protein primarily produced and secreted by osteoblasts and their precursor cells.[21] It is an important mediator of the biomechanical properties of collagen-rich tissues by regulating collagen fibril diameter and cross-linking.[24]

In the present study, increased flexibility of the osteospheres was observed after exposure to the two vitamins despite enhanced mineralization. The improvement of flexibility could be attributed to increased synthesis of periostin and COL-1. Accordingly, *POSTN* and *COL1A1* gene expression levels in these osteospheres were significantly enhanced; however, no evident alterations in the protein levels of periostin and COL-1 were revealed. Still, it is reasonable that MK-4 may have facilitated the formation of more collagen with proper physiological function in the osteospheres. Vitamin K2 has been suggested to promote collagen accumulation in osteoblastic cells via the SXR-signaling pathway.[50] Enhanced collagen mRNA expression has also been reported in 2D cultures of osteogenically differentiated human mesenchymal stem cells from amniotic fluid treated with MK-4; however, protein levels in 3D spheroid cultures were not affected.[51] Vitamins D and K2, as well as the combination of the two, have previously been described to enhance mineralization of osteoblasts in vitro.[52]

In clinical studies, combined administration of vitamins D and K is suggested to improve bone quality and lower the risk of fractures.[33] Moreover, a higher gain in BMD has been reported in postmenopausal women with osteoporosis treated with a combination of the vitamins compared with each vitamin alone or calcium.[38,39]

It is worth noting that the generated osteospheres in our study may comprise osteoblasts in various differentiation stages, similar to the in vivo situation. As previously reported, spheroids with a diameter of 500 μm are made-up of a heterogenic population of cells, depending upon the location within the layer-like structure of the sphere.[53,54] In the outer rim of a sphere, cells are surrounded by media and have the space to proliferate, whereas cells in the inner area have cell-to-cell contact and are dependent on nutrient transport from neighboring cells.[54,55] In contrast to the even periostin staining in our study, immunostaining of unexposed osteospheres revealed COL-1 expressing cells in the outer region of the semispheres. This may indicate that these cells are less differentiated, producing higher amounts of COL-1.[56] The absence of COL-1 expression in the inner region of our osteospheres suggests that these cells are of later osteoblast or early osteocyte differentiation stage,[57] as COL-1 is downregulated when osteoblasts begin to develop into osteocytes in vitro.[56,58] As recently suggested by Kim and Adachi, the cell condensation within spheroids triggers the differentiation of osteoblast-precursor cells to osteocyte-like cells.[59] The uneven differentiation of osteoblasts in 3D cultures has been previously reported by others.[57,60] Alterations in this differentiation pattern within the osteospheres, induced by the vitamins, are reflected in the immunostaining and gene expression analysis.

OC and OPN are major noncollagenous proteins (NCPs) involved in bone matrix organization and deposition, and have been shown to influence bone morphology and mechanical properties.[61] Both proteins interact with collagen and mineral.[23,62] It has been recently suggested that their spatial arrangement in the bone matrix enhances bone toughness.[63]

Among these NCPs, OPN has been proposed to act as a glue that counteracts the separation of the mineralized collagen fibers upon mechanical loading of bone. In this structure, energy may be dissipated through the formation and reformation of intramolecular bonds between OPN and divalent Ca^{2+}, which increases the total energy to fracture bone.[64,65] Moreover, NCPs influence the mechanical properties of bone through dilatational band formation as suggested by Poundarik and colleagues.[63] Dilatational bands are ellipsoidal voids that result from the disassembly of noncollagenous protein complexes, like OC-OPN complexes, which are integrated in the mineralized matrix of bone when a load is applied. Formation of these microcracks within bone allows for the dissipation of large amounts of energy, which reduces the bone's propensity to fracture.[63] The enhanced *BGLAP* and *SPP1* expressions in osteospheres exposed to MK-4 alone and combined with 25(OH)D$_3$, as well as the acute increase in OPN secretion, suggest that the reduced stiffness seen in these osteospheres may be partially mediated by these mechanisms.

The carboxylated form of OC facilitates deposition of calcium into the bone matrix.[66] Both vitamins D and K stimulate synthesis of OC and are also cofactors in the carboxylation,[37] thereby contributing to mineralization.[67–69] In line with this, we observed a rise in OC levels in the 2D cell cultures after 1 and 7 days of vitamin D administration, and after 7 days of exposure to vitamin *K*, no further enhancement occurred when combining the two vitamins.

OPN release in 2D cell cultures was promoted by both vitamins after one day of exposure, but only by the higher concentration of MK-4 (10μM) after 7 days. Vitamin D alone and in combination with MK-4 also induced a transient increase in OPN in 3D osteospheres.

Based on our findings, it is reasonable that the effects of vitamins D and K are partly mediated by these proteins. It is worth noting that we were not able to detect OC in the culture medium of the osteospheres. This could be attributed to the fact that OC is expressed late in the osteoblast maturation process,[70] and therefore not detectable in the medium after a culture period of 14 days.

The rate of bone turnover is another determinant of bone quality. Thus, we assessed the impact of the two vitamins on substances regulating bone metabolism. In 2D cultures, MK-4 administration alone and combined with 25(OH)D$_3$ induced a decline in OPG. In contrast, a sustained increase in OPG by exposure to 25(OH)D$_3$, as well as a decreased *RANKL/OPG* ratio in 3D spheroids by 25(OH)D$_3$ and combined vitamins was seen. These findings may translate to suppression of bone resorption in vivo. In the 3D spheroids, both vitamins induced a rise in IL6. However, data on the effect of IL-6 on bone metabolism are diverging.[71] Moreover, both vitamins induced an increase in DKK1, an inhibitor of bone formation,[72] 25(OH)D$_3$ at several time points, MK-4 and the combination of the vitamins only after 14 days. Finally, G-CSF levels were enhanced by treatment with 25(OH)D$_3$ alone, and to a lesser degree by the combined vitamins compared with control. In summary, the two vitamins induced a rise both in factors stimulating and inhibiting bone resorption, as well as factors favoring and inhibiting bone formation. How this translates to in vivo conditions is, however, impeded by the fact that the osteospheres only contained osteoblasts. We observed enhancement of osteoblast differentiation by 25(OH)D$_3$ and MK-4 alone and in combination, as reflected in increased OC levels. Given the interplay between osteoblasts and osteoclasts, the presence of both cells would have given a more complete picture. Still,

based on our results, it can be hypothesized that combined administration of K2 and 25(OH)D$_3$ could contribute to stronger bone also in vivo. This should be tested in 3D osteospheres containing both osteoblasts and osteoclasts, as well as in rodents and humans.

Disclosures

MS, EAR, JH, BHS, AML, US, and JER state that they have no conflicts of interest. MEM is a shareholder in Axial Vita AS, which sells vitamin K2. JER is a member of Cost Action 16119 CellFit.

Acknowledgments

Author Contributions

Maria Schroeder: Formal analysis; investigation; methodology; visualization; writing-original draft; writing-review and editing. **Elisabeth Riksen:** Formal analysis; visualization; writing-original draft. **Jiannying He:** Formal analysis; investigation; visualization; writing-original draft. **Bjørn Skallerud:** Formal analysis; resources; supervision; writing-review and editing. **Mona Møller:** Resources; writing-review and editing. **Aina Lian:** Formal analysis; investigation. **Unni Syversen:** Writing-original draft; writing-review and editing. **Janne Reseland:** Conceptualization; funding acquisition; methodology; project administration; supervision; validation; writing-original draft; writing-review and editing.

Peer Review

The peer review history for this article is available at https://publons.com/publon/10.1002/jbm4.10394.

References

1. Clarke MS, Sundaresan A, Vanderburg CR, Banigan MG, Pellis NR. A three-dimensional tissue culture model of bone formation utilizing rotational co-culture of human adult osteoblasts and osteoclasts. Acta Biomater. 2013;9(8):7908–16.

2. Penolazzi L, Lolli A, Sardelli L, et al. Establishment of a 3D-dynamic osteoblasts-osteoclasts co-culture model to simulate the jawbone microenvironment in vitro. Life Sci. 2016;152:82–93.

3. Facer SR, Zaharias RS, Andracki ME, Lafoon J, Hunter SK, Schneider GB. Rotary culture enhances pre-osteoblast aggregation and mineralization. J Dent Res. 2005;84(6):542–7.

4. Schneider G, Boehrs JK, Hoopes JV, Seabold D. Use of 3-dimensional environments to engineer osseous-like tissue. J Dev Biol Tissue Eng. 2011;3:42–7.

5. Joon Ko Y, Zaharias R, Seabold D, Lafoon J, Schneider G. Osteoblast differentiation is enhanced in rotary cell culture simulated microgravity environments. J Prosthodont. 2007;16:431–8.

6. Haugen S, He J, Sundaresan A, et al. Adiponectin reduces bone stiffness: verified in a three-dimensional artificial human bone model in vitro. Front Endocrinol. 2018;9:236.

7. Lips P, van Schoor NM. The effect of vitamin D on bone and osteoporosis. Best Pract Res Clin Endocrinol Metab. 2011;25(4):585–91.

8. Jones G, Strugnell SA, DeLuca HF. Current understanding of the molecular actions of vitamin D. Physiol Rev. 1998;78(4):1193–231.

9. Christakos S, Ajibade DV, Dhawan P, Fechner AJ, Mady LJ. Vitamin D: metabolism. Endocrinol Metab Clin North Am. 2010;39(2):243–53.

10. Zerwekh JE. Blood biomarkers of vitamin D status. Am J Clin Nutr. 2008;87(4):1087S–91S.

11. Howard GA, Turner RT, Sherrard DJ, Baylink DJ. Human bone cells in culture metabolize 25-hydroxyvitamin D3 to 1,25-dihydroxyvitamin D3 and 24,25-dihydroxyvitamin D3. J Biol Chem. 1981;256(15): 7738–40.

12. van Driel M, Koedam M, Buurman CJ, et al. Evidence for auto/paracrine actions of vitamin D in bone: 1alpha-hydroxylase expression and activity in human bone cells. FASEB J. 2006;20(13):2417–9.

13. Berger U, Wilson P, McClelland RA, et al. Immunocytochemical detection of 1,25-dihydroxyvitamin D receptors in normal human tissues. J Clin Endocrinol Metab. 1988;67(3):607–13.

14. Boivin G, Mesguich P, Pike JW, et al. Ultrastructural immunocytochemical localization of endogenous 1,25-dihydroxyvitamin D3 and its receptors in osteoblasts and osteocytes from neonatal mouse and rat calvaria. Bone Miner. 1987;3(2):125–36.

15. Wang Y, Zhu J, DeLuca HF. Identification of the vitamin D receptor in osteoblasts and chondrocytes but not osteoclasts in mouse bone. J Bone Miner Res. 2014;29(3):685–92.

16. Lips P. Relative value of 25(OH)D and 1,25(OH)2D measurements. J Bone Miner Res. 2007;22(11):1668–71.

17. Shea MK, Booth SL. Update on the role of vitamin K in skeletal health. Nutr Rev. 2008;66(10):549–57.

18. Beulens JWJ, Booth SL, van den Heuvel EGHM, Stoecklin E, Baka A, Vermeer C. The role of menaquinones (vitamin K2) in human health. Br J Nutr. 2013;110(8):1357–68.

19. Bügel S. Vitamin K and bone health in adult humans. Vitam Horm. 2008;78:393–416. San Diego, CA: Elsevier Academic Press Inc.

20. Ferland G. The vitamin k-dependent proteins: an update. Nutr Rev. 1998;56(8):223–30.

21. Wen L, Chen J, Duan L, Li S. Vitamin K dependent proteins involved in bone and cardiovascular health (review). Mol Med Rep. 2018;18 (1):3–15.

22. Cancela L, Hsieh CL, Francke U, Price PA. Molecular structure, chromosome assignment, and promoter organization of the human matrix Gla protein gene. J Biol Chem. 1990;265(25):15040–8.

23. Lombardi G, Perego S, Luzi L, Banfi G. A four-season molecule: osteocalcin. Updates in its physiological roles. Endocrine. 2015;48(2): 394–404.

24. Norris RA, Damon B, Mironov V, et al. Periostin regulates collagen fibrillogenesis and the biomechanical properties of connective tissues. J Cell Biochem. 2007;101(3):695–711.

25. Koshihara Y, Hoshi K, Okawara R, Ishibashi H, Yamamoto S. Vitamin K stimulates osteoblastogenesis and inhibits osteoclastogenesis in human bone marrow cell culture. J Endocrinol. 2003;176(3):339–48.

26. Tabb MM, Sun A, Zhou C, et al. Vitamin K2 regulation of bone homeostasis is mediated by the steroid and xenobiotic receptor SXR. J Biol Chem. 2003;278(45):43919–27.

27. Yamaguchi M, Weitzmann MN. Vitamin K2 stimulates osteoblastogenesis and suppresses osteoclastogenesis by suppressing NF-kappaB activation. Int J Mol Med. 2011;27(1):3–14.

28. Feskanich D, Weber P, Willett WC, Rockett H, Booth SL, Colditz GA. Vitamin K intake and hip fractures in women: a prospective study. Am J Clin Nutr. 1999;69(1):74–9.

29. Booth SL, Tucker KL, Chen H, et al. Dietary vitamin K intakes are associated with hip fracture but not with bone mineral density in elderly men and women. Am J Clin Nutr. 2000;71(5):1201–8.

30. Szulc P, Chapuy MC, Meunier PJ, Delmas PD. Serum undercarboxylated osteocalcin is a marker of the risk of hip fracture in elderly women. J Clin Invest. 1993;91(4):1769–74.

31. Iwamoto J. Vitamin K_2 therapy for postmenopausal osteoporosis. Nutrients. 2014;6(5):1971–80.

32. Palermo A, Tuccinardi D, D'Onofrio L, et al. Vitamin K and osteoporosis: myth or reality? Metabolism. 2017;70:57–71.

33. Kidd PM. Vitamins D and K as pleiotropic nutrients: clinical importance to the skeletal and cardiovascular systems and preliminary evidence for synergy. Altern Med Rev. 2010;15(3):199–222.

34. Price PA, Baukol SA. 1,25-Dihydroxyvitamin D3 increases synthesis of the vitamin K-dependent bone protein by osteosarcoma cells. J Biol Chem. 1980;255(24):11660–3.

35. Price PA, Baukol SA. 1,25-Dihydroxyvitamin D3 increases serum levels of the vitamin K-dependent bone protein. Biochem Biophys Res Commun. 1981;99(3):928–35.

36. Poon CC, Li RW, Seto SW, et al. In vitro vitamin K(2) and 1alpha,25-dihydroxyvitamin D(3) combination enhances osteoblasts anabolism of diabetic mice. Eur J Pharmacol. 2015;767:30–40.

37. Miyake N, Hoshi K, Sano Y, Kikuchi K, Tadano K, Koshihara Y. 1,25-Dihydroxyvitamin D3 promotes vitamin K2 metabolism in human osteoblasts. Osteoporos Int. 2001;12(8):680–7.

38. Ushiroyama T, Ikeda A, Ueki M. Effect of continuous combined therapy with vitamin K(2) and vitamin D(3) on bone mineral density and coagulofibrinolysis function in postmenopausal women. Maturitas. 2002;41(3):211–21.

39. Iwamoto J, Takeda T, Ichimura S. Effect of combined administration of vitamin D3 and vitamin K2 on bone mineral density of the lumbar spine in postmenopausal women with osteoporosis. J Orthop Sci. 2000;5(6):546–51.

40. Binkley N, Harke J, Krueger D, et al. Vitamin K treatment reduces undercarboxylated osteocalcin but does not alter bone turnover, density, or geometry in healthy postmenopausal north American women. J Bone Min Res. 2009;24(6):983–91.

41. He J, Zhang Z, Kristiansen H. Nanomechanical characterization of single Micron-sized polymer particles. J Appl Polym Sci. 2009;113: 1398–405.

42. Luna LG. Histopathologic methods and color atlas of special stains and tissue artifacts. Gaithersberg, MD: American Histolabs Inc; 1993 pp 255–6.

43. Brauer A, Pohlemann T, Metzger W. Osteogenic differentiation of immature osteoblasts: interplay of cell culture media and supplements. Biotech Histochem. 2016;91(3):161–9.

44. Pfaffl MW. A new mathematical model for relative quantification in real-time RT-PCR. Nucleic Acids Res. 2001;29(9):e45.

45. Wrzesinski K, Fey S. From 2D to 3D–A new dimension for modelling the effect of natural products on human tissue. Curr Pharm Des. 2015;21:5605–16.

46. Burr DB. Bone material properties and mineral matrix contributions to fracture risk or age in women and men. J Musculoskelet Neuronal Interact. 2002;2(3):201–4.

47. Viguet-Carrin S, Garnero P, Delmas PD. The role of collagen in bone strength. Osteoporos Int. 2006;17(3):319–36.

48. Currey JD. The relationship between the stiffness and the mineral content of bone. J Biomech. 1969;2(4):477–80.

49. Boskey AL, Coleman R. Aging and bone. J Dent Res. 2010;89(12): 1333–48.

50. Ichikawa T, Horie-Inoue K, Ikeda K, Blumberg B, Inoue S. Steroid and xenobiotic receptor SXR mediates vitamin K2-activated transcription of extracellular matrix-related genes and collagen accumulation in osteoblastic cells. J Biol Chem. 2006;281(25):16927–34.

51. Mandatori D, Penolazzi L, Pipino C, et al. Menaquinone-4 enhances osteogenic potential of human amniotic fluid mesenchymal stem cells cultured in 2D and 3D dynamic culture systems. J Tissue Eng Regen Med. 2018;12(2):447–59.

52. Lancaster C, Harrison R. Effects of vitamin D, K1, and K2 supplementation on bone formation by osteoblasts in vitro: a meta-analysis. J Biom Biostat. 2017;8(4). https://doi.org/10.4172/2155-6180. 1000365.

53. Lin RZ, Chang HY. Recent advances in three-dimensional multicellular spheroid culture for biomedical research. Biotechnol J. 2008;3 (9–10):1172–84.

54. Mehta G, Hsiao AY, Ingram M, Luker GD, Takayama S. Opportunities and challenges for use of tumor spheroids as models to test drug delivery and efficacy. J Control Release. 2012;164(2):192–204.

55. Khaitan D, Chandna S, Arya MB, Dwarakanath BS. Establishment and characterization of multicellular spheroids from a human glioma cell line; implications for tumor therapy. J Transl Med. 2006;4(12). https:// doi.org/10.1186/1479-5876-4-12.

56. Aubin JE. Advances in the osteoblast lineage. Biochem Cell Biol. 1998; 76(6):899–910.

57. Jähn K, Richards RG, Archer CW, Stoddart MJ. Pellet culture model for human primary osteoblasts. Eur Cell Mater. 2010;20:149–61.

58. Kato Y, Windle JJ, Koop BA, Mundy GR, Bonewald LF. Establishment of an osteocyte-like cell line, MLO-Y4. J Bone Miner Res. 1997;12 (12):2014–23.

59. Kim J, Adachi T. Cell condensation triggers the differentiation of osteoblast precursor cells to osteocyte-like cells. Front Bioeng Biotechnol. 2019;7(288). https://doi.org/10.3389/fbioe.2019.00288.

60. Sun Q, Gu Y, Zhang W, Dziopa L, Zilberberg J, Lee W. Ex vivo 3D osteocyte network construction with primary murine bone cells. Bone Res. 2015;3:15026.

61. Bailey S, Karsenty G, Gundberg C, Vashishth D. Osteocalcin and osteopontin influence bone morphology and mechanical properties. Ann N Y Acad Sci. 2017;1409(1):79–84.

62. Ritter NM, Farach-Carson MC, Butler WT. Evidence for the formation of a complex between osteopontin and osteocalcin. J Bone Miner Res. 1992;7(8):877–85.

63. Poundarik AA, Diab T, Sroga GE, et al. Dilatational band formation in bone. Proc Natl Acad Sci U S A. 2012;109(47):19178–83.

64. Fantner GE, Hassenkam T, Kindt JH, et al. Sacrificial bonds and hidden length dissipate energy as mineralized fibrils separate during bone fracture. Nat Mater. 2005;4(8):612–6.

65. Morgan S, Poundarik AA, Vashishth D. Do non-collagenous proteins affect skeletal mechanical properties? Calcif Tissue Int. 2015;97(3): 281–91.

66. Patti A, Gennari L, Merlotti D, Dotta F, Nuti R. Endocrine actions of osteocalcin. Int J Endocrinol. 2013;2013:846480.

67. van Driel M, Koedam M, Buurman CJ, et al. Evidence that both 1alpha,25-dihydroxyvitamin D3 and 24-hydroxylated D3 enhance human osteoblast differentiation and mineralization. J Cell Biochem. 2006;99(3):922–35.

68. van der Meijden K, Lips P, van Driel M, et al. Primary human osteoblasts in response to 25-hydroxyvitamin D3, 1,25-dihydroxyvitamin D3 and 24R,25-dihydroxyvitamin D3. PLoS One. 2014;9(10):e110283.

69. Koshihara Y, Hoshi K, Ishibashi H, Shiraki M. Vitamin K2 promotes 1alpha,25(OH)2 vitamin D3-induced mineralization in human periosteal osteoblasts. Calcif Tissue Int. 1996;59(6):466–73.

70. Stein GS, Lian JB, Stein JL, Van Wijnen AJ, Montecino M. Transcriptional control of osteoblast growth and differentiation. Physiol Rev. 1996;76(2):593–629.

71. Blanchard F, Duplomb L, Baud'huin M, Brounais B. The dual role of IL-6-type cytokines on bone remodeling and bone tumors. Cytokine Growth Factor Rev. 2009;20(1):19–28.

72. Morvan F, Boulukos K, Clément-Lacroix P, et al. Deletion of a single allele of the Dkk1 gene leads to an increase in bone formation and bone mass. J Bone Miner Res. 2006;21(6):934–45.

Osteoblasts in a Perfusion Flow Bioreactor—Tissue Engineered Constructs of TiO₂ Scaffolds and Cells for Improved Clinical Performance

Maria Schröder, Janne Elin Reseland [ID] and Håvard Jostein Haugen *[ID]

Department of Biomaterials, Institute of Clinical Dentistry, University of Oslo, NO-0317 P.O. Box 1109 Blindern Oslo, Norway; maria.schroder@odont.uio.no (M.S.); j.e.reseland@odont.uio.no (J.E.R.)
* Correspondence: h.j.haugen@odont.uio.no; Tel.: +47-22852170

Abstract: Combining biomaterial scaffolds with cells serves as a promising strategy for engineering critical size defects; however, homogenous cellular growth within large scaffolds is challenging. Mechanical stimuli can enhance bone regeneration by modulating cellular growth and differentiation. Here, we compare dynamic seeding in a perfusion flow bioreactor with static seeding for a synthetic bone scaffold for up to 21 days using the cell line MC3T3-E1 and primary human osteoblast, confocal laser scanning microscopy, and real-time reverse transcriptase-polymerase chain reaction. The secretion of bone-related proteins was quantified using multiplex immunoassays. Dynamic culture improved cellular distribution through the TiO₂ scaffold and induced a five-fold increase in cell number after 21 days. The relative mRNA expression of osteopontin of MC3T3-E1 was 40-fold enhanced after 7 and 21 days at a flow rate of 0.08 mL/min, and that of collagen type I alpha I expression was 18-fold after 21 days. A flow rate of 0.16 mL/min was 10-fold less effective. Dynamic culture increased the levels of dickkopf-related protein 1 (60-fold), osteoprotegrin (29-fold), interleukin-6 (23-fold), interleukin-8 (36-fold), monocyte chemoattractant protein 1 (28-fold) and vascular endothelial growth factor (6-fold) in the medium of primary human osteoblasts after 21 days compared to static seeding. The proposed method may have clinical potential for bone tissue engineering.

Keywords: perfusion bioreactor; synthetic bone scaffold; wall shear stress; fluid flow; bone tissue engineering; human osteoblasts

1. Introduction

Today only a handful of scaffolds lead the craniomaxillofacial market. As a result of increased regulatory restrictions, particularly in Europe (European Tissue and Cells Directive; EUTCD, 2004), and the Medical Device Regulation (MDR, 2017), allografts are less used in clinical practice, and their suppliers may be limited in the future [1,2]. European dentists still prefer xenografts as bone scaffolds. However, under MDR, xenografts experience a more challenging regulatory pathway [3]. More scientific literature and comparative studies are needed to convince dentists that new bone grafts (BGs) can provide more advantages than current xenografts. This may provide a shift from allografts and xenografts to synthetic scaffold BG substitutes [4]. One example of a synthetic scaffold is titanium dioxide (TiO₂), a block ceramic BG substitute with porous architecture which allows the formation of bone and vascularization, and has compressive strength similar to trabecular bone and biocompatible properties [5,6]. The ability of these scaffolds to promote the attachment, growth and differentiation of osteoblastic cells was demonstrated in vitro [7]. In addition, previous studies showed both bone ingrowth and angiogenesis within the structures of the TiO₂ block in vivo minipig and dog models [6,8]. These scaffolds are now in clinical use. Thereon, this is a promising biocompatible material which is also reported to have bioactive properties [9,10].

Although TiO$_2$ scaffolds favor new bone ingrowth in vivo [6,8,11], in chronic bone defects the rate of bone growth was found to be too slow [12]. Therefore, bone tissue engineering (BTE) strategies are needed for these TiO$_2$ scaffolds to increase clinical translation. One strategy may be to harvest osteoprogenitor/osteogenic cells from the patient and combine these with the scaffold in a dynamic culturing system.

Various dynamic culturing systems, including spinner flasks [13], rotating wall vessels [13,14], and perfusion bioreactors [15–17] were applied to BTE to overcome diffusion limitations of nutrients and oxygen in static culture environments. These cause reduced cellular viability and growth in the scaffold center compared to its periphery, limiting the ingrowth of new tissue into the scaffold [18–20]. Among these systems, perfusion bioreactors are most advantageous, as they provide enhanced delivery of nutrients and metabolites as well as the removal of waste products throughout the entire porous scaffold [21]. In addition to enhanced mass transport, fluid flow provides mechanical stimulation to the cells, similar to the bone mechanical environment in vivo. Here, mechanical loading exposes bone cells to mechanical stretch and interstitial fluid flow within the porous lacuna-canalicular bone network [22,23]. Fluid flow through a bone scaffold enhances osteoprogenitor cells' differentiation and improves osteoblast function [15,24,25]. However, the fluid flow and its wall shear stress (WSS) depend on scaffold pore structure and morphology. One cannot translate inlet fluid flow from one scaffold system to another without prior examination of computational fluid dynamics (CFD).

We analyzed the fluid flow and stimuli acting on cells in porous TiO$_2$ scaffolds using CFD under simulated perfusion culture conditions [26]. However, the prolonged effect of fluid flow and shear stress stimuli on bone cells, and their growth and differentiation in the scaffolds under experimental conditions, have not yet been studied.

This study investigated whether the in silico modeling for TiO$_2$ scaffolds can be verified experimentally using a custom-made flow perfusion bioreactor, and whether the system can be a beneficial BTE strategy for the scaffolds. The mouse preosteoblastic cell line MC3T3-E1 represents a standard model to investigate the effect of mechanical stimuli in three-dimensional bone scaffolds; fewer studies use human mesenchymal stem cells or osteoblasts. However, interspecies differences hamper the transfer of the results to clinical use [27].

We aimed to:

(1) Validate whether perfusion seeding of TiO$_2$ scaffold versus static seeding is beneficial for bone scaffolds prior to clinical use based on in silico modeling.

(2) Analyze the effect of shear fluid flow on the growth and differentiation of MC3T3-E1 cells and human osteoblasts cultured on TiO$_2$ scaffolds.

(3) Analyze the validity of the results obtained from the cell line osteoblasts compared to primary human osteoblasts.

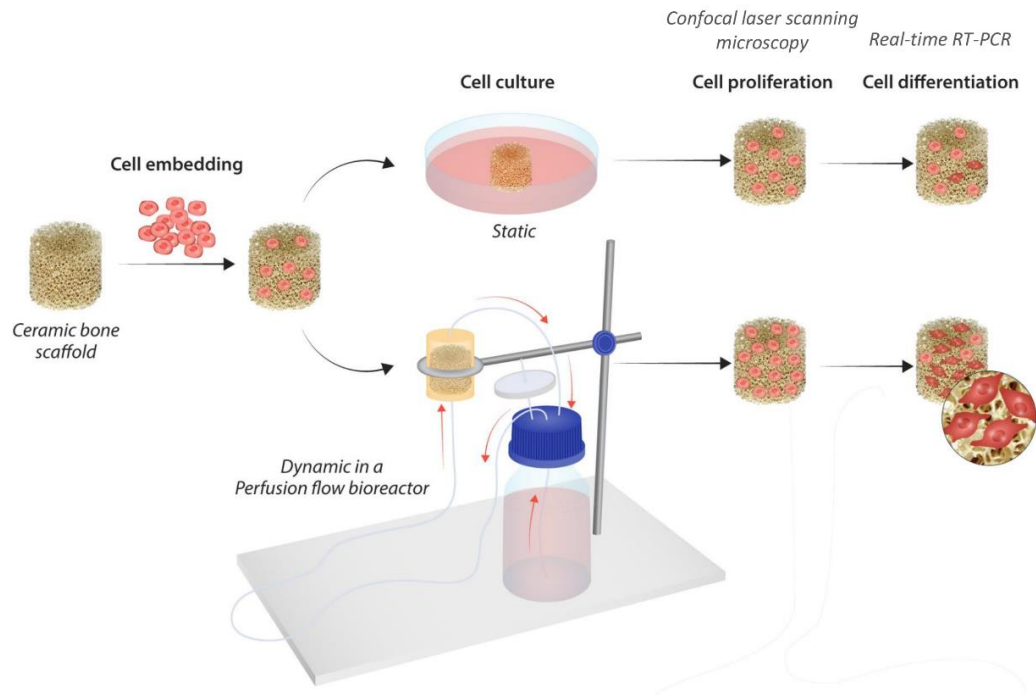An overview of the study's experimental design is shown in Figure 1.

Figure 1. Experimental design of the study.

2. Materials and Methods

2.1. Fabrication of TiO$_2$ Scaffolds

Porous TiO$_2$ scaffolds, with 8 mm height and 9 mm diameter, were produced using commercial TiO$_2$ powder (Kronos 1171, Kronos Titan GmbH, Leverkusen, Germany) and polymer sponge replication as previously described [28]. In brief, cylindrical polyurethane foam templates were coated with TiO$_2$ slurry, dried, the polymer template was burned out, and the scaffolds were sintered at 1500 °C for 40 h. The scaffolds were steam sterilized at 121 °C for 20 min before cell culture.

2.2. Cell Culture and Seeding

The mouse preosteoblastic cell line MC3T3-E1 (ATCC, Manassas, VA, USA) was cultured in α-MEM + GlutaMAX (Gibco) supplemented with 10% fetal bovine serum (FBS, PAA Laboratories GmbH, Pasching, Austria), 100 U mL^{-1} penicillin, 100 µg mL^{-1} streptomycin (Gibco) and primary human osteoblasts (Cambrex Bio Science, Walkersville, MD, USA) from two donors (one from humerus and one from tibia) in osteoblast growth medium supplemented with 10% FBS, 0.1% gentamicin sulphate/amphotericin B and 0.1% ascorbic acid (Lonza, Walkersville, MD, USA) at 37 °C in a humidified atmosphere of 95% air and 5% CO$_2$. As previously described [8], an agitated seeding method was used to ensure homogenous cell distribution throughout the scaffold. In brief, scaffolds were placed in non-adherent 48 well plates, a solution of 2×10^5 cells in culture medium was pipetted against the wall of each sample well, and the plates were agitated for 3 h at 37 °C. The scaffolds were then moved to a new 48 well plate and incubated for 24 h at 37 °C in the corresponding culture medium.

2.3. Perfusion Bioreactor System and Flow Culture

The flow perfusion bioreactor system consisted of a vertical cylindrical polyether ether ketone chamber with a 6 cm height and a 3 cm diameter with a round recess (diameter: 0.9 cm) for the scaffolds, which was connected to a 200 mL medium reservoir bottle with a customized cap of platinum-coated silicon tubing (HECO–Laboratorieutstyr AS, Oslo, Norway). Sterile gas exchange was maintained through a disposable air filter (0.2 µm PES, VWR) on the medium reservoir. Medium flow from the reservoir to the perfusion chamber

and back was generated using a peristaltic roller pump (Masterflex, Cole-Parmer, Vernon Hills, IL, USA). A small segment of the flow circuit consisted of Masterflex PharMed BPT tubing (Cole-Parmer, Vernon Hills, IL, USA) to ensure sufficient mechanical resistance of the tubing in the peristaltic pump. All components were autoclaved at 121 °C for 20 min and assembled under sterile conditions in a laminar flow hood. Each perfusion chamber housed two scaffolds. To allow for a homogenous distribution of medium flow through the seeded constructs, a grid (polytetrafluoroethylene; diameter: 0.9 cm; hole diameter: 0.1 cm) was placed in front of each scaffold. The perfusion chamber was filled with theculture medium, and the bioreactor system was placed in an incubator and operated at 37 °C. Two continuous media flow rates were analyzed in this study: 0.16 mL/min (inlet fluid velocity: 34 µm/s, based on [26]) and 0.08 mL/min (inlet fluid velocity: 17 µm/s). TiO_2 scaffolds cultured without flow were placed in a new 48-well plate and incubated at 37 °C in the corresponding culture medium. The media on both flow and non-flow cultures were changed twice a week. At day 7 and 21, the culture media from both flow and non-flow cultures were collected for analysis and scaffolds were harvested. Scaffolds were washed twice in PBS and stored either in this solution at 4 °C until microscopy or frozen at −80 °C until DNA quantification and RT-PCR.

2.4. DNA Quantification

TiO_2 scaffolds were incubated in lysis buffer (10 mM Tris pH 8, 1 mM EDTA, 0.2% *v/v* Triton X-100) for 1 h on ice. According to the manufacturer's protocol, double-stranded DNA (dsDNA) was quantified using Qubit 1X dsDNA HS Assay Kit and Qubit 4.0 Fluorometer (Thermo Fisher Scientific, Waltham, MA, USA).

2.5. Confocal Laser Scanning Microscopy

TiO_2 scaffolds were washed twice in PBS, fixed in 4% paraformaldehyde and washed again in PBS. Cells were permeabilized with 0.1% triton X-100 for 5 min, washed in PBS and blocked with 1% BSA in PBS for 60 min at room temperature. Following this, cells were stained with Alexa Fluor 568 Phalloidin (Thermo Fisher Scientific, Waltham, MA, USA) at 1:400 dilution in 1% BSA for 60 min and washed twice in PBS. Cells were counterstained with Hoechst 33342 (1 µg/mL in PBS; Sigma-Aldrich, Saint Louis, MO, USA), and scaffolds were stored in this solution until microscopy. Prior to imaging, the scaffolds were halved with a scalpel. Imaging was performed using a Leica SP8 confocal microscope (Leica Microsystems CMS GmbH, Mannheim, Germany) using 405- and 552-nm excitation and 420- to 480-nm and 580- to 630-nm emission filters for Hoechst 33342 and Alexa Fluor 568, respectively. Confocal images were processed using ImageJ software (NIH, Bethesda, MD, USA).

2.6. RNA Isolation and Real-Time RT-PCR Analysis

Total RNA from TiO_2 scaffolds was isolated using RNeasy mini kit (Qiagen, Hilden, Germany) with some modifications to the manufacturer's protocol. In brief, scaffolds were incubated in a lysis buffer for 1 h at 4 °C and agitated on an orbital shaker for 10 min. Then the lysate was sonicated (UP50H; Hielscher Ultrasonics GmbH, Teltow, Germany) for 10 s. The rest of the isolation followed the manufacturer's protocol. cDNA was synthesized using RevertAid First Strand cDNA Synthesis Kit and oligo dT primers according to the manufacturer's protocol (Thermo Fisher Scientific, Waltham, MA, USA). Real-time PCR was carried out in BioRad CFX Connect System (Bio-Rad Laboratories, Hercules, CA, USA), using SYBR green-based assay iQ SYBR supermix (Bio-Rad Laboratories, Hercules, CA, USA). Real-time RT-PCR data were analyzed using the $2^{-\Delta\Delta Ct}$ method 2 (Delta Delta C(T)) [29]. The primer sequences are listed in Table 1.

Table 1. Primer sequences used for real-time RT-PCR analysis.

Protein	Gene	Primer Sequence (5′–3′)
Mouse glyceraldehyde-3-phosphate dehydrogenase	m-*GAPDH*	f ACCCAGAAGACTGTGGATGG
	m-*GAPDH*	r CACATTGGG-GGTAGGAACAC
Mouse collagen type I alpha 1	m-*COL1A1*	f AGAGC-ATGACCGATGGATTC
	m-*COL1A1*	r CCTTCTTGAGGTTGCCAGTC
Mouse alkaline phosphatase	m-*ALPL*	f AACCCAGACACAAGCATTCC
	m-*ALPL*	r GAGAGCGAAGGGTC-AGTCAG
Mouse bone sialoprotein	m-*BSP*	f GAAA-ATGGAGACGGCGATAG
	m-*BSP*	r ACCCGAGAGTGTGGAAAGTG
Mouse osteopontin	m-*SPP1*	f TCTGCGGCAGGCATTCTCGG
	m-*SPP1*	r GTCA-CTTTCACCGGGAGGGAGGA
Mouse osteocalcin	m-*BGLAP*	f CCGGGAGCAG-TGTGAGCTTA
	m-*BGLAP*	r TAGATGC-GTTTGTAGGCGGTC
Mouse osterix	m-*SP7*	f AC-TGGCTAGGTGGTGGTCAG
	m-*SP7*	r GGTAGGGAGC-TGGGTTAAGG
Human-glyceraldehyde-3-phos-phate dehydrogenase	h-*GAPDH*	f CTCTGCTCCTCCTGTTCGAC
	h-*GAPDH*	r ACGACCAAATCCGTTGACTC
Human collagen type I alpha 1	h-*COL1A1*	f CCAAATCCG-ATGTTTCTGCT
	h-*COL1A1*	r CATCTCCCCTTCGTTTTTGA
Human alkaline phosphatase	h-*ALPL*	f AGACGCGCCTGGTAGTTGT
	h-*ALPL*	r GACAAGAAGCCCTTCACTGC
Human osteopontin	h-*SPP1*	f TGAGGTGATGTCCTCGTCTG
	h-*SPP1*	r GCC-GAGGTGATAGTGTGGTT
Human osteocalcin	h-*BGLAP*	f GCTTCACCCTCGAAATGGTA
	h-*BGLAP*	r GCAAGTAGCGCCAATCTAGG
Human osterix	h-*SP7*	f TACCCC-ATCTCCCTTGACTG
	h-*SP7*	r GCTGCAAGCTCTCCATAACC

2.7. Quantification of Proteins Secreted in the Cell Culture Medium

Multianalyte profiling of protein levels in the culture media was performed on the Luminex 200 system employing xMAP technology (Luminex Corp., Austin, TX, USA). Acquired fluorescence data were analyzed using xPONENT 3.1 software (Luminex, Austin, TX, USA). The secretion of dickkopf-related protein 1 (DKK-1), osteoprotegerin (OPG), interleukin-6 (IL-6), interleukin-8 (IL-8), monocyte chemoattractant protein 1 (MCP1) and vascular endothelial growth factor (VEGF) to the culture medium were measured using the Milliplex Human Bone Panel and a Cytokine/Chemokine kit. For the analysis, aliqouts of the culture media from the respective groups, the static samples and perfused samples, were pooled. The culture media from the perfused samples were concentrated five- to eight-fold using MicrosepTM centrifugal tubes with a 3 kDa cut-off. All further analyses were performed according to the manufacturer's protocols.

2.8. Statistical Analysis

Statistical analysis was performed using SigmaPlot software version 14.0 (Systat Software, San Jose, CA, USA). Data obtained using DNA assay and real-time RT-PCR ($\Delta\Delta$Ct values) were compared between the groups using a *t*-test or a Mann–Whitney U test, depending on their normal distribution. Data obtained using Luminex assay were compared between static and perfused samples using a Holm–Sidak test. A probability of ≤ 0.05 was considered significant.

3. Results

3.1. Effect of Medium Flow and Influence of Flow Rate on Growth and Distribution of MC3T3-E1 Cells Cultured on TiO₂ Scaffolds

Confocal microscopy revealed an uneven distribution of MC3T3-E1 cells on TiO$_2$ scaffolds cultured statically for 7 and 21 days. While the scaffold side (surface) exposed to the medium was highly populated with cells, fewer cells were found inside and on

the bottom of the scaffold. Perfusion culture at both the higher (0.16 mL/min) and lower (0.08 mL/min) flow rates resulted in a homogenous cellular distribution throughout the TiO_2 scaffold after 7 days. After 21 days of perfusion culture at both the higher and lower flow rates, the scaffold side from which the flow entered (inlet) was covered with a dense layer of cells, with most pores completely bridged by the cells. Compared to the inlet side, fewer cells were observed inside and on the side of the scaffold from which the flow exited (outlet). However, perfusion culture still increased the number of cells in these areas compared to the static group (Figure 2A). Confocal microscopy observations resembled the DNA assay. Determination of dsDNA content of the scaffolds showed that perfusion culture increased the proliferation of MC3T3-E1 cells after 7 and 21 days compared to static culture. A flow rate of 0.08 mL/min enhanced the dsDNA content 3.2-fold compared to the static group after 7 days ($p = 0.002$); a flow rate of 0.16 mL/min induced a 5.3-fold increase ($p < 0.001$). The increase at flow rate 0.16 mL/min was significantly higher than at 0.08 mL/min ($p = 0.001$). After 21 days, the dsDNA content of constructs perfused at 0.16 mL/min and 0.08 mL/min increased 4.7-fold and 4.9-fold compared to statically cultured scaffolds ($p = 0.003$ and $p = 0.004$), respectively (Figure 2B).
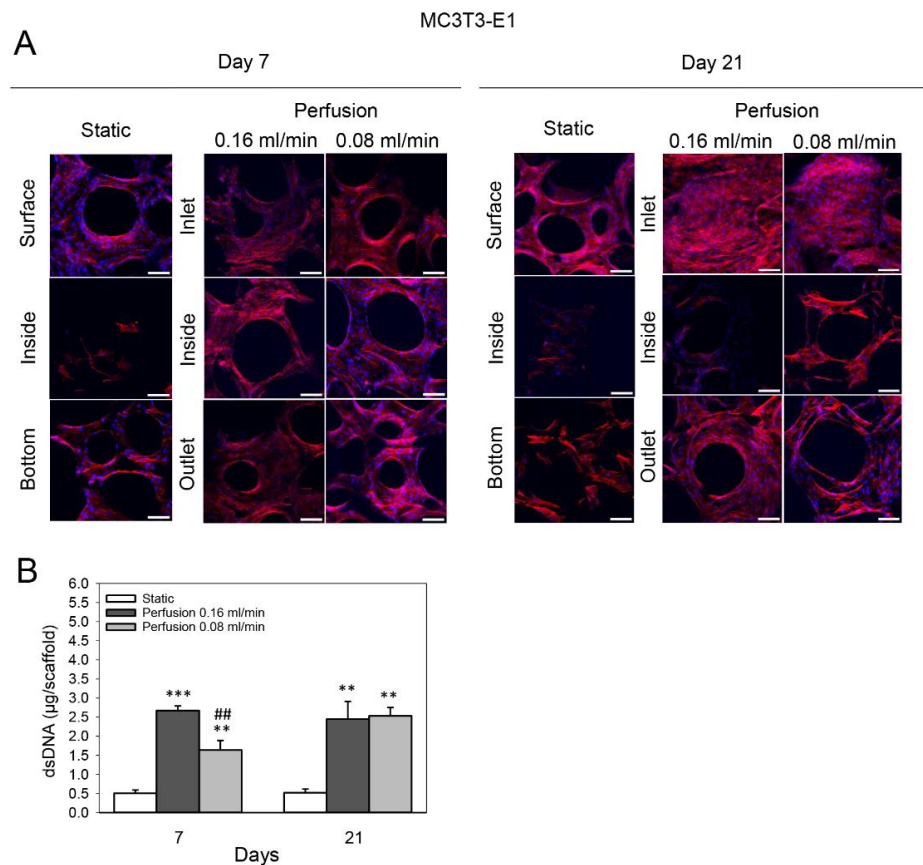

Figure 2. Effect of medium flow and influence of flow rate on growth and distribution of MC3T3-E1 cells cultured on TiO_2 scaffolds without flow (static) and with continuous flow (flow rates of 0.16 mL /min and 0.08 mL/min) for 7 and 21 days. (**A**) Immunofluorescence images of F-actin (red) and cell nuclei (blue). The top and bottom refer to the scaffold surfaces exposed to the medium and touching the well plate, respectively. Inlet and outlet refer to scaffold surfaces from which the flow entered and exited, respectively. Scaffolds were cut with a scalpel to observe the cellular distribution inside the scaffold. Scalebar = 100 μm. (**B**) Cultured scaffolds' double-stranded DNA (dsDNA) (shown in μg/scaffold) was quantified. Values represent the mean ± SD. Significant differences were analyzed with a SigmaPlot *t*-test. ** $p < 0.01$ and *** $p < 0.001$ indicate significance compared to the static group; ## $p < 0.01$ indicates significance compared to the perfusion 0.16 mL/min group.

3.2. Effect of Medium Flow on Growth and Distribution of Primary Human Osteoblasts Cultured on TiO₂ Scaffolds

The distribution of primary human osteoblasts on statically cultured TiO2 scaffolds after 7 and 21 days was similar to that of MC3T3-E1 cells. However, more cells were observed inside and at the bottom of the constructs at both time points. Perfusion culture at 0.08 mL/min enhanced cellular growth after 7 and 21 days mainly on the flow inlet side of the scaffolds compared to statically cultured constructs, and slightly more cells were observed inside and at the flow outlet side (Figure 3A). In line with this, the dsDNA content of these scaffolds was 2.5-fold greater compared to the static group on day 7 ($p < 0.001$) and 5.2-fold greater on day 21 ($p = 0.029$) (Figure 3B).
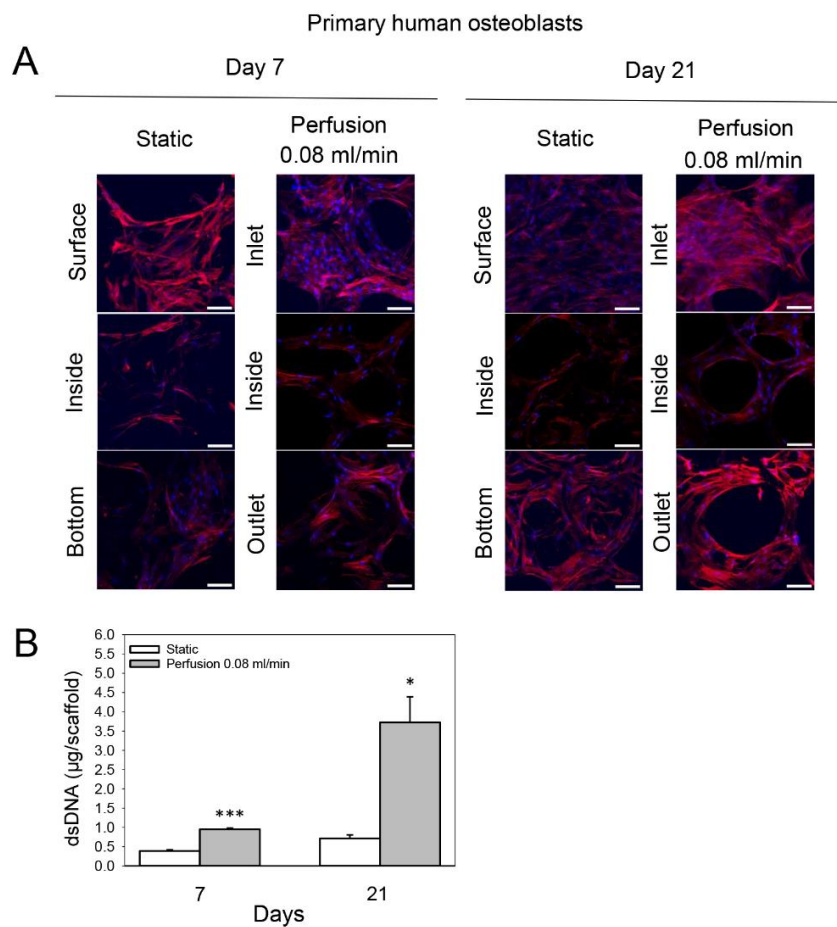

Figure 3. Effect of medium flow on growth and distribution of primary human osteoblasts cultured on TiO₂ scaffolds without flow (static) and with continuous flow (flow rate of 0.08 mL/min) for 7 and 21 days. (**A**) Immunofluorescence images of F-actin (red) and cell nuclei (blue). The top and bottom refer to the scaffold surfaces exposed to the medium and touching the well plate, respectively. Inlet and outlet refer to scaffold surfaces from which the flow entered and exited, respectively. Scaffolds were cut with a scalpel to observe the cellular distribution inside the scaffold. Scalebar = 100 μm. (**B**) Cultured scaffolds' double-stranded DNA (dsDNA) (shown in μg/scaffold) was quantified. Values represent the mean ± SD. Significant differences were analyzed with a SigmaPlot *t*-test. * $p < 0.05$ and *** $p < 0.001$ indicate significance compared to static group.

3.3. Effect of Medium Flow and Influence of Flow Rate on Osteogenic Gene Expression of MC3T3-E1 Cells Cultured on TiO₂ Scaffolds

Real-time RT-PCR analysis revealed that both the higher (0.16 mL/min) and lower (0.08 mL/min) flow rates enhanced the mRNA expression of *COL1A1* of MC3T3-E1 cells after 21 days compared to the static group ($p < 0.001$ for both; 2.8-fold and 18.3-fold,

respectively). The increase at flow rate 0.08 mL/min was significantly higher than at 0.16 mL/min ($p < 0.001$) (Figure 4A). The mRNA expression of *ALPL* of MC3T3-E1 cells was 3-fold reduced at flow rate 0.16 mL/min after 7 days compared to the static group ($p = 0.004$), and even more so at flow rate 0.08 mL/min (12.8-fold, $p < 0.001$) (0.16 mL/min vs. 0.08 mL/min, $p = 0.002$) (Figure 4B). Moreover, perfusion culture elevated the mRNA expression of *SPP1* of MC3T3-E1 cells after 7 and 21 days compared to static culture. At day 7, flow rate 0.16 mL/min induced a 3.9-fold increase compared to the static group, and flow rate 0.08 mL/min induced an even higher increase (42.7-fold, $p < 0.001$ for both) (0.16 mL/min vs. 0.08 mL/min, $p < 0.001$); a similar pattern was observed after 21 days (Figure 4C). In addition, perfusion culture reduced the mRNA expression of *BSP* of MC3T3-E1 cells after 7 days compared to static culture (flow rate 0.16 mL/min, 3.3-fold ($p < 0.001$), flow rate 0.08 mL/min, 6.3-fold); however, no significant difference was found between the two groups ($p = 0.055$). After 21 days, the lower flow rate induced a slight increase in the mRNA expression of *BSP* (1.4-fold, $p = 0.003$) (Figure 4D). The mRNA expression of *BGLAP* of MC3T3-E1 cells was reduced 16.4-fold at flow rate 0.16 mL/min after 7 days compared to the static group, and 32.8-fold at flow rate 0.08 mL/min ($p < 0.001$ for both); however, no significant difference was found between the two groups ($p = 0.061$). After 21 days, the higher flow rate induced a 1.7-fold reduction in the mRNA expression of *BGLAP* and the lower flow rate induced an even greater reduction (3.6-fold, $p < 0.001$ for both) (0.16 mL/min vs. 0.08 mL/min, $p = 0.004$) (Figure 4E). The mRNA expression of *SP7* of MC3T3-E1 cells was 2-fold enhanced at flow rate 0.16 mL/min after 7 days compared to the static group ($p = 0.004$), and 3.9-fold after 21 days ($p < 0.001$) (Figure 4F).
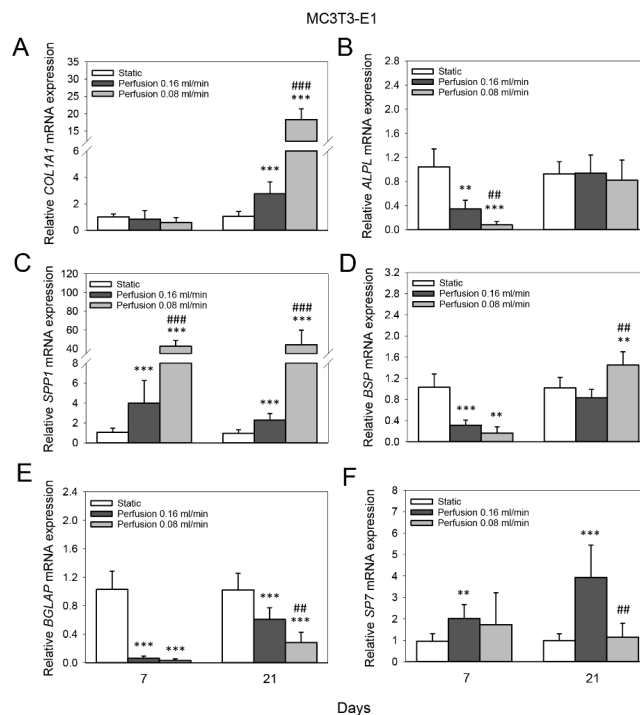

Figure 4. Effect of medium flow and influence of flow rate on osteogenic gene expression of MC3T3-E1 cells cultured on TiO$_2$ scaffolds. Relative mRNA levels of (**A**) collagen type I alpha 1 (*COL1A1*), (**B**) alkaline phosphatase (*ALPL*), (**C**) osteopontin (*SPP1*), (**D**) bone sialoprotein (*BSP*), (**E**) osteocalcin (*BGLAP*) and (**F**) osterix (*SP7*) without flow (static) and with continuous flow (flow rates of 0.16 mL /min and 0.08 mL/min) at day 7 and 21. Data represent fold changes of target genes normalized to reference gene *GAPDH* (glyceraldehyde-3-phosphate dehydrogenase). Values represent the mean ± SD. Significant differences were analyzed using a SigmaPlot *t*-test. ** $p < 0.01$ and *** $p < 0.001$ indicate significance compared to the static group; ## $p < 0.01$ and ### $p < 0.001$ indicate significance compared to perfusion 0.16 mL/min group.

3.4. Effect of Medium Flow on Osteogenic Gene Expression of Primary Human Osteoblasts Cultured on TiO$_2$ Scaffolds

Perfusion culture at 0.08 mL/min induced a 2.2-fold increase in the mRNA expression of *COL1A1* of primary human osteoblasts after 21 days compared to the static group ($p < 0.001$) (Figure 5A). The mRNA expression of *ALPL* of primary human osteoblasts was 4-fold enhanced at a flow rate of 0.08 mL/min after 7 days compared to static culture ($p < 0.001$), while after 21 days, a 4.9-fold reduction was observed ($p < 0.001$) (Figure 5B). Furthermore, *SPP1* mRNA expression of primary human osteoblasts was elevated 61.5-fold at a flow rate of 0.08 mL/min after 7 days compared to static culture and 3.3-fold after 21 days ($p < 0.001$ for both) (Figure 5C). The mRNA expression of *BGLAP* of primary human osteoblasts on TiO$_2$ scaffolds was not significantly altered after 7 or 21 days by perfusion culture at 0.08 mL/min compared to the static group (Figure 5D). However, the mRNA expression of *SP7* was 2.3-fold enhanced at a flow rate of 0.08 mL/min after 7 days compared to static culture ($p = 0.013$) (Figure 5E).
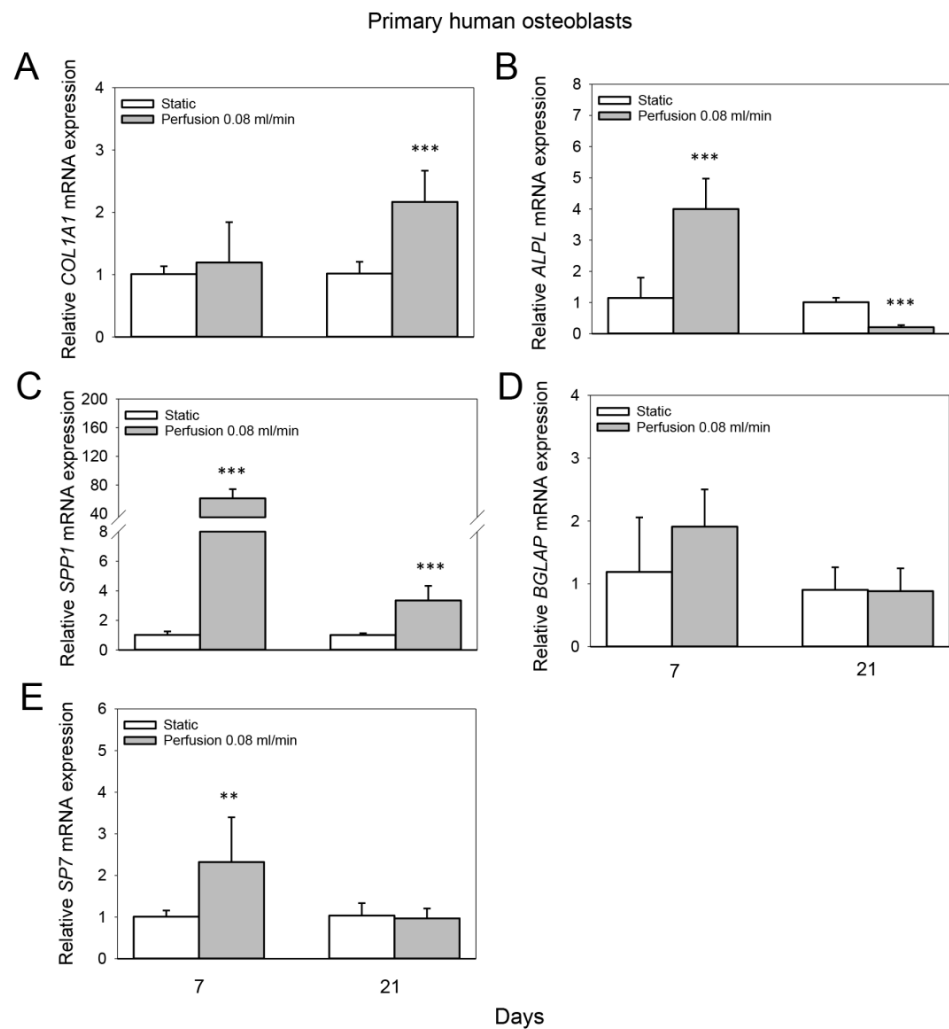

Figure 5. Effect of medium flow on osteogenic gene expression of primary human osteoblasts cultured on TiO$_2$ scaffolds. Relative mRNA levels of (**A**) collagen type I alpha 1 (*COL1A1*), (**B**) alkaline phosphatase (*ALPL*), (**C**) osteopontin (*SPP1*), (**D**) osteocalcin (*BGLAP*) and (**E**) osterix (*SP7*) without flow (static) and with continuous flow (flow rate of 0.08 mL/min) at day 7 and 21. Data represent fold changes of target genes normalized to reference gene *GAPDH* (glyceraldehyde-3-phosphate dehydrogenase). Values represent the mean ± SD. Significant differences were analyzed using a SigmaPlot *t*-test. ** $p < 0.01$ and *** $p < 0.001$ indicate significance compared to static group.

3.5. Effect of Medium Flow on the Secretion of Bone-Related Proteins from Primary Human Osteoblasts Cultured on TiO$_2$ Scaffolds

The concentration of DKK-1 in the culture medium of primary human osteoblasts increased in the perfusion group after 7 days compared to the static group (donor 1: 10.7-fold; donor 2: 4.3-fold; $p < 0.001$ for both) and after 21 days (donor 1: 60-fold, $p < 0.001$; donor 2: 6.5-fold, $p = 0.013$) (Figure 6A). Moreover, perfusion culture induced 5.5-fold and 29.3-fold increases in OPG levels in the culture medium of primary human osteoblast donor 1 compared to static culture after 7 and 21 days ($p < 0.001$ for both), respectively (Figure 6B). The concentration of IL-6 in the culture medium of primary human osteoblasts increased 3.7-fold in the perfusion group after 7 days compared to the static group (donor 1, $p = 0.042$; donor 2, $p = 0.03$); after 21 days, 23.4-fold and 17-fold increases were observed for donor 1 and donor 2 ($p < 0.001$), respectively (Figure 6C). In line with this, IL-8 levels in the culture medium of primary human osteoblasts increased 35.8-fold (donor 1) and 15.4-fold (donor 2) after 21 days in the perfusion group compared to the static group ($p < 0.001$ for both) (Figure 6D). Furthermore, perfusion culture induced 27.9-fold (donor 1, $p < 0.001$) and 11.3-fold (donor 2, $p = 0.002$) increases in the amount of MCP-1 in the culture medium after 21 days compared to static culture (Figure 6E), and a 5.5-fold rise (donor 1; p=0.001) in VEGF (Figure 6F).
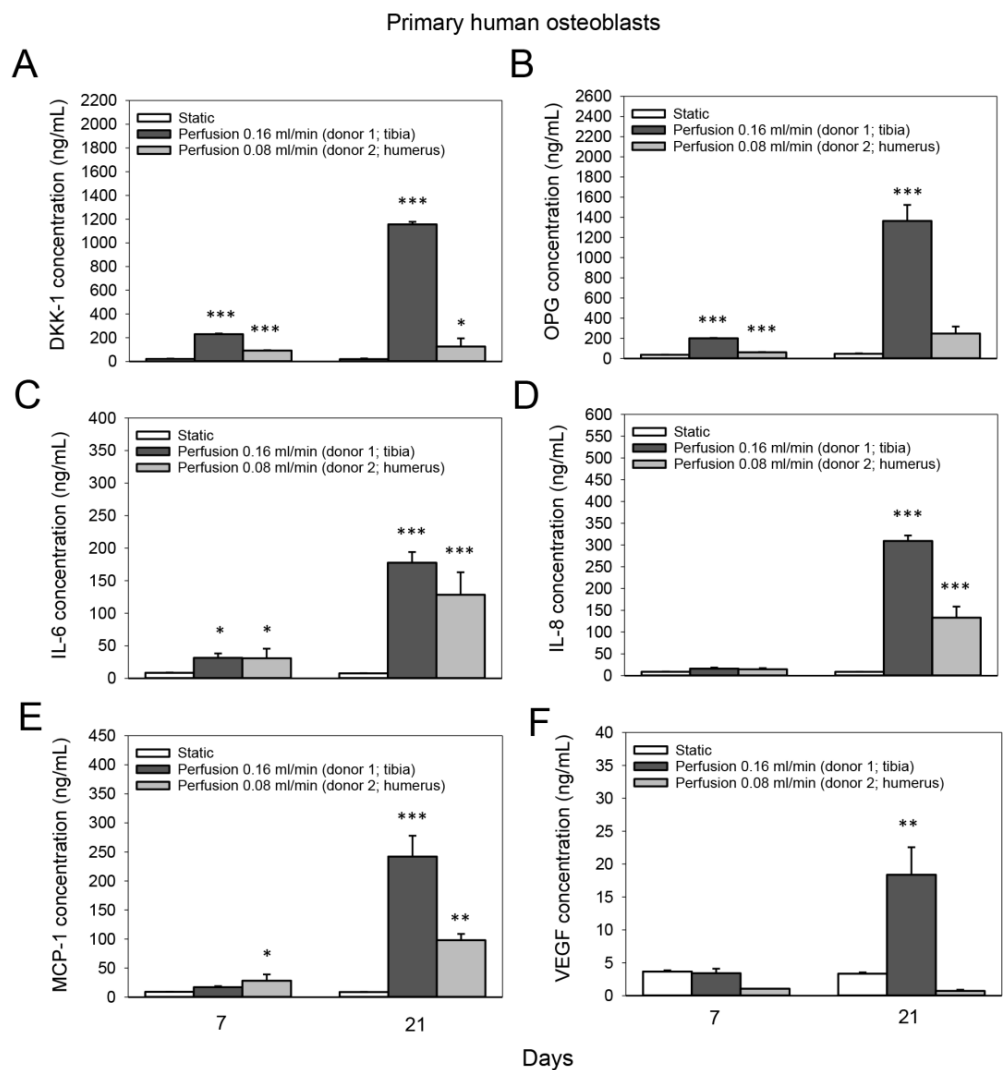

Figure 6. Effect of medium flow on the secretion of bone-related proteins from primary human osteoblasts cultured on TiO$_2$ scaffolds. Concentration (in ng/mL) of (**A**) dickkopf-related protein 1

(DKK-1), (**B**) osteoprotegrin (OPG), (**C**) interleukin-6 (IL-6), (**D**) interleukin-8 (IL-8), (**E**) monocyte chemoattractant protein 1 (MCP-1) and (**F**) vascular endothelial growth factor (VEGF) in the culture media of two different human osteoblasts donors without flow (static) and with continuous flow. The culture media of the static and perfused samples were pooled from two scaffolds. A flow rate of 0.16 mL/min was conducted with donor 1 (isolated from the tibia), and a flow rate of 0.08 mL/min was conducted with donor 2 (isolated from the humerus). Values represent the mean $\pm$ SD. Significant differences were analyzed using a SigmaPlot Holm-Sidak test. * $p < 0.05$, ** $p < 0.01$ and *** $p < 0.001$ indicate significance compared to staticgroup. Statistical comparison between the two perfusion groups was not performed due to the use of two different osteoblast donors.

The fluid flow and induced WSS can be viewed in Figure 7 based on previously performed CFDs.
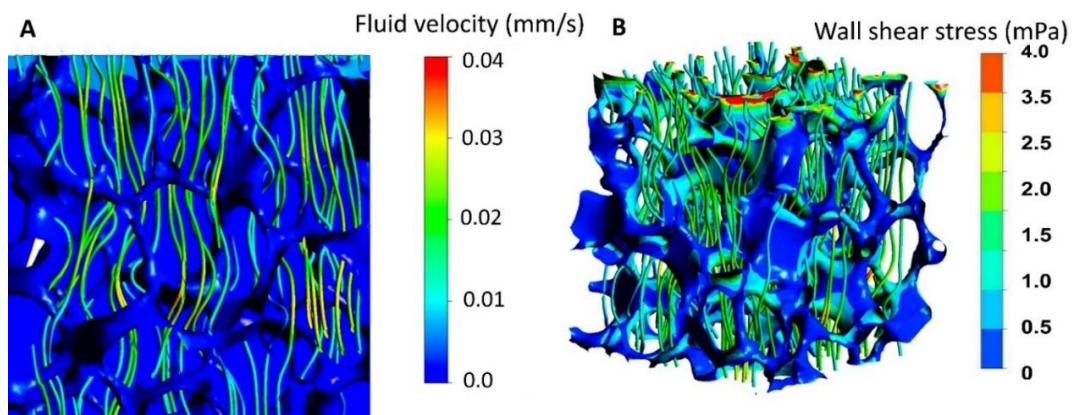

Figure 7. (A) The cross-sectional view of static pressure on the walls combined with streamlines, color coded according to velocity magnitude, when the inlet velocity was 0.08 mL/min. **(B)** Wall shear stress distribution in combination with streamlines, color coded according to velocity magnitude, when the inlet velocity was 34 μm/s. Reprinted with permission from Copyright Clearance Center's RightsLink® service reference number 5302731494559 [26].

4. Discussion

The BTE approach using in vitro expansion of cells on a scaffold prior to grafting into bone represents a promising alternative to current clinical treatments. TiO$_2$ scaffolds, as used here, show promising results in various in vivo experiments [6,8,11]. However, in a recent study [12] using a chronic non-contained bone defects application, less bone formation was observed in the TiO$_2$ groups compared to membrane alone at the final time point of 12 weeks of healing. To improve the clinical performance of bone scaffolds, various bioreactor systems are suggested, including spinner flasks, rotating wall bioreactors, and perfusion systems [21]. Perfusion systems expose cells to shear stress and more efficiently enhance nutrient transfer than other systems [30]; for this reason it was chosen as the bioreactor in this study. Shear influences osteoblastic differentiation [31–36], but the magnitude of shear stress cells are exposed to in various bioreactor systems is not always known. Modeling can be a tool for calculating the magnitude of shear stress and yield information on an ideal inlet fluid velocity. Although such modeling for the TiO$_2$ scaffolds was performed, it was never validated with in vitro experiments; nevertheless, the inlet fluid velocities were chosen as suggested in Zhang et al.'s simulation [26]. To validate the inlet fluid velocity, we exposed both human and cell line osteoblasts to shear stress to provide insight into the bone cell behavior pathways affected by long-term shear stress. Determining this effect will allow for a greater understanding of perfusion systems, lead to more effective optimization of these systems and potentially lead to a more effective introduction of these systems into clinical BTE.

The ability of material exchange can be characterized by interconnectivity and permeability in a bone scaffold. The predicted permeability of these scaffolds [26] was found to be within the range of cancellous bone by comparative analysis, and should positively influence the cell migration rate [37] when compared to static seeding. The present study clearly illustrates this effect, as significantly more bone cells were found after days 7 and 21. Our findings are comparable to other similar studies [38,39].

TiO_2 has higher pore interconnectivity and higher permeability (1.678×10^{-9} m^2) than other commercial scaffolds, which was more conducive to nutrient transport and metabolic product excretion and improved in vivo bone ingrowth [40,41]. Variations in inlet fluid velocity and fluid viscosity produce proportional and independent changes in fluid velocity, fluid shear stress and fluid pressure. These variations, here with two different inlet velocities, should cause different levels of mechanical stimuli within the scaffold [42,43]. According to Sandino et al. and Cartmell et al., 37–46 mPa shear stress can stimulate osteoblast differentiation into bone cells [39,44]. Furthermore, differentiation of the cells adhered to the surface wall of the TiO_2 scaffold should occur with the inlet fluid flow used, as it will provide a WSS from 1.35 to 2.55 mPa [44,45]. Indeed, the osteogenic gene expression of both the cell line and human osteoblasts were altered with the applied fluid flow. For instance, a flow rate of 0.08 mL/min highly upregulated collagen type I and osteopontin gene expression in MC3T3-E1 cells. This is in agreement with similar studies [46–48]. The phosphorylated glycoprotein osteopontin is an important factor in the formation of bone. It is secreted by osteoblasts during the early stage of bone development and binds to hydroxyapatite to promote the cell attachment and spreading necessary for bone formation and mineralization [49]. Since a flow rate of 0.16 mL/min was 10-fold less effective in upregulating osteopontin and collagen type I gene expression of the MC3T3-E1, we concentrated our efforts for the primary human osteoblasts on a flow rate of 0.08 mL/min. Here, we also observed a strong effect of fluid flow on the gene expression of osteopontin after 7 days; additionally, the gene expression of alkaline phosphatase, a crucial enzyme in the initiation of the bone mineralization process [50], was moderately enhanced. It slightly increased osterix expression, a transcription factor involved in osteoblast differentiation and bone formation [51], after 7 days. This is in contrast to the cell line osteoblasts and may be explained by interspecies differences in cellular response to fluid flow [52], highlighting the importance of validating the obtained results from the standardized osteoblast model in this study with primary human cells to improve the clinical performance of the TiO_2 scaffolds. Another reason for the discrepant results may be differences in the osteogenic differentiation stage of the two cell types during the flow culture [53]. In line with this, we observed that the gene expression of alkaline phosphatase, bone sialoprotein and osteocalcin (proteins involved in early and late osteogenic differentiation [54]) in cell line osteoblasts was remarkably reduced after 7 days of flow culture, while the expression of osteopontin was upregulated after 7 and 21 days. Osteopontin is expressed during two stages of osteogenesis, the early proliferative stage and prior to mineralization [54]. Hence, it is reasonable that human osteoblasts were at a more advanced stage of osteogenic differentiation than the cell line osteoblasts during the flow culture. However, using a culture medium specific to each cell type during the long-term perfusion may have also influenced the osteogenic gene expression.

We also aimed to analyze how applied shear stress affects the communication of primary human osteoblasts to the bone microenvironment. We observed that fluid flow increased the release of DKK-1, OPG, IL-6 and IL-8, factors modulating bone remodeling [55–58] from the human osteoblasts. In addition, fluid flow enhanced the release of the angiogenic factor MCP-1, which stimulates angiogenesis by upregulating VEGF [59], a key factor in promoting vascular growth during bone regeneration. VEGF is also involved in the coupling of angiogenesis and osteogenesis [60]. This may further promote vascularization in the TiO_2 scaffold interior during bone regeneration [6].

This study analyzed the effect of long-term shear stress on osteoblasts in the porous TiO_2 scaffolds. Several studies analyze the short-term responses of osteoblasts to fluid

flow in bone scaffolds [44,61,62]. However, these are less suitable for BTE approaches, as they cannot provide insights into essential stages during bone formation, such as the late osteogenic differentiation of osteoprogenitor cells, collagen matrix deposition or mineralization. For a BTE approach, it is vital to carefully study the long-term effect of shear stress on cells inside a bone scaffold to determine the ideal bioreactor culture duration prior to implantation. Furthermore, it has to be considered that the flow profile will change with time as the cells proliferate and start to deposit matrix.

5. Conclusions

In this study, we verified in silico modeling with an experimental approach using a custom-made perfusion flow bioreactor system and a synthetic bone graft substitute that is in clinical use. We used a standardized osteoblast model to investigate the effect of fluid flow generated by the system on the cellular response and were able to validate the results with primary human osteoblasts. We show that the perfusion system with the examined TiO_2 bone scaffolds had a positive effect on cellular growth and distribution. In addition, the gene expression of osteopontin and collagen type I alpha I was upregulated by the applied fluid flow, suggesting an effect on osteogenic differentiation. Primary human osteoblasts cultured in the flow bioreactor system communicated to the bone microenvironment by an increase in factors related to bone remodeling and angiogenesis. The proposed method may facilitate an increase in the clinical performance of synthetic bone scaffolds.

Author Contributions: Conceptualization, H.J.H., J.E.R. and M.S.; methodology, formal analysis, investigation, data curation, writing—original draft preparation, M.S.; writing—review and editing, H.J.H. and J.E.R.; supervision, H.J.H. and J.E.R.; project administration, H.J.H. and J.E.R.; funding acquisition, H.J.H. and J.E.R. All authors have read and agreed to the published version of the manuscript.

Institutional Review Board Statement: Not applicable.

Informed Consent Statement: Not applicable.

Data Availability Statement: Data are available upon request from the corresponding author.

Conflicts of Interest: Haugen holds patents behind the technology for the TiO2 scaffolds (EP Patent 2,121,053, US Patent 9,629,941, US Patent App. 14/427,901, US Patent App. 14/427,683, and US Patent App. 14/427,854). The rights for these patents are shared between the University of Oslo and Corticalis AS. Haugen is a shareholder and board member of Corticalis AS.

References

1. Bostrom, M.P.G.; Seigerman, D.A. The Clinical Use of Allografts, Demineralized Bone Matrices, Synthetic Bone Graft Substitutes and Osteoinductive Growth Factors: A Survey Study. *HSS J.®: Musculoskelet. J. Hosp. Spéc. Surg.* **2005**, *1*, 9–18. [CrossRef]
2. Bohner, M. Resorbable biomaterials as bone graft substitutes. *Mater. Today* **2010**, *13*, 24–30. [CrossRef]
3. Haugen, H.J.; Lyngstadaas, S.P.; Rossi, F.; Perale, G. Bone grafts: Which is the ideal biomaterial? *J. Clin. Periodontol.* **2019**, *46* (Suppl. S21), 92–102. [CrossRef] [PubMed]
4. Larsson, S.; Hannink, G. Injectable bone-graft substitutes: Current products, their characteristics and indications, and new developments. *Injury* **2011**, *42*, S30–S34. [CrossRef]
5. Tiainen, H.; Wiedmer, D.; Haugen, H.J. Processing of highly porous TiO_2 bone scaffolds with improved compressive strength. *J. Eur. Ceram. Soc.* **2013**, *33*, 15–24. [CrossRef]
6. Tiainen, H.; Wohlfahrt, J.C.; Verket, A.; Lyngstadaas, S.P.; Haugen, H.J. Bone formation in TiO_2 bone scaffolds in extraction sockets of minipigs. *Acta Biomater.* **2012**, *8*, 2384–2391. [CrossRef]

7.	Gómez-Florit, M.; Rubert, M.; Ramis, J.M.; Haugen, H.J.; Tiainen, H.; Lyngstadaas, S.P.; Monjo, M. TiO$_2$ Scaffolds Sustain Differentiation of MC3T3-E1 Cells. *J. Biomater. Tissue Eng.* **2012**, *2*, 336–344. [CrossRef]

8.	Haugen, H.J.; Monjo, M.; Rubert, M.; Verket, A.; Lyngstadaas, S.P.; Ellingsen, J.E.; Rønold, H.J.; Wohlfahrt, J.C. Porous ceramic titanium dioxide scaffolds promote bone formation in rabbit peri-implant cortical defect model. *Acta Biomater.* **2013**, *9*, 5390–5399. [CrossRef]

9.	Jokinen, M.; Pätsi, M.; Rahiala, H.; Peltola, T.; Ritala, M.; Rosenholm, J.B. Influence of sol and surface properties onin vitro bioactivity of sol-gel-derived TiO$_2$ and TiO$_2$-SiO$_2$ films deposited by dip-coating method. *J. Biomed. Mater. Res.* **1998**, *42*, 295–302. [CrossRef]

10.	Nygren, H.; Tengvall, P.; Lundström, I. The initial reactions of TiO$_2$ with blood. *J. Biomed. Mater. Res.* **1997**, *34*, 487–492. [CrossRef]

11.	Le Thieu, M.K.; Homayouni, A.; Hæren, L.R.; Tiainen, H.; Verket, A.; Ellingsen, J.E.; Rønold, H.J.; Wohlfahrt, J.C.; Gonzalez Cantalapiedra, A.; Guzon Muñoz, F.M.; et al. Impact of simultaneous placement of implant and block bone graft substitute: An in vivo peri-implant defect model. *Biomater. Res.* **2021**, *25*, 43. [CrossRef] [PubMed]

12.	Le Thieu, M.K.; Haugen, H.J.; Sanz-Esporrin, J.; Sanz, M.; Lyngstadaas, S.P.; Verket, A. Guided bone regeneration of chronic non-contained bone defects using a volume stable porous block TiO2 scaffold: An experimental in vivo study. *Clin. Oral Im-plant. Res.* **2021**, *32*, 369–381. [CrossRef] [PubMed]

13.	Sikavitsas, V.I.; Bancroft, G.N.; Mikos, A.G. Formation of three-dimensional cell/polymer constructs for bone tissue engineering in a spinner flask and a rotating wall vessel bioreactor. *J. Biomed. Mater. Res.* **2002**, *62*, 136–148. [CrossRef] [PubMed]

14.	Botchwey, E.A.; Pollack, S.R.; Levine, E.M.; Laurencin, C.T. Bone tissue engineering in a rotating bioreactor using a microcarrier matrix system. *J. Biomed. Mater. Res.* **2001**, *55*, 242–253. [CrossRef]

15.	Bancroft, G.N.; Sikavitsas, V.I.; Dolder, J.V.D.; Sheffield, T.L.; Ambrose, C.G.; Jansen, J.A.; Mikos, A.G. Fluid flow increases mineralized matrix deposition in 3D perfusion culture of marrow stromal osteoblasts in a dose-dependent manner. *Proc. Natl. Acad. Sci. USA* **2002**, *99*, 12600–12605. [CrossRef]

16.	Grayson, W.L.; Bhumiratana, S.; Cannizzaro, C.; Chao, P.-H.G.; Lennon, D.P.; Caplan, A.; Vunjak-Novakovic, G. Effects of Initial Seeding Density and Fluid Perfusion Rate on Formation of Tissue-Engineered Bone. *Tissue Eng. Part A* **2008**, *14*, 1809–1820. [CrossRef]

17.	Janssen, F.W.; Oostra, J.; Van Oorschot, A.; van Blitterswijk, C. A perfusion bioreactor system capable of producing clinically relevant volumes of tissue-engineered bone: In vivo bone formation showing proof of concept. *Biomaterials* **2006**, *27*, 315–323. [CrossRef]

18.	Goldstein, A. Effect of convection on osteoblastic cell growth and function in biodegradable polymer foam scaffolds. *Biomaterials* **2001**, *22*, 1279–1288. [CrossRef]

19.	Ishaug-Riley, S.L.; Crane, G.; Yaszemski, M.J.; Mikos, A.G. Three-dimensional culture of rat calvarial osteoblasts in porous biodegradable polymers. *Biomaterials* **1998**, *19*, 1405–1412. [CrossRef]

20.	Ishaug, S.L.; Crane, G.M.; Miller, M.J.; Yasko, A.W.; Yaszemski, M.J.; Mikos, A.G. Bone formation by three-dimensional stromal osteoblast culture in biodegradable polymer scaffolds. *J. Biomed. Mater. Res.* **1997**, *36*, 17–28. [CrossRef]

21.	Gaspar, D.; Gomide, V.; Monteiro, F. The role of perfusion bioreactors in bone tissue engineering. *Biomatter* **2012**, *2*, 167–175. [CrossRef] [PubMed]

22.	Birru, B.; Mekala, N.K.; Parcha, S.R. Mechanistic role of perfusion culture on bone regeneration. *J. Biosci.* **2019**, *44*, 23. [CrossRef] [PubMed]

23.	Duncan, R.L.; Turner, C.H. Mechanotransduction and the functional response of bone to mechanical strain. *Calcif. Tissue Res.* **1995**, *57*, 344–358. [CrossRef] [PubMed]

24.	Yamada, S.; Yassin, M.A.; Schwarz, T.; Hansmann, J.; Mustafa, K. Induction of osteogenic differentiation of bone marrow stromal cells on 3D polyester-based scaffolds solely by subphysiological fluidic stimulation in a laminar flow bioreactor. *J. Tissue Eng.* **2021**, *12*. [CrossRef]

25.	Moser, C.; Bardsley, K.; El Haj, A.J.; Alini, M.; Stoddart, M.J.; Bara, J.J. A Perfusion Culture System for Assessing Bone Marrow Stromal Cell Differentiation on PLGA Scaffolds for Bone Repair. *Front. Bioeng. Biotechnol.* **2018**, *6*. [CrossRef]

26.	Zhang, X.; Tiainen, H.; Haugen, H.J. Comparison of titanium dioxide scaffold with commercial bone graft materials through micro-finite element modelling in flow perfusion. *Med. Biol. Eng. Comput.* **2018**, *57*, 311–324. [CrossRef]

27.	Wittkowske, C.; Reilly, G.C.; Lacroix, D.; Perrault, C.M. In Vitro Bone Cell Models: Impact of Fluid Shear Stress on Bone Formation. *Front. Bioeng. Biotechnol.* **2016**, *4*, 87. [CrossRef]

28.	Tiainen, H.; Lyngstadaas, S.P.; Ellingsen, J.E.; Haugen, H.J. Ultra-porous titanium oxide scaffold with high compressive strength. *J. Mater. Sci. Mater. Med.* **2010**, *21*, 2783–2792. [CrossRef]

29.	Pfaffl, M.W. A new mathematical model for relative quantification in real-time RT-PCR. *Nucleic Acids Res.* **2001**, *29*, e45. [CrossRef]

30.	Sampson, K.; Koo, S.; Gadola, C.; Vasiukhina, A.; Singh, A.; Spartano, A.; Gollapudi, R.; Duley, M.; Mueller, J.; James, P.F.; et al. Cultivation of hierarchical 3D scaffolds inside a perfusion bioreactor: Scaffold design and finite-element analysis of fluid flow. *SN Appl. Sci.* **2021**, *3*, 884. [CrossRef]

31.	Mikos, A.G.; Bao, Y.; Cima, L.G.; Ingber, N.E.; Vacanti, J.P.; Langer, R. Preparation of poly(glycolic acid) bonded fiber structures for cell attachment and transplantation. *J. Biomed. Mater. Res.* **1993**, *27*, 183–189. [CrossRef] [PubMed]

32.	Martínez-Vázquez, F.; Cabañas, M.; Paris, J.; Lozano, D.; Vallet-Regí, M. Fabrication of novel Si-doped hydroxyapatite/gelatine scaffolds by rapid prototyping for drug delivery and bone regeneration. *Acta Biomater.* **2015**, *15*, 200–209. [CrossRef] [PubMed]

33. Karageorgiou, V.; Kaplan, D. Porosity of 3D biomaterial scaffolds and osteogenesis. *Biomaterials* **2005**, *26*, 5474–5491. [CrossRef] [PubMed]

34. Melchels, F.P.W.; Barradas, A.W.C.; van Blitterswijk, C.A.; de Boer, J.; Feijen, J.; Grijpma, D.W. Effects of the architecture of tissue engineering scaffolds on cell seeding and culturing. *Acta Biomater.* **2010**, *6*, 4208–4217. [CrossRef] [PubMed]

35. Otsuki, B.; Takemoto, M.; Fujibayashi, S.; Neo, M.; Kokubo, T.; Nakamura, T. Pore throat size and connectivity determine bone and tissue ingrowth into porous implants: Three-dimensional micro-CT based structural analyses of porous bioactive titanium implants. *Biomaterials* **2006**, *27*, 5892–5900. [CrossRef]

36. Jones, A.C.; Arns, C.; Hutmacher, D.W.; Milthorpe, B.K.; Sheppard, A.; Knackstedt, M.A. The correlation of pore morphology, interconnectivity and physical properties of 3D ceramic scaffolds with bone ingrowth. *Biomaterials* **2009**, *30*, 1440–1451. [CrossRef]

37. Jones, J.R.; Atwood, R.C.; Poologasundarampillai, G.; Yue, S.; Lee, P. Quantifying the 3D macrostructure of tissue scaffolds. *J. Mater. Sci. Mater. Electron.* **2008**, *20*, 463–471. [CrossRef]

38. Yeatts, A.; Fisher, J.P. Bone tissue engineering bioreactors: Dynamic culture and the influence of shear stress. *Bone* **2011**, *48*, 171–181. [CrossRef]

39. Sandino, C.; Planell, J.; Lacroix, D. A finite element study of mechanical stimuli in scaffolds for bone tissue engineering. *J. Biomech.* **2008**, *41*, 1005–1014. [CrossRef]

40. Mitsak, A.G.; Kemppainen, J.M.; Harris, M.T.; Hollister, S.J. Effect of Polycaprolactone Scaffold Permeability on Bone Regeneration in vivo. *Tissue Eng. Part A* **2011**, *17*, 1831–1839. [CrossRef]

41. Zhao, F.; Xiong, Y.; Ito, K.; van Rietbergen, B.; Hofmann, S. Porous Geometry Guided Micro-mechanical Environment Within Scaffolds for Cell Mechanobiology Study in Bone Tissue Engineering. *Front. Bioeng. Biotechnol.* **2021**, *9*, 736489. [CrossRef] [PubMed]

42. Zhang, X.; Gong, H. Simulation on tissue differentiations for different architecture designs in bone tissue engineering scaffold based on cellular structure model. *J. Mech. Med. Biol.* **2015**, *15*, 1550028. [CrossRef]

43. Olivares, A.L.; Marsal, È.; Planell, J.A.; Lacroix, D. Finite element study of scaffold architecture design and culture conditions for tissue engineering. *Biomaterials* **2009**, *30*, 6142–6149. [CrossRef] [PubMed]

44. Cartmell, S.H.; Porter, B.D.; García, A.J.; Guldberg, R.E. Effects of Medium Perfusion Rate on Cell-Seeded Three-Dimensional Bone Constructs in Vitro. *Tissue Eng.* **2003**, *9*, 1197–1203. [CrossRef] [PubMed]

45. McCoy, R.J.; O'Brien, F.J. Influence of Shear Stress in Perfusion Bioreactor Cultures for the Development of Three-Dimensional Bone Tissue Constructs: A Review. *Tissue Eng. Part B Rev.* **2010**, *16*, 587–601. [CrossRef]

46. Mueller, S.M.; Mizuno, S.; Gerstenfeld, L.C.; Glowacki, J. Medium Perfusion Enhances Osteogenesis by Murine Osteosarcoma Cells in Three-Dimensional Collagen Sponges. *J. Bone Miner. Res.* **1999**, *14*, 2118–2126. [CrossRef]

47. Bjerre, L.; Bünger, C.E.; Kassem, M.; Mygind, T. Flow perfusion culture of human mesenchymal stem cells on silicate-substituted tricalcium phosphate scaffolds. *Biomaterials* **2008**, *29*, 2616–2627. [CrossRef]

48. Su, W.-T.; Wang, Y.-T.; Chou, C.-M. Optimal fluid flow enhanced mineralization of MG-63 cells in porous chitosan scaffold. *J. Taiwan Inst. Chem. Eng.* **2014**, *45*, 1111–1118. [CrossRef]

49. Butler, W.T. The Nature and Significance of Osteopontin. *Connect. Tissue Res.* **1989**, *23*, 123–136. [CrossRef]

50. Golub, E.; Boesze-Battaglia, K. The role of alkaline phosphatase in mineralization. *Curr. Opin. Orthop.* **2007**, *18*, 444–448. [CrossRef]

51. Zhou, X.; Zhang, Z.; Feng, J.Q.; Dusevich, V.M.; Sinha, K.; Zhang, H.; Darnay, B.G.; de Crombrugghe, B. Multiple functions of Osterix are required for bone growth and homeostasis in postnatal mice. *Proc. Natl. Acad. Sci. USA* **2010**, *107*, 12919–12924. [CrossRef] [PubMed]

52. Sinlapabodin, S.; Amornsudthiwat, P.; Damrongsakkul, S.; Kanokpanont, S. An axial distribution of seeding, proliferation, and osteogenic differentiation of MC3T3-E1 cells and rat bone marrow-derived mesenchymal stem cells across a 3D Thai silk fibroin/gelatin/hydroxyapatite scaffold in a perfusion bioreactor. *Mater. Sci. Eng. C* **2016**, *58*, 960–970. [CrossRef] [PubMed]

53. Kreke, M.; Huckle, W.; Goldstein, A. Fluid flow stimulates expression of osteopontin and bone sialoprotein by bone marrow stromal cells in a temporally dependent manner. *Bone* **2005**, *36*, 1047–1055. [CrossRef] [PubMed]

54. Stein, G.S.; Lian, J.B. Molecular Mechanisms Mediating Proliferation/Differentiation Interrelationships During Progressive Development of the Osteoblast Phenotype. *Endocr. Rev.* **1993**, *14*, 424–442. [CrossRef] [PubMed]

55. Boyce, B.F.; Xing, L. Functions of RANKL/RANK/OPG in bone modeling and remodeling. *Arch. Biochem. Biophys.* **2008**, *473*, 139–146. [CrossRef]

56. Pinzone, J.J.; Hall, B.M.; Thudi, N.K.; Vonau, M.; Qiang, Y.-W.; Rosol, T.J.; Shaughnessy, J.D., Jr. The role of Dickkopf-1 in bone development, homeostasis, and disease. *Blood* **2009**, *113*, 517–525. [CrossRef]

57. Blanchard, F.; Duplomb, L.; Baud'Huin, M.; Brounais, B. The dual role of IL-6-type cytokines on bone remodeling and bone tumors. *Cytokine Growth Factor Rev.* **2009**, *20*, 19–28. [CrossRef]

58. Bendre, M.S.; Montague, D.C.; Peery, T.; Akel, N.S.; Gaddy, D.; Suva, L.J. Interleukin-8 stimulation of osteoclastogenesis and bone resorption is a mechanism for the increased osteolysis of metastatic bone disease. *Bone* **2003**, *33*, 28–37. [CrossRef]

59. Hong, K.H.; Ryu, J.; Han, K.H. Monocyte chemoattractant protein-1–induced angiogenesis is mediated by vascular endothelial growth factor-A. *Blood* **2005**, *105*, 1405–1407. [CrossRef]

60. Grosso, A.; Burger, M.G.; Lunger, A.; Schaefer, D.J.; Banfi, A.; Di Maggio, N. It Takes Two to Tango: Coupling of Angiogenesis and Osteogenesis for Bone Regeneration. *Front. Bioeng. Biotechnol.* **2017**, *5*, 68. [CrossRef]

61.   Jaasma, M.J.; O'Brien, F.J. Mechanical Stimulation of Osteoblasts Using Steady and Dynamic Fluid Flow. *Tissue Eng. Part A* **2008**, *14*, 1213–1223. [CrossRef] [PubMed]

62.   Tanaka, S.M.; Sun, H.B.; Roeder, R.K.; Burr, D.B.; Turner, C.H.; Yokota, H. Osteoblast Responses One Hour After Load-Induced Fluid Flow in a Three-Dimensional Porous Matrix. *Calcif. Tissue Res.* **2005**, *76*, 261–271. [CrossRef] [PubMed]

Name of candidate: Maria Elisabeth Schröder

Title of thesis: 3D *in vitro* models as tool for studying tissue repair and remodelling of soft and hard tissues

Errata list

Page number	Line	Original text	Type of correction	Corrected text
4	116	forth	Correction of language	fourth
9	273	.. Type I collagen type mRNA expression	Delete text	… Type I collagen mRNA expression
22	674	.. dynamic culture environment (128)).	Delete sign	.. dynamic culture environment (128).
22	682	… it provide very low shear stress	Correction of language	… it provides very low shear stress
27	866	… stiffness of osteoblast spheroids	Add text	… stiffness of the osteoblast spheroids
28	897	… OPG, RANKL)	Delete sign	… OPG, RANKL.
37	1179	… cells surround by	Correction of language	… cells surrounded by
37	1192	… endothelial linage,	Correction of language	… endothelial lineage,
77	323-327	The nominal stress-strain relationship of the PDLC-spheroids (...), and considerably lower in the 25(OH)D3+MK-4 group (12.4 MPa).	Text double. Delete	

3D *in vitro* models as tool for studying tissue repair and remodelling of soft and hard tissues

Maria Elisabeth Schröder

Doctoral Thesis for the degree of Philosophiae Doctor (Ph.D)

Department of Biomaterials

Institute of Clinical Dentistry

Faculty of Dentistry

University of Oslo

Norway

2023